EFFICIENT APPROACH FOR PROCESSING OF HEXAGONALLY SAMPLED EXPLORATION SEISMIC DATA USING SPIRAL ARCHITECTURE

BY

Haroon Ashraf

A Thesis Presented to the

DEANSHIP OF GRADUATE STUDIES

KING FAHD UNIVERSITY OF PETROLEUM & MINERALS

DHAHRAN, SAUDI ARABIA

In Partial Fulfillment of the
Requirements for the Degree of

MASTER OF SCIENCE

In

ELECTRICAL ENGINEERING

May, 2015

KING FAHD UNIVERSITY OF PETROLEUM & MINERALS
DHAHRAN 31261, SAUDI ARABIA

DEANSHIP OF GRADUATE STUDIES

This thesis, written by **HAROON ASHRAF** under the direction of his thesis adviser and approved by his thesis committee, has been presented to and accepted by the Dean of Graduate Studies, in partial fulfillment of the requirements for the degree of **MASTER OF SCIENCE IN ELECTRICAL ENGINEERING DEPARTMENT**.

Thesis Committee

Dr. Wail A. Mousa (Adviser)

Dr.Abdullatif A. Al-Shuhail (Member)

Dr.Azzedine M. Zerguine (Member)

Dr.Ali A. Al-Shaikhi
Department Chairman

Dr. Salam A. Zummo
Dean of Graduate Studies

20/5/15
Date

EFFICIENT APPROACH FOR PROCESSING OF HEXAGONALLY SAMPLED EXPLORATION SEISMIC DATA USING SPIRAL ARCHITECTURE

by

HAROON ASHRAF

A Thesis Presented to the
DEANSHIP OF GRADUATE STUDIES

In Partial Fulfillment of the Requirements
for the degree
MASTER OF SCIENCE

IN

ELECTRICAL ENGINEERING DEPARTMENT
KING FAHD UNIVERSITY
OF PETROLEUM & MINERALS

Dhahran, Saudi Arabia

MAY, 2015

KING FAHD UNIVERSITY OF PETROLEUM & MINERALS
DHAHRAN 31261, SAUDI ARABIA

DEANSHIP OF GRADUATE STUDIES

This thesis, written by **HAROON ASHRAF** under the direction of his thesis adviser and approved by his thesis committee, has been presented to and accepted by the Dean of Graduate Studies, in partial fulfillment of the requirements for the degree of **MASTER OF SCIENCE IN ELECTRICAL ENGINEERING DEPARTMENT**.

Thesis Committee

Dr. Wail A. Mousa (Adviser)

Dr.Abdullatif A. Al-Shuhail (Member)

Dr.Azzedine M. Zerguine (Member)

Dr.Ali A. Al-Shaikhi
Department Chairman

Dr. Salam A. Zummo
Dean of Graduate Studies

Date

Dedicated to my late father, my teacher,
my best friend and my ideal.
I miss you Abbu.

And to all those who are trying to find a cure to cancer.

ACKNOWLEDGMENTS

First of all, I would like to thank Allah (S.W.T) for guiding me towards right path and for showering his blessings upon me. I would like to thank KFUPM for giving me this opportunity to complete my master's degree in such a challenging environment. I would like to thank my mother, her prayers specifically, my wife, my cute daughter and my sister for the unconditional support throughout the research and building confidence in me during difficult times. I would also like to thank my thesis advisor Dr. Wail A. Mousa for encouraging me to take seismic signal processing as my research area and for guiding me throughout the research. It was his enthusiasm and guidance which made me accomplish my thesis objectives. The experience has been interesting and rewarding one.

I would also like to thank my thesis committee members, Dr. Abdellatif Shuhail and Dr. Azzedine Zerguine for providing me their support and guidance at every level. The valuable suggestions provided to me by Dr. Azzedine during my independent research assisted me a lot. Dr. Abdellatif Shuhail's experience and understanding of seismic exploration played a pivotal part in this thesis. Moreover, I would like to humbly appreciate the efforts of my committee members in proof reading the drafts. They have been an invaluable help throughout my thesis.

Dr.Saleh Al-Dossary, Exploration Application Services Department, Saudi Aramco, has been instrumental in this research work. His observations from an industrial point of view played a pivotal part in the seismic interpretation stages of my thesis. He was kind enough to provide me with Aramco's data to be utilized in my research work. This data assisted me tremendously and helped me in fine tuning my research.

Second last and not the least, rather not at all the least, I would like to acknowledge the contributions of my beloved wife. She has stood by me at every level in the toughest phase of my life. Not only did she support me in every possible way she even helped me at technical level. I would like to thank my wife for her unwavering motivation and support. This could not have been possible without her.

In the end I would like to acknowledge the seismic group in EE department (SEA Group), KFUPM, for helping me with the technical and research work, I would like to thank my friends Fazal and Naveed, for their help and assistance, I would like to thank Dr.Ahmad Masood, for being an awesome teacher. And lastly a lot of thanks to Ahmad Rafiq for giving me a good company and playing C&C Generals with overlord tanks and aurora bombers when the stress of research was too much to handle. Thank you everyone.

TABLE OF CONTENTS

LIST OF TABLES

LIST OF FIGURES

THESIS ABSTRACT

NAME: Haroon Ashraf

TITLE OF STUDY: Efficient Approach For Processing Of Hexagonally Sampled Exploration Seismic Data Using Spiral Architecture

MAJOR FIELD: Electrical Engineering Department

DATE OF DEGREE: May, 2015

Natural resources such as oil and gas, hidden in sub-earth structures, are extremely important in our daily lives. The gap between increasing demand and new discoveries is increasing. In order to make new successful explorations, it is imperative to employ higher resolution subsurface imaging techniques. Thus, we are faced with a huge data, data handling and processing time related hurdles. Hexagonal sampling in the spatial domain offers a solution to the previously mentioned hurdles associated with increased resolution. The seismic data is circularly band limited in the wavenumber domain. It has been proven that spatial hexagonal sampling is the optimum sampling scheme for seismic data. Yet, with the existence of no efficient technique to handle such a hexagonal scheme, it was not feasible to do so. In this thesis, an attempt has been made to prove the efficiency of hexago-

nal sampling as compared to the regular rectangular sampling. A MATLAB based toolbox has been developed which deals with hexagonal processing. As a proof of concept, hexagonal sampling has been successfully employed on the acquisition and interpretation stages of seismic signal processing.

ملخص الرسالة

الاسم الكامل: هارون أشرف

عنوان الرسالة: المنهجية الفعالية في معالجة عينة البيانات الزلزالية المكتشفة السداسية باستخدام العمارة اللولبية

التخصص: الهندسة الكهربائية

تاريخ الدرجة العلمية: مايو, 2015

المصادر الطبيعية كالزيت والغاز والمخبأة في باطن الأرض تكتسب أهمية كبيرة في حياتنا اليومية. فالفجوة بين زيادة الطلب والاكتشافات الجديدة في ازدياد. فمن الواجب لعمل المزيد من الاكتشافات الناجحة أن نوظف تقنيات التصوير تحت السطحية عالية الدقة. وهكذا فنحن نواجه عقبات متعلقة بضخامة البيانات، والتعامل معها ومعالجتها. فالعينات السداسية في المدى اللولبي يقدم الحل للعقبات المذكورة آنفا والمتعلقة بزيادة الدقة. فالبيانات الزلزالية محدودة بشكل دائري في نطاق رقم الموجة. لقد أثبت أن العينات السداسية اللولبية هي مخطط العينات الأمثل للبيانات الزلزالية. وحتى الآن، مع عدم وجود أي تقنية فعالة للتعامل مع مثل هذه المخططات السداسية، فمن غير المجدي عمل ذلك. في هذه الرسالة، تمت المحاولة لاثبات فعالية العينات السداسية مقارنة لتلك العينات المستطيلة المنتظمة. فتم تطوير الأدوات المبنية على الماتلاب والتي تتعامل مع المعالجة السداسية. ولاثبات لهذا المفهوم، تم تطبيق العينات السداسية بنجاح باقتناء وتفسير مراحل معالجة الاشارات الزلزالية.

CHAPTER 1

INTRODUCTION

1.1 Introduction

Natural resources such as oil, gas and coal are extremely important in our day-to-day life. Such resources are hidden in deep land or marine sub-surface structures. In particular, the process of oil exploration locates possible drilling locations. These are the locations where the actual drilling of an oil well is used to determine the possibility of oil to exist [1], [2]. Obtaining a vivid and accurate image of the sub-surface is a prerequisite for oil production. This can be achieved by a technique called reflection seismology [1]. Such a geophysical technique depends on the production of artificial seismic waves and the recording of their reflections from various geological layers by the help of receivers. However, such acquired seismic data does not reveal an accurate image of the sub-surface unless we use appropriate seismic data processing techniques.

The acquired seismic data contains reflections from different earth layers. By analyzing these layers, geologists and geophysicists, after obtaining the final image of the subsurface, can predict the most likely structures that may contain hydrocarbons. Due to the complex geological conditions, different kinds of reflections are generated.

The major constraints in seismic reflection data processing arise from the huge data set involved. The seismic data is received with the help of receiver lines. Each receiver line contains multiples of receivers. The number of receivers is directly proportional to the resolution of sub-surface image. In the past few decades, the number of receivers used in the exploration stage has witnessed an exponential increase [3], [4]. The higher the resolution of the seismic image the better identification of hydrocarbons can be made. With the advancement in computational technology, the number of live receiver channels used for geological surveys has increased exponentially from less than a 100 in 1970 to nearly 200,000 channels nowadays and up to 1 million live channels by 2020 are expected [3], [5], [6].

Owing to higher resolution, the raw data acquired is huge. For example, the amount of data recorded by CGG Veritas (an oil exploration service company) during just one medium sized marine three dimensional (3D) survey would fill 20,000 compact discs forming a stack over 650 feet high, where most of the 3D

surveys uses rectangular sampling. It has been shown in literature that seismic data in the wavenumber domain is circularly band limited. Hence, one way to reduce the size of data is to use hexagonal sampling instead of rectangular sampling.

Little research work has been carried out on hexagonally sampled seismic data processing. 1n 1992, the work was carried out by applying McClellan transformations on a hexagonal sampling grid [7]. In 1997, the work was carried out on hexagonal sampling grid [8]. In 2004, work was carried out for 3D filter design on a hexagonal grid with applications to point receiver land acquisitions [9] and in 2007 pre stack depth migration was researched for hexagonally sampled seismic data [10].

Hexagonal sampling strategy has the alternative rows/columns placed half sample interval with respect to the other rows/columns. It is called hexagonal because each sample has six equidistant neighbors, when the sampling, in horizontal and vertical directions, is evenly dense. Hexagonal sampling offers the best approximation of circularly band limited signals and requires 13.4% less number of samples to represent the same data in comparison to rectangular sampling [8], [11], [12], [13]. Since seismic signals are circularly band-limited in the wavenumber domain, hexagonal approach is more appropriate in comparison to rectangular sampling [8], [11], [12], [13], [14] .

1.2 Thesis Contribution

The fundamental strength of hexagonal sampling lattice is its great symmetry; a regular hexagon is 50% more symmetric than a square, exhibiting a 12 fold as opposed to 8 fold symmetry. This forms the basis of the efficiency of the hexagonal sampling technique [11], [15]. Hexagonal sampling has been applied in a limited amount in signal processing. Every location in a rectangular sampling grid has four nearest neighbors (vertical and horizontal) and four diagonal neighbors located at a greater distance. Whereas, in a hexagonal grid each location has six nearest neighbors, each of which is the same distance away [15]. This is convenient for certain image processing problems involving boundary tracing, cluster separation etc. Thus, the application of hexagonal sampling to seismic data can help in increasing the processing speed and quality of results obtained even at the interpretation stage [13], particularly for the case of 3D seismic data set.

Extensive work has been carried on hexagonal sampling in the image processing and computer vision domains [16], [17]. However, the work done so far deals with hexagonal sampling from a rectangular sampling viewpoint. This approach definitely utilizes the fact that 13.4% less samples are required but the computation power for dealing with this hexagonal structure renders its sampling efficiency less effective than it could have been if hexagonal sampling had been approached in a way independent of rectangular sampling [18], [19]. Similar

approaches have also been applied on seismic signal processing, which employ rectangular addressing techniques to deal with hexagonally sampled data.

The spiral architecture (SA) was introduced in 1996 for machine vision on a hexagonal lattice [20]. The spiral architecture provides a model closer to biological vision systems, while offering advantages over the regular rectangular pixel image representation [15]. The pixel in SA has the shape of a hexagon. While the basic concept of hexagonal pixels is not new, SA introduces a special addressing algorithm, which identifies each hexagon of the structure with a unique one dimensional (1D) address in base seven. The addressing algorithm, spiral addition and spiral multiplication, provides the spiral architecture with the algebraic feature of a Euclidean ring. This addressing allows the handling of two-dimensional (2D) signals as 1D signals [21], [22]. Application of SA on image processing has been performed several times but no work has been carried out for the application of SA on seismic data, which will not only reduce the number of samples required for the same resolution but will also assist in treating a 3D problem as a 2D problem.

In this thesis, we propose a 3D SA hexagonal signal processing approach to 3D seismic data problems. The inherent ability of hexagonal sampling to deal with large data has been explored. In order to implement hexagonal processing on seismic data, a MATLAB-based toolbox has been developed but utilizing the

SA. Existing work has been done on 2D SA data. A 3D hexagonally sampled data can be processed using the proposed framework. This is the first attempt to deal with 3D hexagonally sampled data. Interestingly, the proposed 3D SA framework is highly efficient, when dealing with huge amounts of data in comparison to the rectangular approach. This will be seen in various applications of 3D seismic data interpretation. Furthermore, quality of the results is subjectively better in the hexagonal case especially during seismic interpretation.

Previously, attempts have been made to apply hexagonal approach to digital group forming problem for the acquisition of 3D seismic data where the data is hexagonally sampled [9]. Since previous attempts to this problem were not hexagonal in the true sense, the attempts introduced certain problems such as aliasing. In this work, we design 3D digital group forming filters using projection on convex sets but using the proposed SA, where true locations are handled and huge data saving is present. Most importantly aliasing is avoided by not inserting zeros between samples, as will be shown later in this work.

One 3D seismic interpretation application is presented as follows. 3D Sobel filters have been designed for edge detection of 3D seismic data that is hexagonally sampled in the spatial domain. It has been shown that not only the edge detection is significantly fast in case of hexagonal approach as compared to rectangular approach. Also the quality of results is improved

due to the inherent increased symmetry of a hexagon. Keeping in mind the huge size of seismic data, the spiral approach's efficiency makes it ideal for seismic signal processing. The rectangular approach requires nearly 45% more additions and multiplications as compared to the SA approach. The SA is hundreds time faster than rectangular approach as will be shown in this research work.

Another application is edge preserving smoothing (EPS) algorithm [23]. The EPS algorithm attempts to simultaneously reduce the noise while preserving the edges. Such a commonly used algorithm in the seismic data processing industry has been designed for hexagonally sampled data using the SA for 3D seismic data. It has been shown that this preprocessing step of edge detection result in even better quality of edge detection. The processing speed of spiral architecture is nearly two times faster in comparison to regular approach. This is the first attempt of edge preserving smoothing on hexagonally sampled data. In both interpretation cases, 2D synthetic and 3D real seismic data sets were used for testing the robustness, efficiency and the quality of the results.

1.3 Thesis Organization

The thesis is structured as follows. Chapter 2 provides an introduction and background of hexagonal signal processing. The fundamentals of hexagonal sampling are discussed. Also, the spiral architecture used for hexagonal sampling is explained. In chapter 3, spiral architecture is used to design 3D digital

group forming filters for seismic acquisition, on both rectangular and hexagonal sampled data. Later on, in chapter 4, an attempt is made to compare seismic edge detection based on hexagonal and rectangular approaches. Chapter 5 introduces the edge preserving smoothing algorithm for simultaneous noise suppression and edge preservation on the spiral architecture. Finally, conclusions and future work are given in chapter 6.

CHAPTER 2

HEXAGONAL SIGNAL PROCESSING

2.1 Introduction

This chapter explains the concept of hexagonal sampling and its relevance to circularly band-limited seismic signals. Furthermore, the advantages of using hexagonal approach for seismic signals are discussed. Moreover, the proposed spiral architecture (SA) for dealing with hexagonally sampled seismic signals is also explored in depth. The addressing scheme and basic arithmetic operation for hexagonally sampled data will be discussed. The data handling capability of the spiral architecture is also explained when dealing with two dimensional (2D) and three dimensional (3D) signals. The frequency domain processing is also explored in this chapter. The MATLAB toolbox and some basic simulation results are shown at the end of this chapter.

2.2 Tiling

A two dimensional spatial signal's sampling can be regarded akin to tiling of the Euclidean plane. Sampling can be studied on the basis of tiling. It can be regarded as a special case of tiling. In tiling, a plane is covered to analyze the characteristics of each tile. In a similar manner, sampling is required to gather maximum information of the underlying signal extending over the plane in an efficient manner. The process of sampling is achieved by first dividing the Euclidean plane into reproducible and regular regions and afterwards by analyzing the signal in each region[15].

A tiling wherein all tiles are same shaped and have an equal size, is called a monohedral tiling. It has been proved that only three such monohedral tilings are physically possible [24]. These three possible tilings namely triangles, squares and hexagons are shown in Fig. 2.1.

The corners of individual tiles must meet at a point. Furthermore all interior angles of tiles meeting at a point should sum to 2π radians as given by Eq. 2.1.

$$InteriorAngle = \frac{(n-2)\pi}{n}. \tag{2.1}$$

In the Eq. 2.1 n is the number of sides. Moreover, there should also be no gap between the tiles.

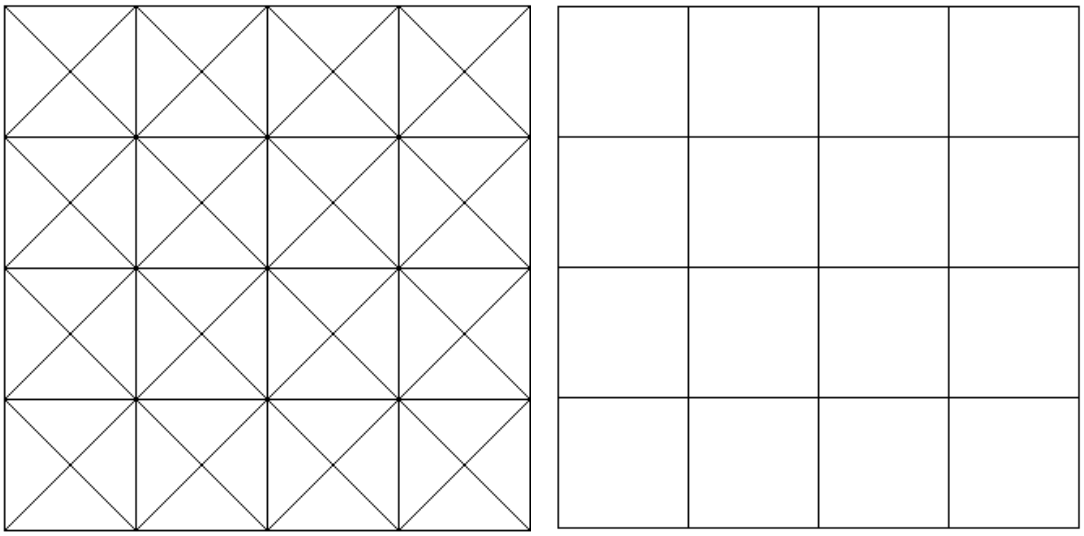

(a) (b)

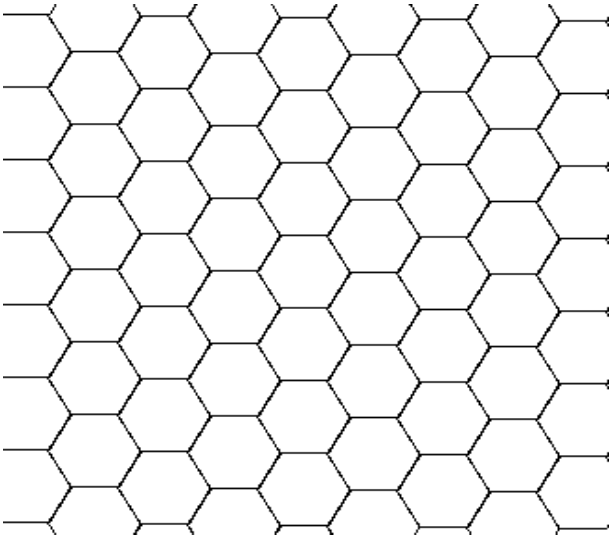

(c)

Figure 2.1: Three possible monohedral tilings. (a) Triangular tiling. (b) Rectangular tiling. (c) Hexagonal tiling.

Several significant features of tilings are based on symmetry. Isometry can be used to define symmetry. Isometries are of four types namely reflection, rotation, glide reflection and translation. The sense of points is preserved in rotation and translation isometries so they are called direct whereas reflection type isometries are known as indirect. The reflection type isometries are shown in Fig. 2.2.

A square has rotation symmetry at multiples of $\pi/2$ radians as compared to $\pi/3$ radians in case of hexagons. Moreover, hexagon has 12 symmetries 6 reflections, 5 rotations and 1 identity. On the other hand, a square has eight symmetries, three rotations, four reflections and one identity. If a tiling fulfils at least one of the four symmetries in addition to identity, it is known as symmetric tiling.

A continuous function is defined in the 2D Euclidean $\mathbb{R}^2$ space. To carry out uniform sampling of this function, it must be divided into regular fashion and samples taken. There is no restriction to only use rectangular sampling. A possible alternative is shown in Fig. 2.3 whose basis $\mathbf{V} = \{\mathbf{v_1}, \mathbf{v_2}\}$ where $\mathbf{v_1}$ and $\mathbf{v_2}$ are the two axes.

The problem of uniform sampling is similar to periodic monohedral tiling. If only regular shapes are to be considered, we have only three options, triangle, square and hexagon. Of these possibilities, hexagons provide the highest number

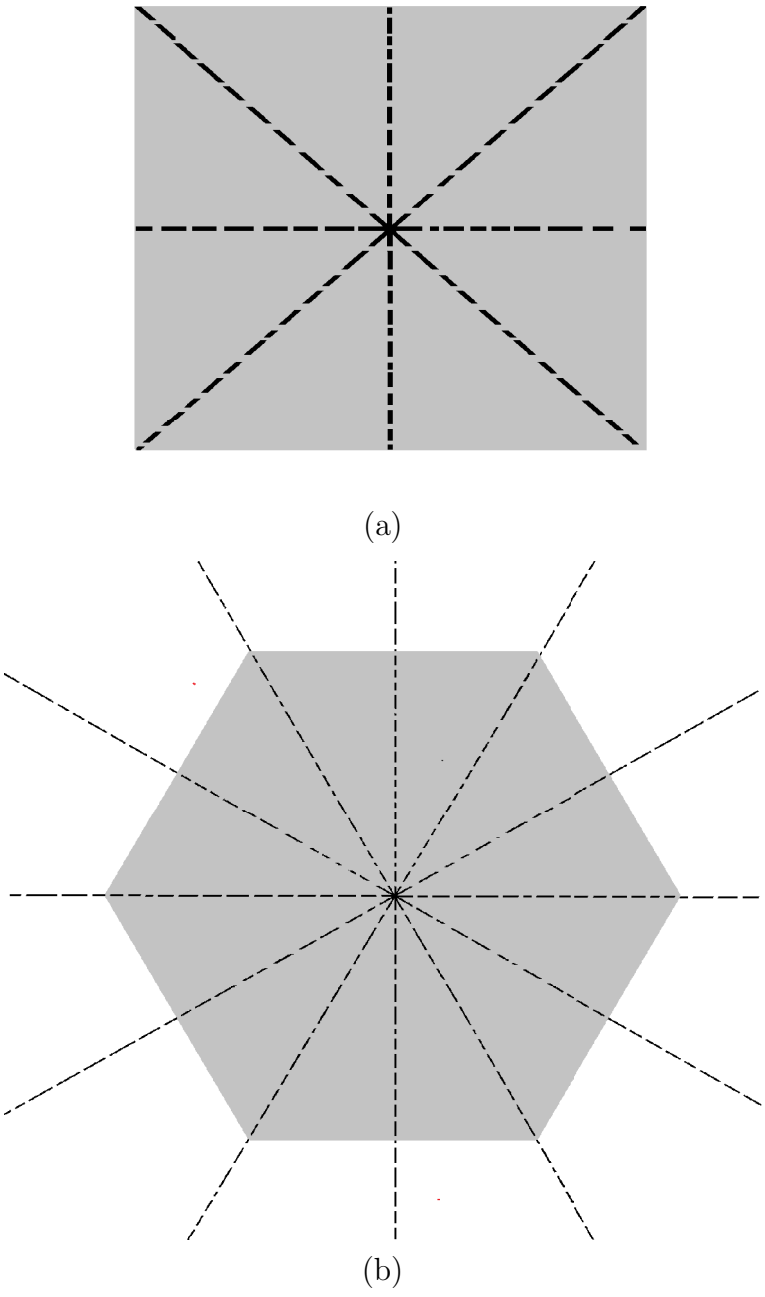

Figure 2.2: Symmetry. (a) Rectangular. (b) Hexagonal.

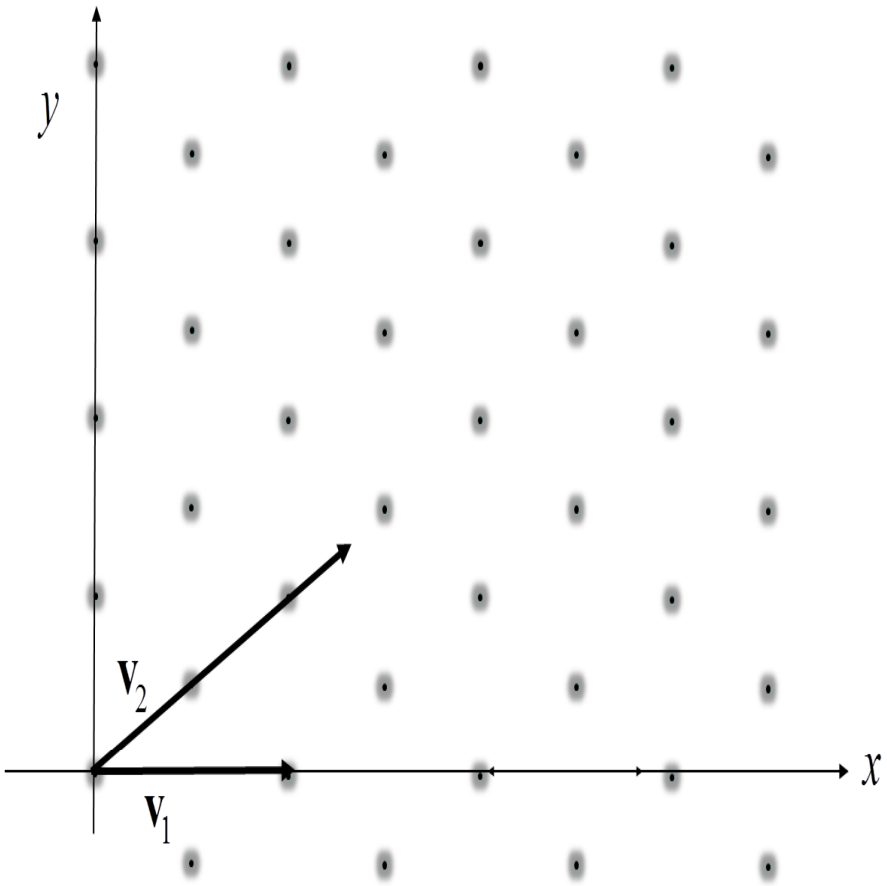

Figure 2.3: Possible uniform sampling of a Euclidean plane.

of tiles/samples per unit. For band-limited signals effective sampling and reconstruction, it is optimum to fit the entire spectrum into a tile. The size and shape of tile can be determined easily if the signal is circularly band-limited. A hexagon is the best fit for such a spectrum as will be shown in next section. Please refer to [11], [15], [19], [24] for more details on tiling.

2.3 Hexagonal Sampling

Two dimensional band-limited signals may be sampled and processed as arrays of numbers. This is a well known and a fundamental fact. But, this fact is not well recognized that there are many strategies by which this sampling can be performed. These sampling strategies represent a different generalization of one-dimensional periodic sampling. These alternate sampling strategies vary in their assumptions regarding how the continuous waveform is band-limited, in the number of samples that must be taken, and in the efficiency of the resulting signal processing algorithms. It must be mentioned that rectangular sampling, which is the most regular approach, is mostly not the best approach [11].

In rectangular sampling, a band-limited signal of two independent variables is sampled at evenly spaced values of each of those variables [11]. Rectangular sampling, thus, corresponds to sampling a waveform at the sampling locations indicated by the filled circles in Fig. 2.4(a). Rectangular sampling assumes that the signal to be sampled is band-limited over such a region as shown in Fig. 2.4(b).

It has been the method of choice for all signal processing applications for a variety of reasons:

- Algorithms for processing signals which have been rectangularly sampled can be straightforwardly generalized from the one dimensional case.
- The resulting expressions can be readily understood and implemented in software.
- Hardware to perform the sampling (scanning) is straightforward to build.

We have become so comfortable with rectangularly sampled arrays that the alternatives are rarely considered [11]. Hexagonal sampling (see Fig. 2.5(a)) considers that the signal to be sampled is band-limited over such a region as shown in Fig. 2.5(b). It is the optimal sampling scheme for signals which are band-limited over a circular region of the Fourier plane, in the sense that exact reconstruction of the waveform requires a lower sampling density than with alternative schemes.

For these signals hexagonal sampling utilizes 13.4% fewer samples than the regular approach of using rectangular sampling [7], [8], [11], [13], [19]. Since several signal processing algorithms are recursive, the computational savings of using hexagonal sampling over rectangular sampling can be several times this factor [11], [19].

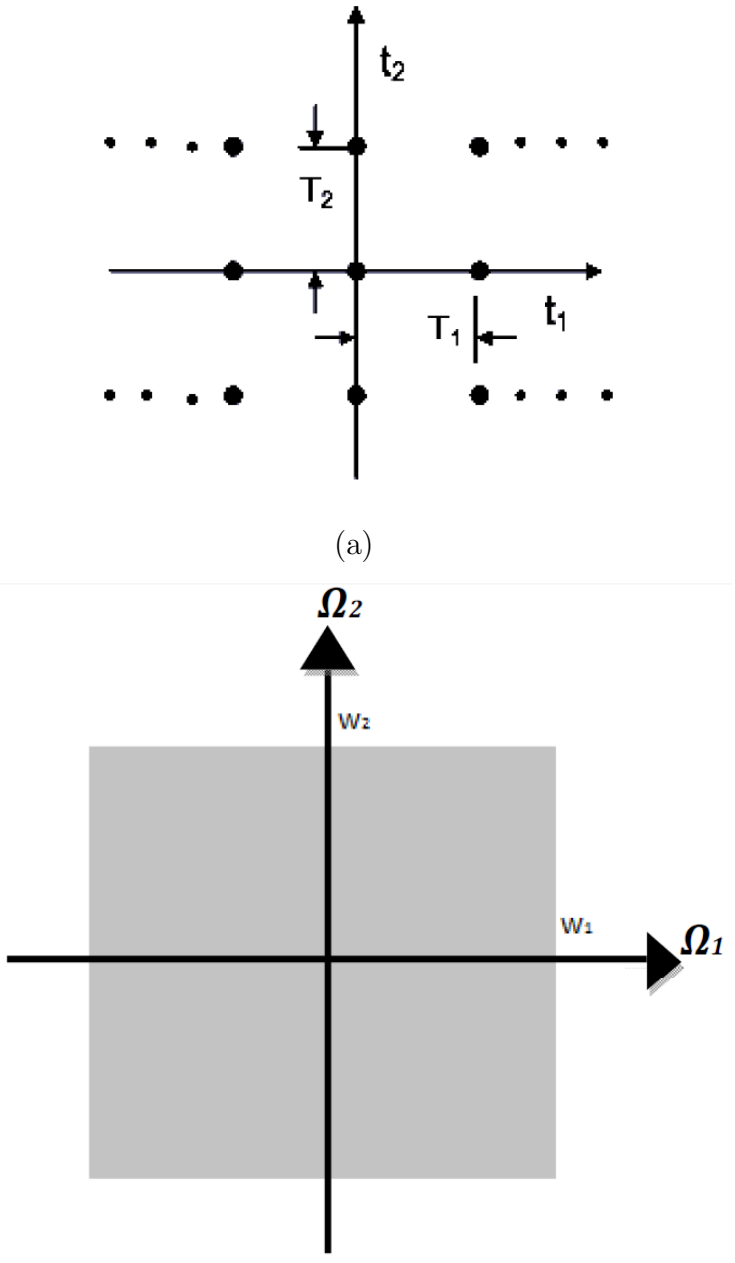

Figure 2.4: Rectangular approach. (a) Sampling raster. (b) Band region.

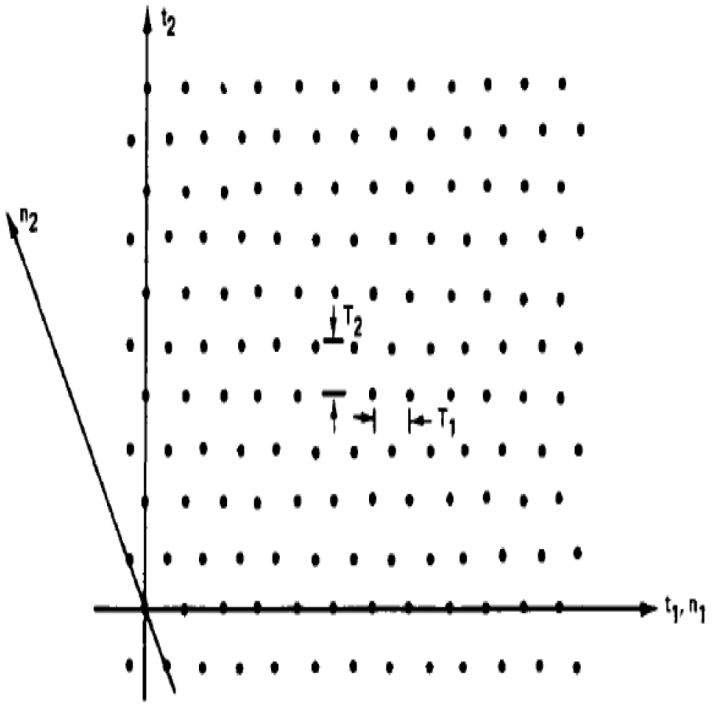

(a)

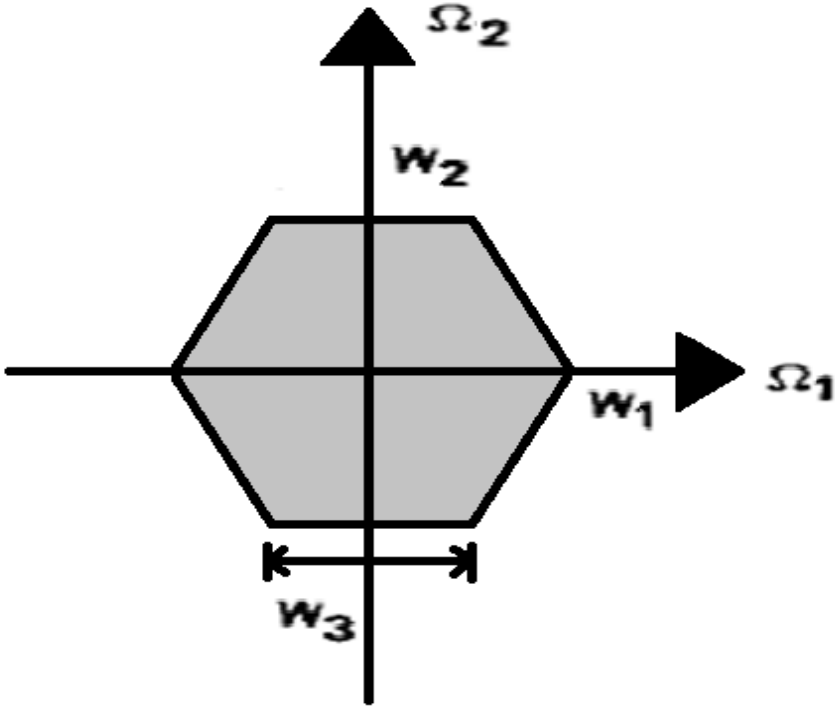

(b)

Figure 2.5: Hexagonal approach. (a) Sampling raster. (Courtesy of [11]). (b) Band region.

For rectangularly sampled waveform the maximum sampling periods are:

$$T_1 = \pi/W, \tag{2.2}$$

and

$$T_2 = \pi/W, \tag{2.3}$$

where W stands for radius. In order to sample the same waveform in a hexagonal manner we can choose:

$$T_1 = 2\pi/\sqrt{3}W, \tag{2.4}$$

and

$$T_2 = \pi/W, \tag{2.5}$$

For a 3D seismic data set, the frequency wave number domain can be approximated by a domain bounded by two cones as shown in Fig. 2.6(a) [8], [13], [25]. The $k-\omega$ axis view of this bounded region is shown in Fig. 2.6(b). The seismic signal is circular band-limited in the $k_x - k_y$ plane [9], [26]. This circular band-limited region is shown in Fig. 2.6(c). The approximation of a circle is more accurately performed with the help of a hexagon rather than a square [13], [15]. This is evident from Fig. 2.7.

The mean sampling density in the spatial domain is less for hexagonal sampling. Generally, it can be shown that the mean sampling density is proportional to the area of the assumed band shape [11]. The mean sampling density for rect-

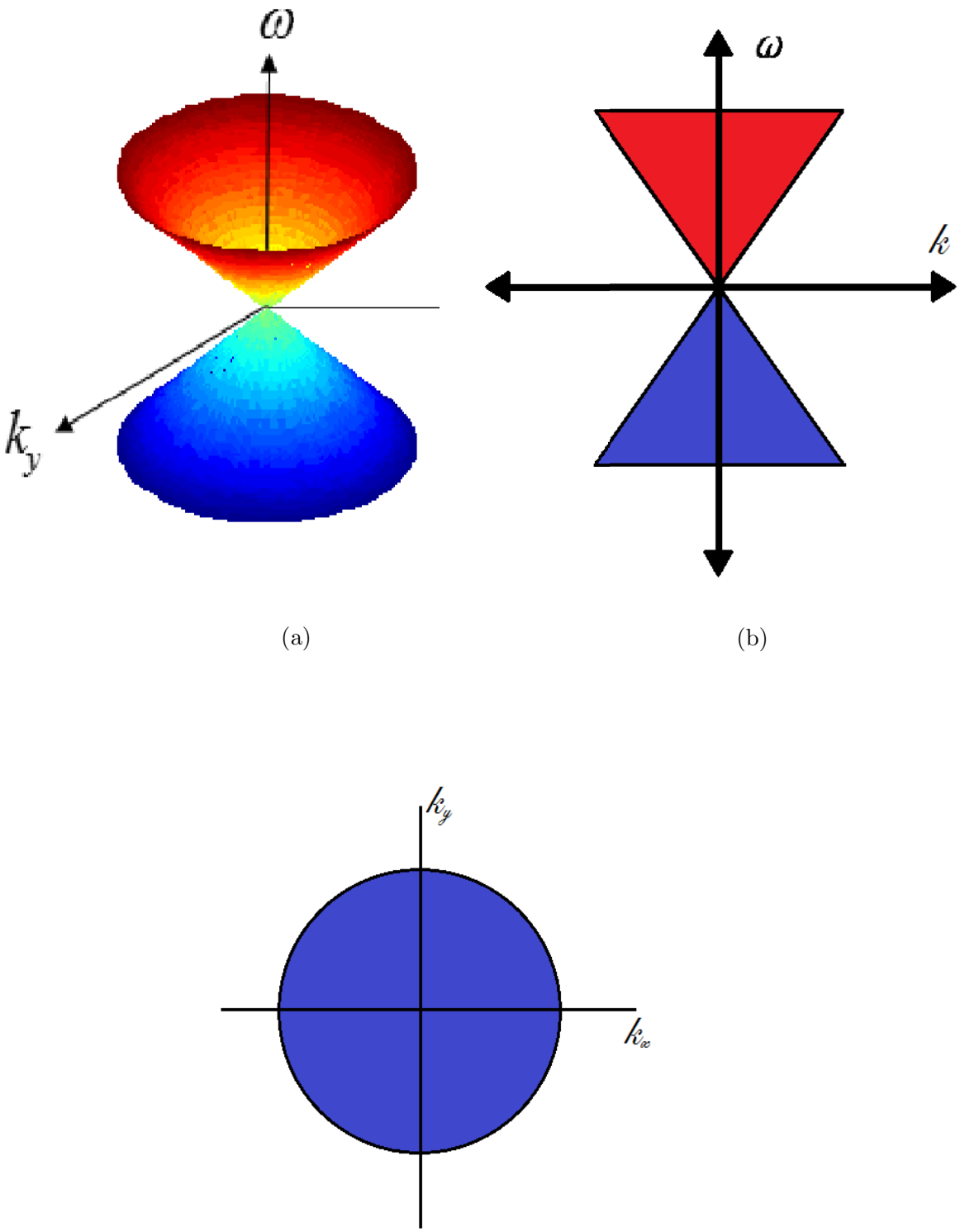

(a) (b)

(c)

Figure 2.6: Seismic band region. (a) In the $k_x - k_y - \omega$ space. (b) In the $k - \omega$ plane. (c) In the $k_x - k_y$ plane.

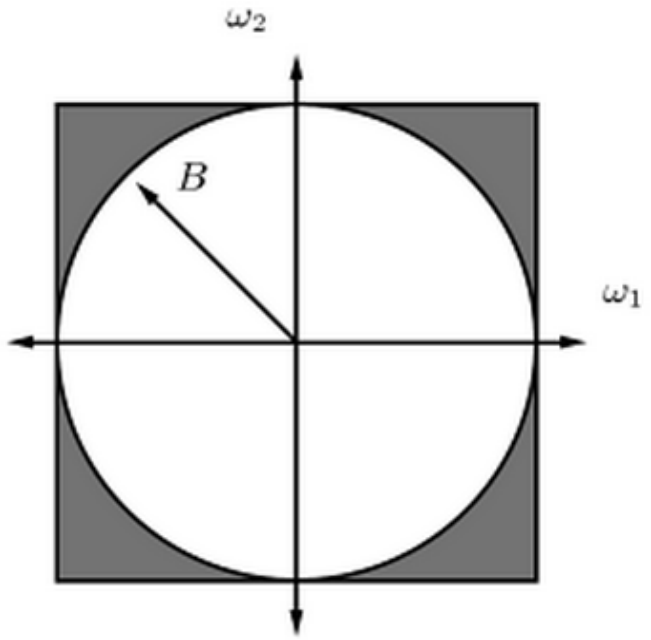

(a)

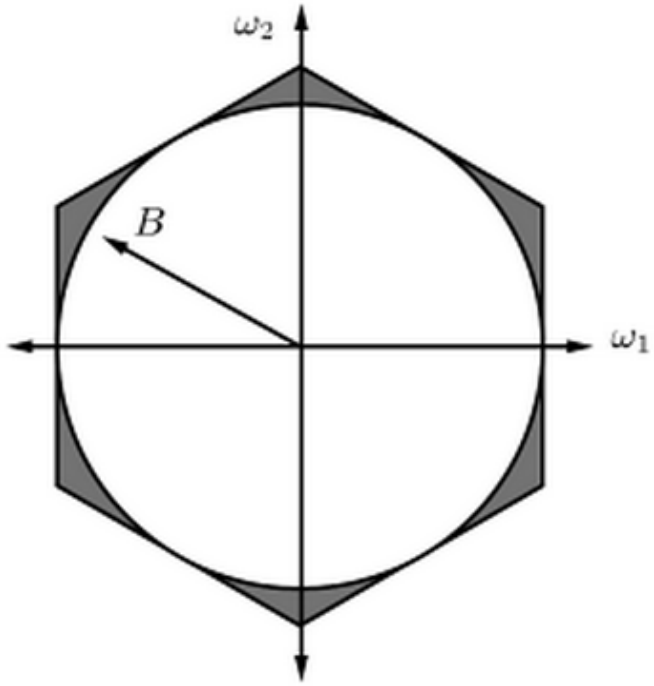

(b)

Figure 2.7: A circularly band-limited signal. (a) Inscribed in a square. (b) Inscribed in a hexagon. (Courtesy of [15].)

angular approach is greater in the spatial domain than for the hexagonal case. Consequently, in case of a circularly band-limited waveform, hexagonal sampling uses 13.4% fewer samples than rectangular sampling [12]. For representation of circularly band-limited waveforms, it has been proven that hexagonal sampling is the best in the sense that no other sampling approach utilizes a lower sampling density [12].

It has also been researched that processing algorithms for hexagonal systems are 25-50% more efficient than those for rectangular systems with the same frequency resolution [12], [27]. Since seismic signal care circularly band limited, usage of hexagonal sampling could theoretically enhance the efficiency of regular two-dimensional surveys by 13-50% [11] . This is particularly interesting for 3D seismic applications, where processing costs are often prohibitively high. A brief comparison is shown in Table 2.1.

Table 2.1: Comparison of features between rectangular and hexagonal sampling.

Features	Rectangular Sampling	Hexagonal Sampling
Symmetry	8 Fold[15]	12 Fold[15]
Equidistant Neighbours	4[15]	6[15]
Approximation of a Circular Region	27.3 % inaccurate	10.2% inaccurate
No. of samples for covering a region wrt Rectangular approach	-	13.4% less[11]
Processing Efficiency wrt Rectangular approach	-	25-50% better [27]
Overall Efficiency wrt Rectangular Approach	-	13-50 % better[11]

2.4 Approaches to Handle Hexagonally Sampled Signals

There are various approaches to deal with hexagonally sampled signals. Most of them are based on the rectangular sampling approach. One of the approaches involves moving alternate axes and then applying rectangular methodologies on alternate rows. This can be seen in the Fig. 2.8(a) [11]. Another approach is using skewed axes as shown in Fig. 2.8(b) [11]. Insertion of alternate zeros has also been employed as shown in Fig. 2.8(c) [9].

All these approaches are based fundamentally on the rectangular approach. As such these hexagonal approaches are not truly hexagonal in terms of processing and data handling rather are a derived version of the rectangular approach. The comparison of these approaches can be seen in Table 2.2. The only true approach to hexagonally sampled signals is the spiral architecture discussed in next section.

2.5 Spiral Architecture

This section introduces Spiral Architecture (SA) for the processing of hexagonally sampled data. The points in a hexagonal grid, unlike the case of square grid, lie along non orthogonal directions to each other. A logical consequence of this non orthogonal sampling is that Cartesian coordinates, which are a normal choice for representation of points in a rectangularly sampled data, are unsuitable in

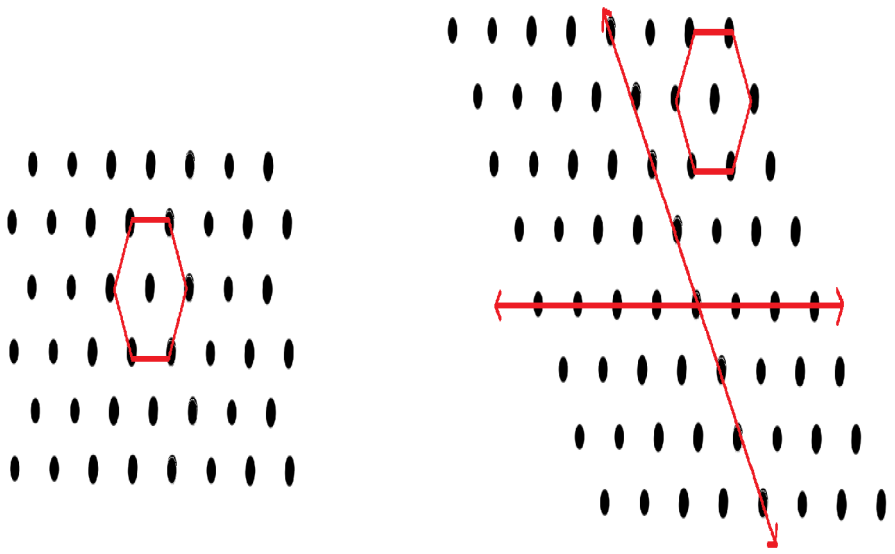

(a) (b)

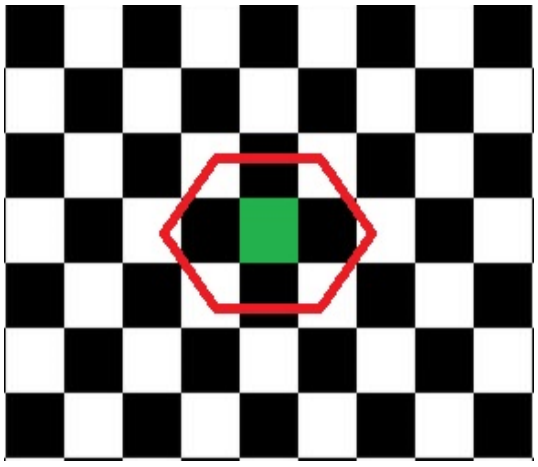

(c)

Figure 2.8: Approaches to handle hexagonally sampled data. (a) Alternate rows approach. (b) Skewed axes approach. (c) Insertion of zeros approach.

Table 2.2: Approaches to handle hexagonally sampled signals.

Approaches	Advantages	Disadvantages
Alternate rows approach	13.4% lesser data	Rectangular processing results in an inability to fully utilize hexagonal processing advantages.
Skewed axes approach	13.4% lesser data	Rectangular processing results in an inability to fully utilize hexagonal processing advantages.
Zero insertion approach	Existing algorithms can be easily utilized.	Rectangular processing results in an inability to fully utilize hexagonal processing advantages. Double size of data due to extra zeros.

the case of hexagonally sampled data. The absence of orthogonality in hexagonal sampling leads to a number of different options based on various sets of skewed axes. Consequently this leads to different possible representations. Nevertheless, such representations are difficult and are unable to completely utilize the hexagonal nature of the underlying lattice. Hence, it is necessary to develop an efficient representation strategy for hexagonal data, because it can affect the performance of a system in a significant manner [20].

2.5.1 Addressing Scheme

Hexagonal sampled 2D data can be considered as a periodic monohedral tiling. A more complex aggregate tile can be made by grouping individual hexagonal tiles. A circular complex arrangement may consist of seven hexagons, containing six hexagons surrounding a central hexagon. This is called circular since six hexagons

are equidistant from central hexagon as shown in Fig. 2.9(a). Linear aggregate tiles consist of lines of four hexagons as shown in Fig. 2.9(b). There are numerous other methods of hexagonal aggregate tiles [15].

Linear aggregate tile contain less degrees of symmetry in comparison to the circular aggregate tiles. 2D plane can be regularly sampled using integer multiples of basis vectors. One vector can be along the horizontal axis and second vector can be at 120 degrees from the horizontal. This results in the following basis vectors [1, 0] and [-0.5, 0.866] as shown in Fig. 2.10.

An addressing scheme can be established on these basis vectors. The central tile, in the Fig. 2.10, can be called a prototile labeled (0, 0). This is the zeroth level. The circular aggregate (light green color), first level aggregate can be considered of seven points. This naming pattern can be continued by moving in an anti clockwise direction, starting from the horizontal axis gives the following hexagonal coordinates for the first seven hexagons:

$$A_1 = \left\{ \begin{bmatrix} 0 \\ 0 \end{bmatrix}, \begin{bmatrix} 1 \\ 0 \end{bmatrix}, \begin{bmatrix} 1 \\ 1 \end{bmatrix}, \begin{bmatrix} 0 \\ 1 \end{bmatrix}, \begin{bmatrix} -1 \\ 0 \end{bmatrix}, \begin{bmatrix} -1 \\ -1 \end{bmatrix}, \begin{bmatrix} 0 \\ -1 \end{bmatrix} \right\}. \tag{2.6}$$

Coordinates for other pixels/tiles can be easily derived on the basis of aggregate level 1 and so by simple addition as shown in Fig. 2.11.

It is evident that level 2 aggregate addresses have been obtained by addition of $(3, 2)$ in the A_1 addresses. Thus the translation symmetry of the original tiling is exploited in case of hexagonal addressing. The translations of each of center tiles of second level aggregate are (3,2),(1,3),(-2,1),(-3,-2),(-1,-3), (2,-1). All these

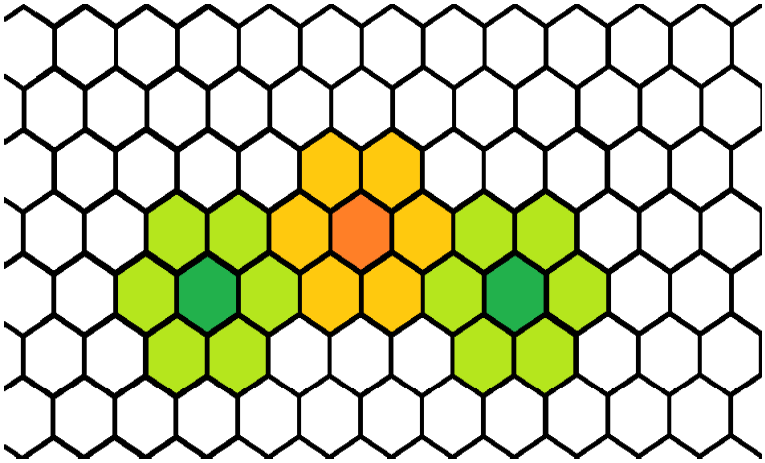

(a)

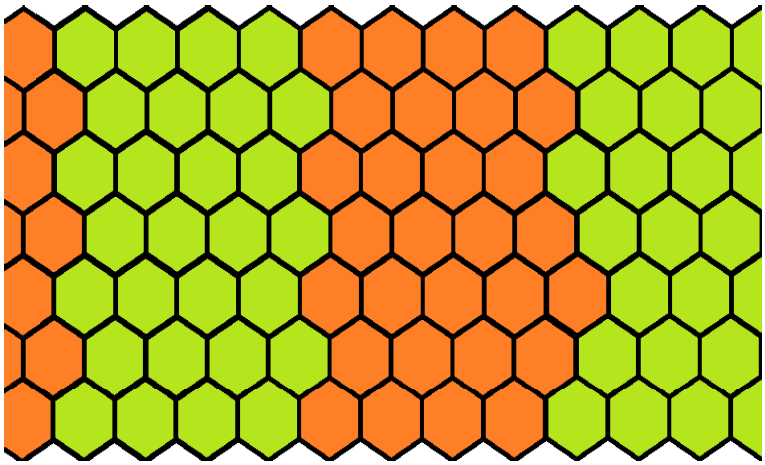

(b)

Figure 2.9: (a) Circular aggregate tiling. (b) Linear aggregate tiling.

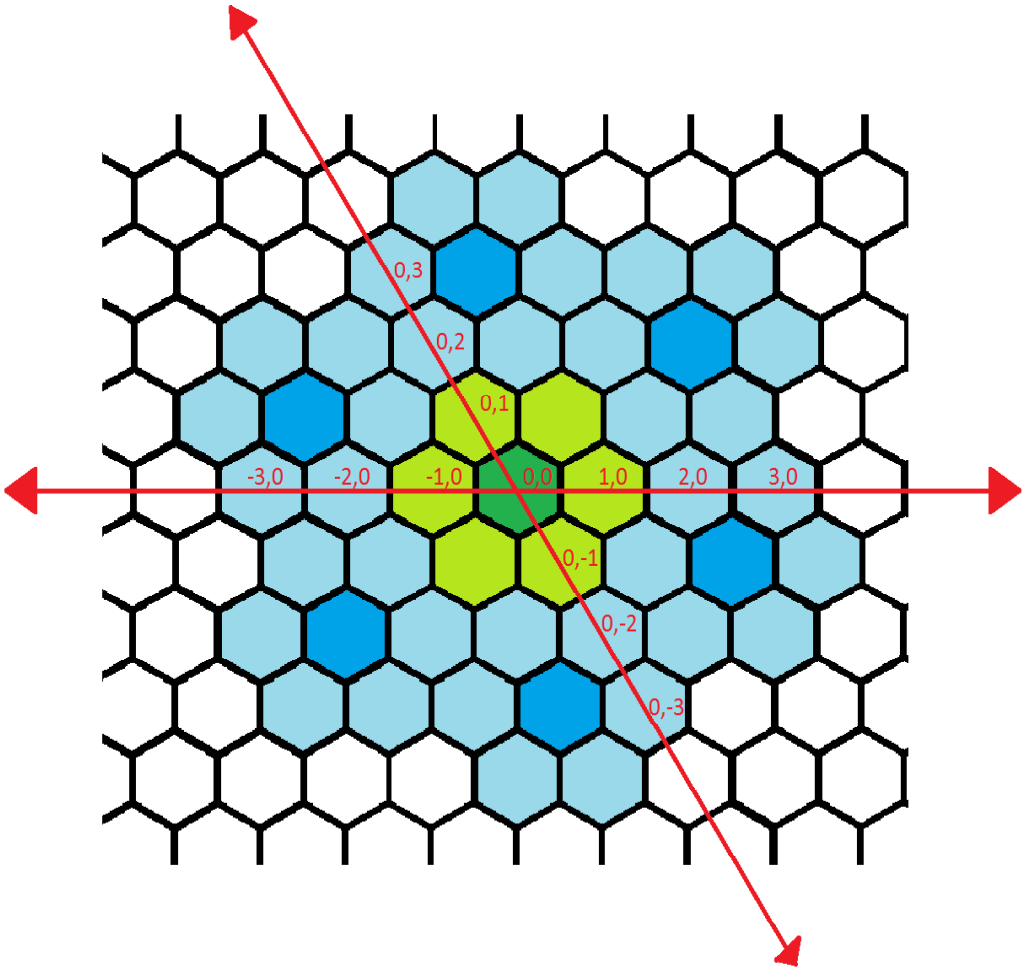

Figure 2.10: Linear hexagonal aggregate basis vectors and coordinates for aggregate level 1.

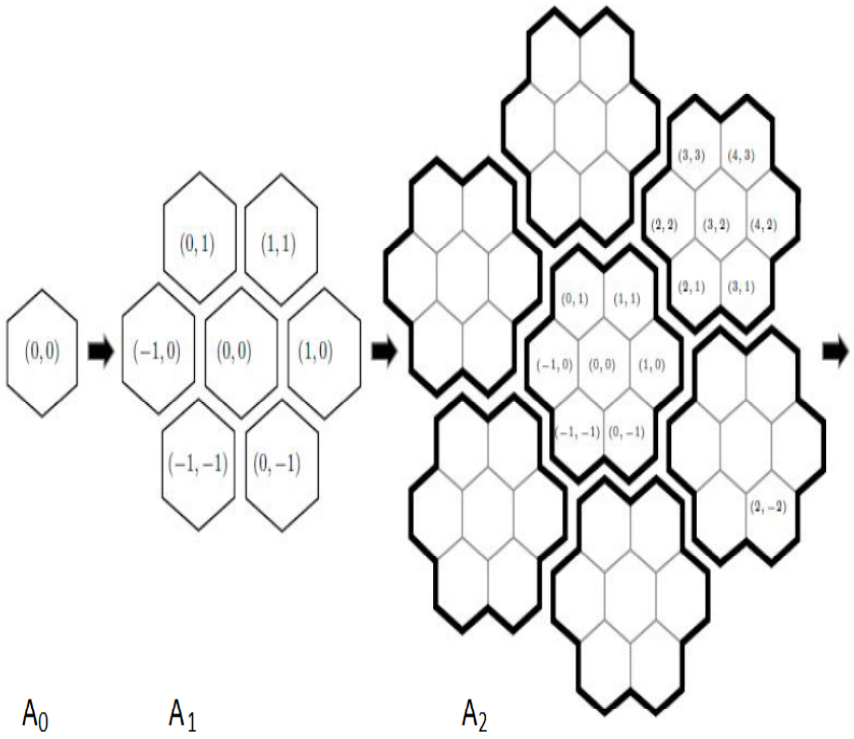

Figure 2.11: Hierarchical tiling based upon the circular aggregate. (Courtesy of [15]).

points are a rotation about the origin by 60 degrees as shown in Fig. 2.12. The aggregate level 2 points are given as :

$$A_2 = \left\{ A_1, \begin{bmatrix} 3 \\ 2 \end{bmatrix}, \begin{bmatrix} 4 \\ 2 \end{bmatrix}, \begin{bmatrix} 4 \\ 3 \end{bmatrix}, \begin{bmatrix} 3 \\ 3 \end{bmatrix}, \begin{bmatrix} 2 \\ 2 \end{bmatrix}, \begin{bmatrix} 2 \\ 1 \end{bmatrix}, \begin{bmatrix} 3 \\ 1 \end{bmatrix}, ..., \begin{bmatrix} 2 \\ -2 \end{bmatrix} \right\}, \tag{2.7}$$

If the points in the first level aggregate are given, then by using the translation property, the points in second level aggregate can be derived. If the points $(3, 2)$ and $(-2, 1)$ are chosen as the basis, then the points mentioned earlier can be reduced to first level aggregate relative to the new axes. Thus, a matrix $\mathbf{N_1}$ can be calculated to perform these translations as shown below :

$$\mathbf{N_1} = \begin{bmatrix} 3 & -2 \\ 2 & 1 \end{bmatrix}. \tag{2.8}$$

Similarly, the next level can be found using the second level aggregate. We have seen that the first tile makes a positive increase in angle from the previous level. So there is only one location for first tile of level 3 $(5, 8)$. Thus, a matrix $\mathbf{N_2}$ can be computed to perform these translations:

$$\mathbf{N_2} = \begin{bmatrix} 5 & -8 \\ 8 & -3 \end{bmatrix}. \tag{2.9}$$

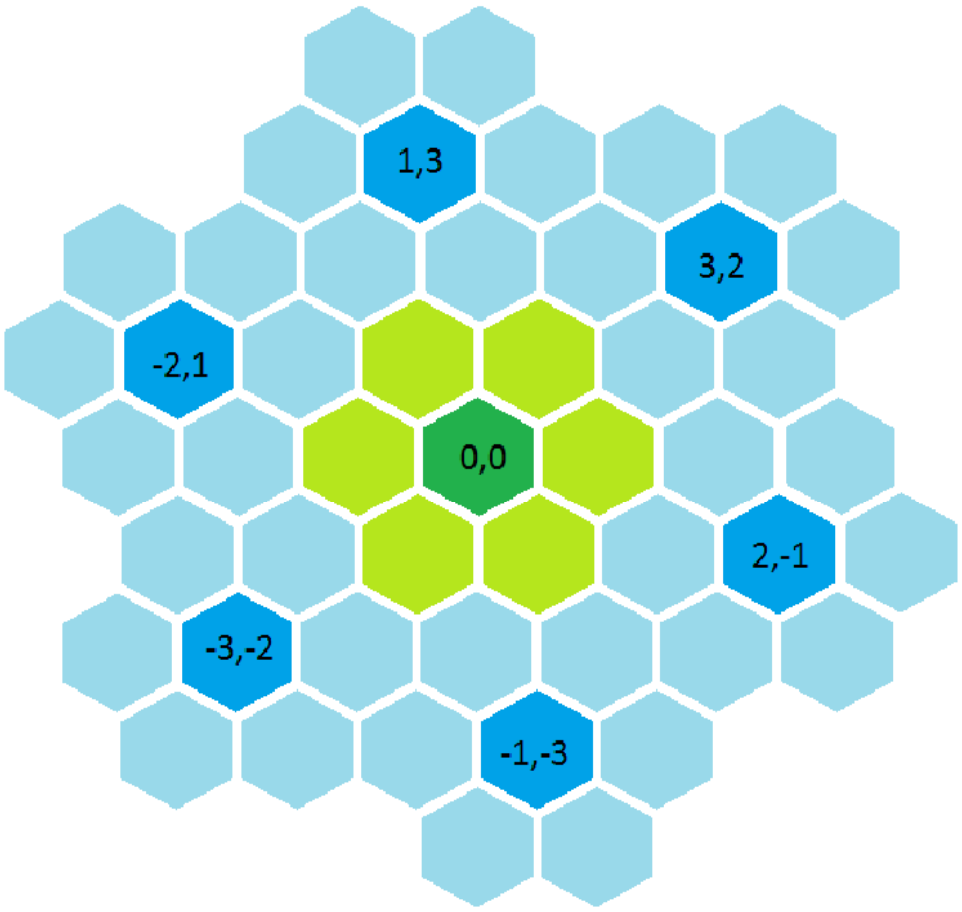

Figure 2.12: Translations of central tiles of second level aggregate.

The general form of this matrix for λ-level aggregate is as follows:

$$\mathbf{N}_\lambda = \begin{bmatrix} 5 & -8 \\ 8 & -3 \end{bmatrix}^{\lambda-1} . \tag{2.10}$$

Using previous sets and translation a complete set of all points in a λ-level aggregate by can be calculated by:

$$A_\lambda = \mathbf{N_{\lambda-1}} A_1 + ... + \mathbf{N_1} A_1 + A_1. \tag{2.11}$$

The number of points in a current aggregate level is seven times more than that of the previous aggregate level. In a λ-level aggregate, the number of points are 7^λ. Another feature is that the angle between the first vector of the basis and the center of each successive aggregate increases as the aggregate level increases. For a λ-level aggregate this rotation is given by:

$$\Theta_\lambda = (\lambda - 1) \arctan \frac{\sqrt{3}}{2}. \tag{2.12}$$

In comparison to a square sampled image of size $M \times N$, the corresponding number of layers/aggregates for spiral architecture can be computed as given below:

$$\lambda = (\log M + \log N) / \log 7. \tag{2.13}$$

Addressing of hexagonal tiles is carried out in the manner shown in Fig. 2.13(a). We can see the level 2 aggregate tile have addresses in two digits. The number

of digits represent the layer. The first digit indicates the index lies within which position of the layer.

2.5.2 Data Handling of Spiral Architecture

An important aspect of the Spiral Architecture (SA) addressing scheme is that 2D data can simply be represented with the help of one dimensional (1D) array. Exploration seismic data is huge in size. In order to efficiently handle this huge data, SA is a suitable alternative since its ability to handle 2D data as a 1D data. In this thesis the ability of SA has been extended to deal with 3D data as well. Consequently, 3D seismic data is handled by SA as a 2D data. This data handling capability is uniquely associated to the spiral architecture approach.

Let us consider the address "34" in Fig. 2.13(a). Here the number of digits demonstrates the aggregate level, i.e., aggregate level 2 in our case. '3' represents the position within the second layer and '4' represents its position within the 3^{rd} first level aggregate. While saving data, the pixel addresses are saved in incremental order as 0,1,2,3,4,5,6,10,11,12,...,65,66,100,...,666. A 2D data can be represented by a single vector as shown in Fig. 2.13(a) and Fig. 2.13(b).

Similarly, a 3D data set can be represented by a 2D array using the spiral architecture as shown in Fig. 2.14(a) and Fig. 2.14(b). This addressing scheme is called spiral due to nature of consecutive addresses [28] (see Fig. 2.15).

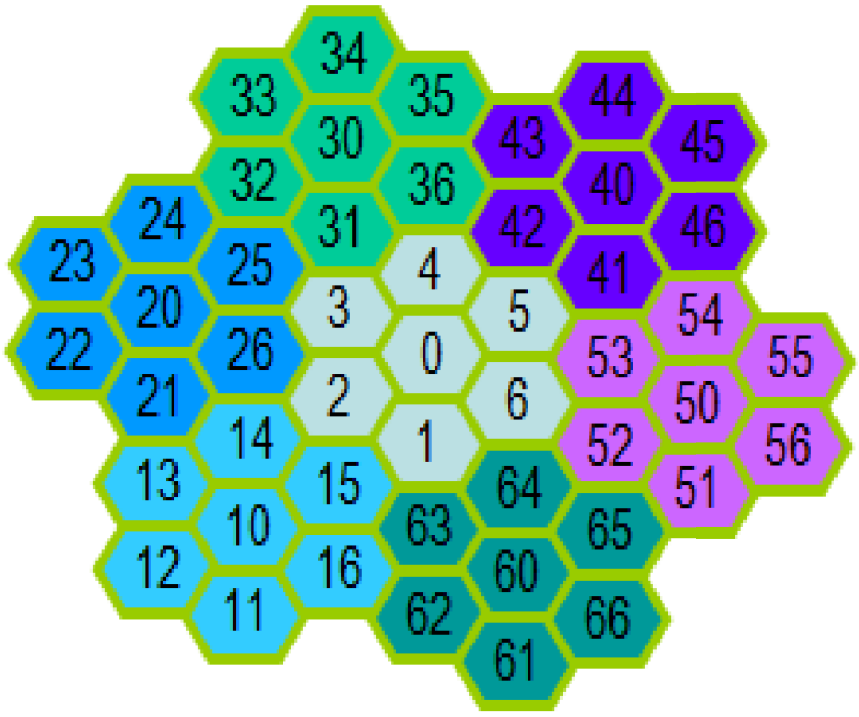

(a)

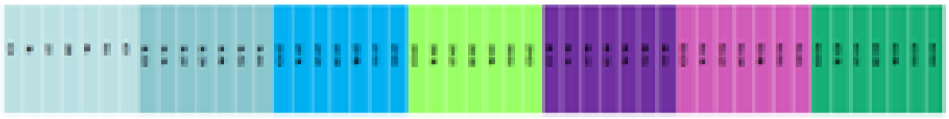

(b)

Figure 2.13: (a) Physical location of addresses in SA. (b) Data storage of two dimensional data in SA.

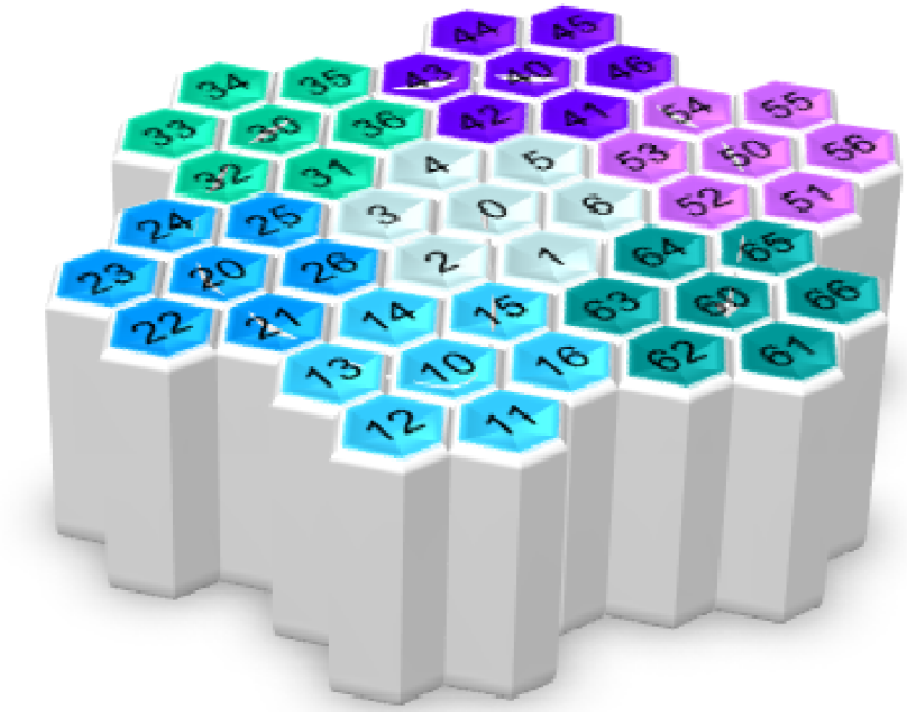

(a)

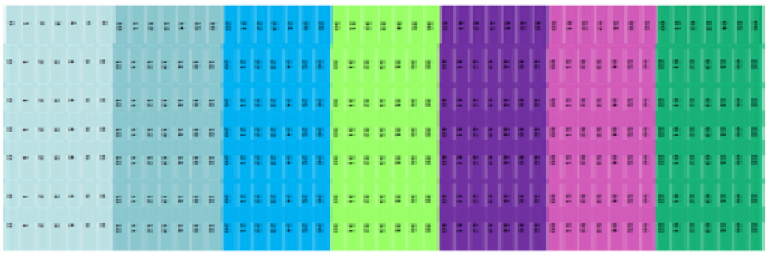

(b)

Figure 2.14: (a) Three dimensional data in SA. (b) Proposed data storage of three dimensional data.

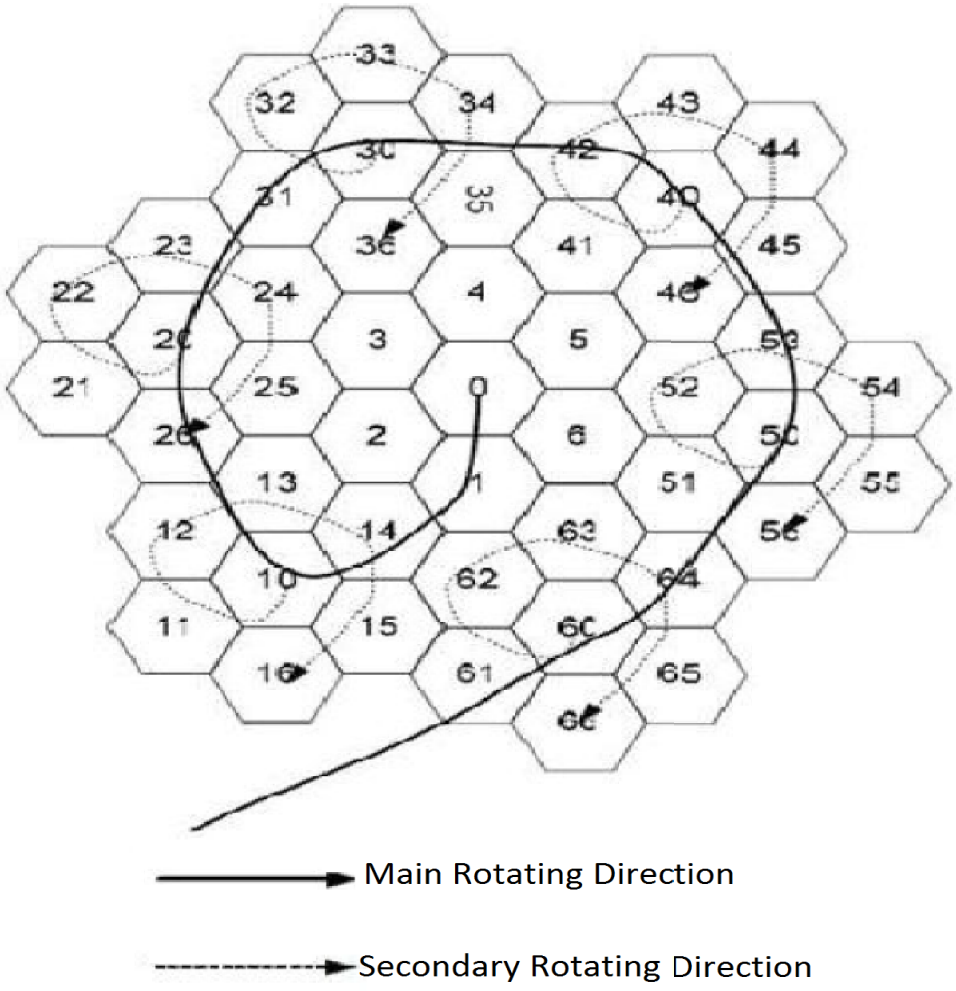

Figure 2.15: Spiral rotating direction. (Courtesy of [28]).

2.5.3 Spiral Arithmetic

The spiral architecture addressing scheme can be considered as a positional number system with base 7. The addresses indicate spatial location in the Euclidian plane with respect to the origin. Thus, each digit within an address gives angle and distance from origin. In this case, the addresses behave like vector quantities. The addresses are vectorial in nature. So the addresses that need to be added can be considered as vectors with one end at the origin and other at the corresponding address.

For example to display 15 in vector form, a line needs to be drawn from origin 0 to 15 as shown in Fig. 2.16. Similarly 26 has been shown. Since these two are vectors there addition is performed just like vector addition which results in 13 as shown in Fig. 2.16. In a similar manner subtraction is performed. The general rule for addition which is given as follows in Table 2.3.

Table 2.3: Spiral addition rule

+	**0**	**1**	**2**	**3**	**4**	**5**	**6**
0	0	1	2	3	4	5	6
1	1	63	15	2	0	6	64
2	2	15	14	26	3	0	1
3	3	2	26	25	31	4	0
4	4	0	3	31	36	42	5
5	5	6	0	4	42	41	53
6	6	64	1	0	5	53	52

Spiral multiplication can be defined in vectorial terms. The effect of multipli-

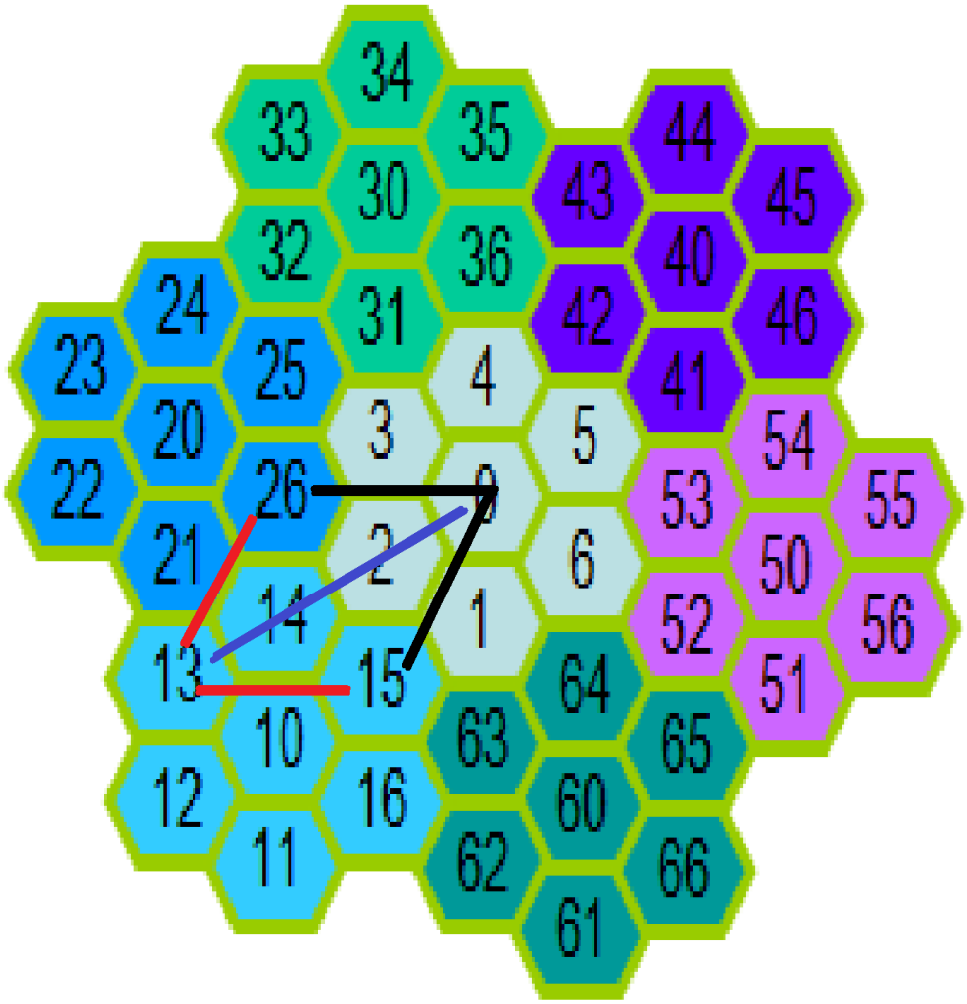

Figure 2.16: Spiral addition example.

cation is scaling and rotation. The following formula tells us about the effect of multiplication:

$$General\,Multiplication\,by\,n = Rotation\,by\,(n-1) \times 60\,degrees. \tag{2.14}$$

If we multiply, for example 14 by 2, the result will be rotation of 14 by $(2-1)\times 60$ degrees which is equal to 60 degrees rotation of 14. This results in 25 in this case which can be seen by observing the addresses 14 and 25 in Fig. 2.16. The general rule of multiplication can be seen from Table 2.3 .

Table 2.4: Spiral multiplication rule

x	**0**	**1**	**2**	**3**	**4**	**5**	**6**
0	0	0	0	0	0	0	0
1	0	1	2	3	4	5	6
2	0	2	3	4	5	6	1
3	0	3	4	5	6	1	2
4	0	4	5	6	1	2	3
5	0	5	6	1	2	3	4
6	0	6	1	2	3	4	5

The arithmetic operations can result in answers which may lie outside the aggregate level for example addition of 62 with 62 will result in an answer which will lie in aggregate three. In order to tackle this problem, we use closed arithmetic techniques. The general rules of closed arithmetic operations are given as follows:

$$Closed\,Addition\, = a + b\,mod\,[10^{\lambda}]. \tag{2.15}$$

$$Closed\,Subtraction\, = a - b\,mod\,[10^{\lambda}]. \tag{2.16}$$

$$Closed\,Multiplication\, a \times b = a \times b \, mod\, 10^{\lambda} \quad if\, b\, is\, not\, a\, multiple\, of\, 10. \quad (2.17)$$

$$Closed\,Multiplication\, a \times b = \left((a \times b) + \left(\frac{a \times b}{10^{\lambda}} \right) \right) mod\, [10^{\lambda}]. \quad (2.18)$$

An example of closed multiplication by 20 has been shown in Fig. 2.17. We can see in this, multiplication with 20 results in the re arrangement of all the pixels.

2.5.4 Spiral Neighborhood and Processing Operations

The hexagonal addressing scheme that has been devised covers an infinite space. Seismic signals and images are, however, finite space. Consequently, a limited number of layers need to be considered when dealing with hexagonal sampled data. Addresses in a λ-level 2D data belong to G^{λ}. However, operations may lead to addresses which lie outside the originally defined region. The first approach to deal with such scenario is to use closed arithmetic which has already been discussed. The second approach is to consider these addresses as boundary addresses. There are a total of 7^{λ} addresses for a λ-level 2D data. These addresses are numbered 0 to $7^{\lambda} - 1$. The addresses of external points start from 7^{λ} and extend to infinity.

In aggregate level 2 we have total 49 pixels with addresses ranging between 0 and 66 and stored like a vector 0,1,2,3,.48. $7^2 = 49$ thus the 49^{th} element in hexagonal addressing scheme i.e., 100 (base 7 address) is an external point . Any point greater than 100 is also an external point. It must be noted that external points extend to infinity.

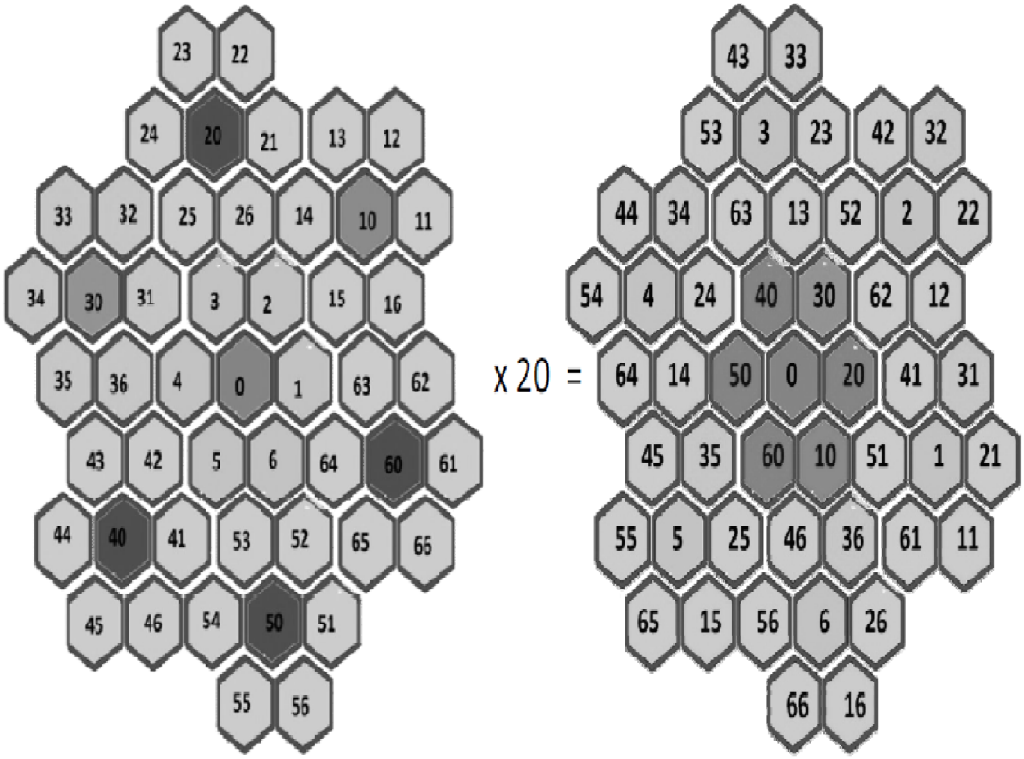

Figure 2.17: Spiral closed multiplication example.

The usage of addresses of external points to specify the data set boundary in not the most optimum approach. The addresses which have at least one out of six neighboring hexagonal addresses as external addresses are called boundary addresses. A boundary address will have at least one neighbor outside the layer level. A boundary address is itself a part of the λ-level image. The boundary addresses for aggregate level 2, i.e., 49 addresses are shown in Fig. 2.18. The white points are external points is Fig. 2.18.

A valid distance measure has the following properties:

- Positive definiteness

  $d\,(a\,,\,b) \geq 0$ Equality only if $a = b$.

- Symmetry

  $d\,(a\,,\,b) = d\,(b\,,\,a)$.

- Triangluar Inequality

  $d\,(a\,,\,b) \leq d\,(a\,,\,c) + d\,(c\,,\,b)$.

In spiral architecture, these properties of distance measures are valid because of the vectorial nature of hexagonally sampled SA addressing scheme. Generally distance measures are defined with respect to a set of axes. Since SA employs positional numbering system, it is difficult measure distance directly. Thus, distance

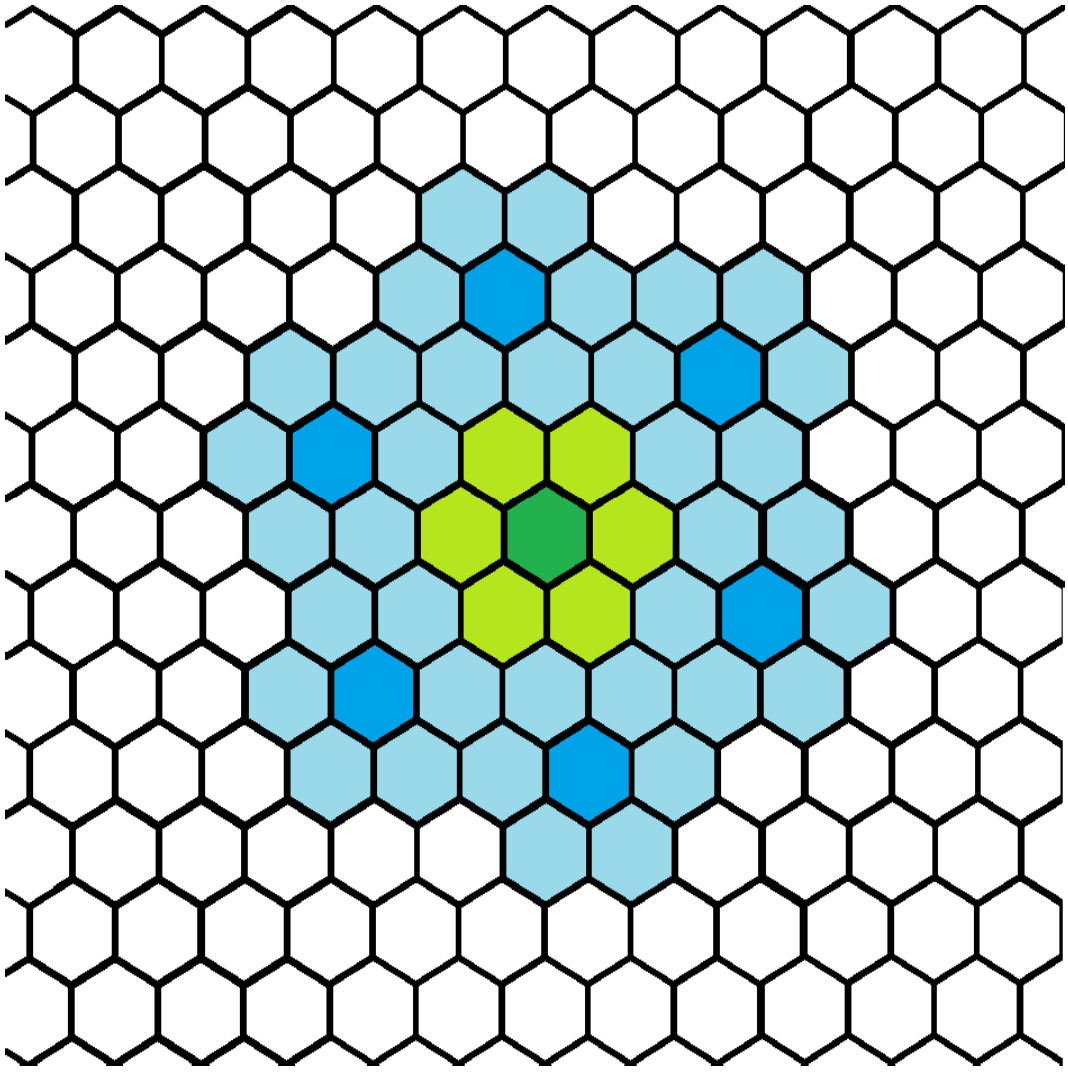

Figure 2.18: External points for aggregate level 2.

measures are calculated by employing different coordinate schemes. Using Hers 3 coordinate system the distance of a (a_1,a_2,a_3) and b(b_1,b_2, b_3) is given as:

$$d(a,b) = (\frac{1}{2}) \times (|a_1 - b_1| + |a_2 - b_2| + |a_3 - b_3|). \tag{2.19}$$

In Hers coordinate system there are 3 axes, each at 60 degrees to each other. A two axis approach can also be used to define distance measures. The Her's distance measures are shown in Fig. 2.19.

Neighborhood is one of the basic relationships which are used in many processing techniques. Neighbours have either a common edge or a corner. In SA framework, neighbors share common edges. In SA, an address contains 6 neighbors. This group of seven hexagonal tiles is the fundamental neighborhood that can be characterized as a first level aggregate. In the neighborhood shown for address 0 all the neighbors are equidistant from the address under consideration as shown in Fig. 2.20

This neighborhood can be defined as $N_1(x) = x, x+1, x+2, x+6$. The second level neighborhood can be derived by using the formula of the first level neighborhood. Thus, the second neighborhood is the first neighborhood N_1 along with the first neighborhoods of every address in the first neighborhood $N_2(x) = N_1(x)UN_1(x+1)UN_1(x+2), UN_1(x+6)$. Thus the neighborhood of any distance level can be recursively found using:

$$N_n(x) = N_{n-1}(x)UN_{n-1}(x+1)UN_{n-1}(x+2), UN_{n-1}(x+6). \tag{2.20}$$

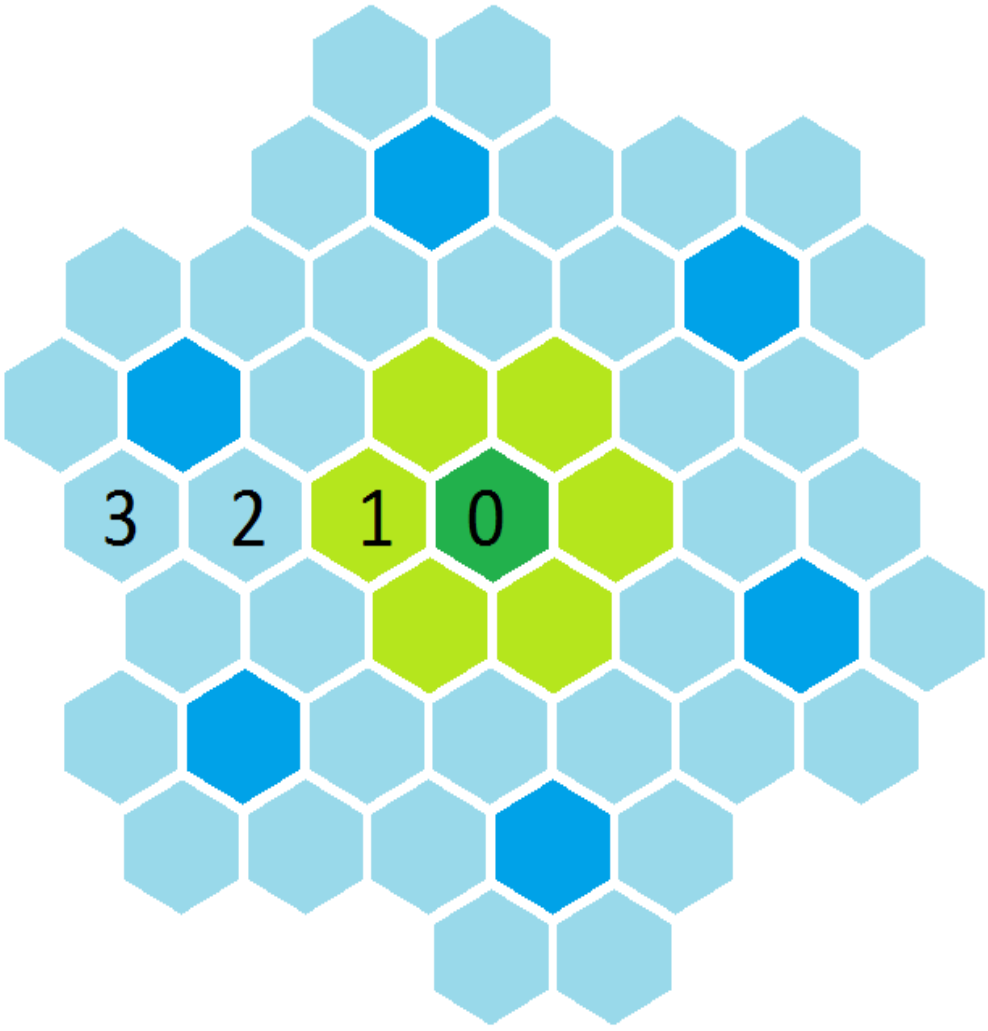

Figure 2.19: Her's Distances.

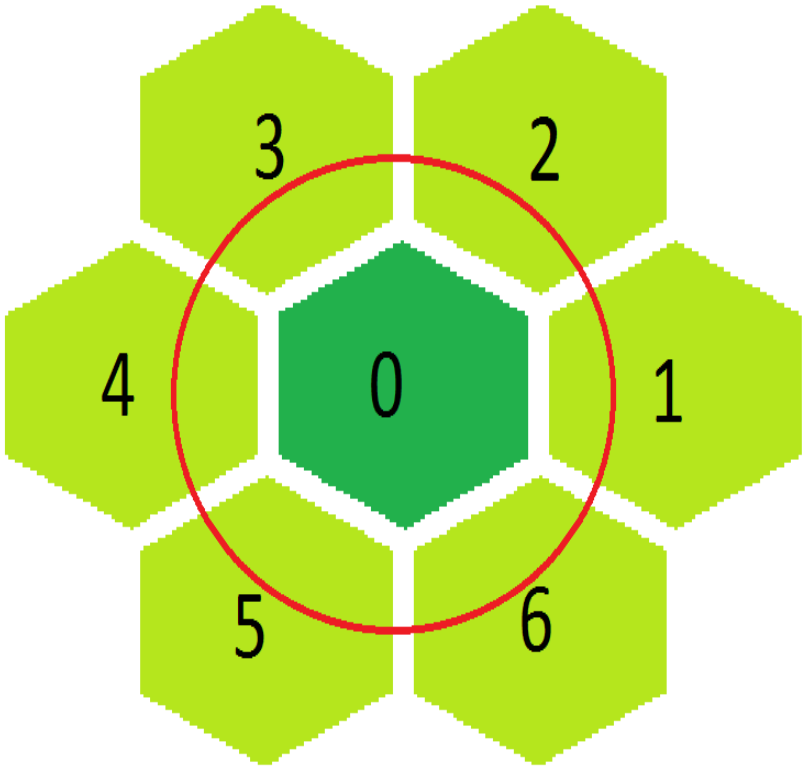

Figure 2.20: Address 0's six equidistant neighbors.

If x is taken 0 the second neighborhood gives the following points:

$$N_2(0) = 0, 1, 2, 3, 4, 5, 6, 14, 15, 25, 26, 36, 31, 41, 42, 52, 53, 63, 64, \tag{2.21}$$

N_2 contains 19 elements:

- Original address.
- 6 immediate neighbors.
- Another 12 neighbors which are the unique neighbors of the original N_1 neighborhood.

The number of elements, cardinality, in this definition of neighborhood can be generally given as follows:

$$card(N_n) = 3n^2 + 3n + 1, \tag{2.22}$$

We also can define the neighborhood using aggregate levels. The first level neighborhood is similar to previous definition. The second level can be defined as follows:

$$N_2^h = N_1^h(x)\, U\, N_1^h(x+10)\, U\, N_1^h(x+20)\, U\, ...N_1^h(x+60), \tag{2.23}$$

Thus, a general definition of this neighborhood can be given as follows

$$N_n^h = N_{n-1}^h(x)\, U\, N_{n-1}^h(x{+}10)\, U\, N_{n-1}^h(x{+}2{\times}10^{n-1}\, U\, ...N_{n-1}^h(x{+}6{\times}10^{n-1}), \tag{2.24}$$

Convolution is extensively employed in signal processing. Convolution is a neighborhood process where the value of a location/address is replaced by the weighted sum of values in its neighborhood. The addresses of neighboring elements can be easily calculated by employing the neighborhood definitions explained earlier. Convolution of a 2D data I with a λ-level mask can be given by Eq. 2.25.

$$M(x) * I(x) = \sum M(k) \times I(x - k) \tag{2.25}$$

In equation 2.25 * denotes convolution and negative sign represents spiral architecture's subtraction. It is noteworthy that Eq. 2.25 employs utilizes single summation. Thus from a computational point of view, a 2D data convolution employs one loop only. This is due to the two dimensional data being represented as a one dimension array. This implies that the computation of convolution of an entire 3D data with a 3D mask requires only a couple of loops. On the other hand the convolution on rectangular sampled data requires four loops i.e., double than the spiral convolution scheme.

2.5.5 Frequency Domain Processing

Hexagonal sampled data is periodic with a periodicity matrix. The images are periodic in an image of order one higher than the original image. For a given hexagonal sampled image x of order λ:

$$x(n) = x(n + N_\lambda r). \tag{2.26}$$

In the Eq. (2.26), n and r are integer vectors. The number of sample points in a period is equal to det $[N_\lambda]$ which is 7, where

- the set of points in the spatial domain samples be I_{N_λ}, or
- the set of points in the spectral domain samples be J_{N_λ}.

The sequence $x(n)$ can be expanded as a Fourier series with coefficients denoted as $X(k)$, where:

$$X(k) = \sum_{n \epsilon G^\lambda} x(n)\, exp\left(-2\pi j k^T N_\lambda^{-1} n\right), \tag{2.27}$$

$$x(n) = \frac{1}{|det N_\lambda|} \sum_{k \epsilon G^\lambda} X(k)\, exp\left(2\pi j k^T N_\lambda^{-1} n\right). \tag{2.28}$$

Eq. (2.27) and Eq. (2.28) are the famous discrete Fourier transform pair. The fast Fourier transform (FFT) equations have also been derived for SA [15]. It is beyond the scope of this thesis to give the detailed explanation of the FFT equations.

2.6 MATLAB Toolbox

A MATLAB toolbox has been developed for the purpose of processing of 2D and 3D hexagonally sampled data. There is no open source toolbox available to deal with hexagonally sampled data using SA. For the first time, we have successfully implemented 3D SA processing. The toolbox is capable of performing resampling from rectangular domain to hexagonal domain (see resampling details in Appendix). The toolbox can handle signal processing operations on spatial and

spectral domains. This toolbox has been used to prove that hexagonal approach is an efficient alternative to the rectangular approach used for seismic signal processing field. Some of the results of this toolbox have been shown in this appendix.

2.7 Summary

In this chapter, the fundamentals of hexagonal signal processing have been explained. The regular tiling problem and various hexagonal approaches have also been discussed. Circularly band-limited signals like seismic signal can be optimally sampled using the hexagonal approach. The SA is an excellent method to deal with hexagonally sampled data. The SA approach not only yields the benefits of hexagonal sampling but also assists in dealing with 2D-data as a 1D-problem. Similarly for higher dimensions, when we extended the concept to 3D datasets, SA was able to process it as a 2D-problem. This ability of SA makes it ideal for seismic signal processing where the size of data is increasing exponentially and consequently the problems associated with huge data sets are also arising. Since, no open source SA-based-toolbox is available, it was necessary to develop our own toolbox.

CHAPTER 3

3D FILTER DESIGN FOR HEXAGONALLY SAMPLED DATA USING SPIRAL ARCHITECTURE FOR SEISMIC DATA ACQUISITION

3.1 Introduction

This chapter discusses the design of a 3D filter for a hexagonal grid that is used in this digital group forming step at the acquisition stage. The chapter will briefly explain the process of seismic acquisition and the relevance of hexagonal sampling to the seismic signal acquisition will be presented. Afterwards, the concept of

digital group forming (DGF) and the application of alternate methods of hexagonal signal processing for DGF will be explained. Finally, the application of SA for hexagonal DGF will be proposed and 3D seismic DGF finite impulse response (FIR) filters will be presented.

3.2 Seismic Acquisition

The process of seismic data acquisition can be understood with the help of the procedure shown in Fig. 3.1.

The fundamental elements are a source and a receiver. The source generates a signal that propagates through various layers and gets reflected back and recorded via receivers. This signal is recorded in the recording unit. The resolution of the seismic data is directly proportional to the number of receivers. By increasing the number of receivers, the resolution can be increased [3]. Greater resolution of the seismic data corresponds to higher successful exploration.

With an increase in the computational power, the oil and gas industry demanded higher resolution of seismic data [3]. An exponential increase (see Fig. 3.2) in the number of recording channels over the last four decades has been witnessed [3].

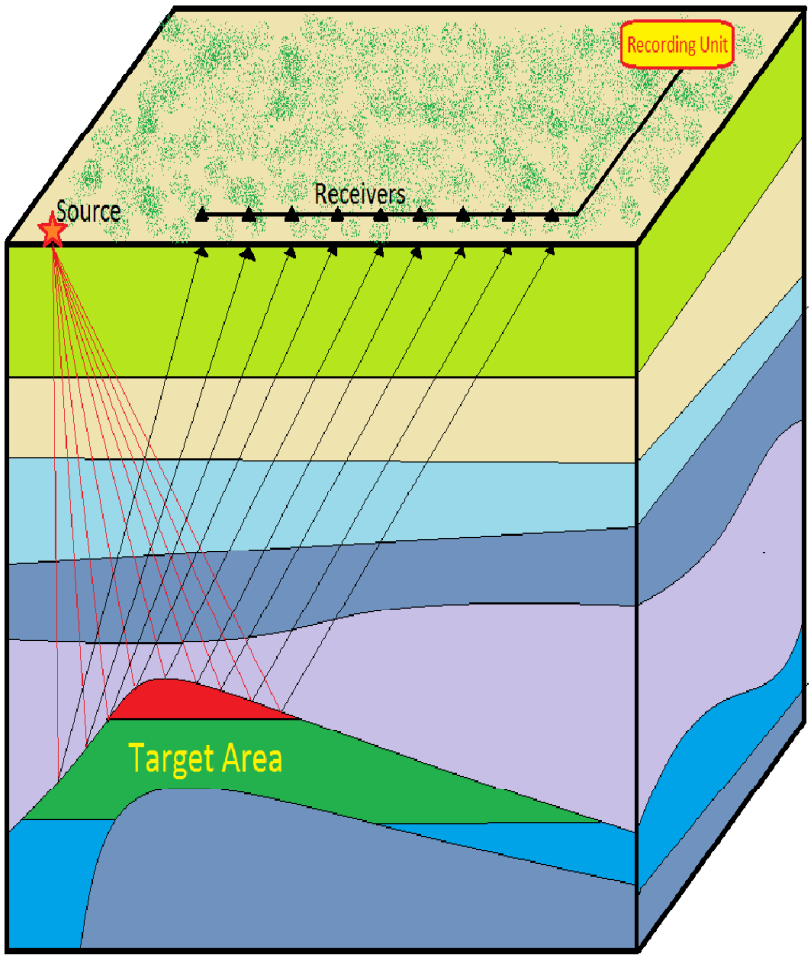

Figure 3.1: Seismic acquisition process.

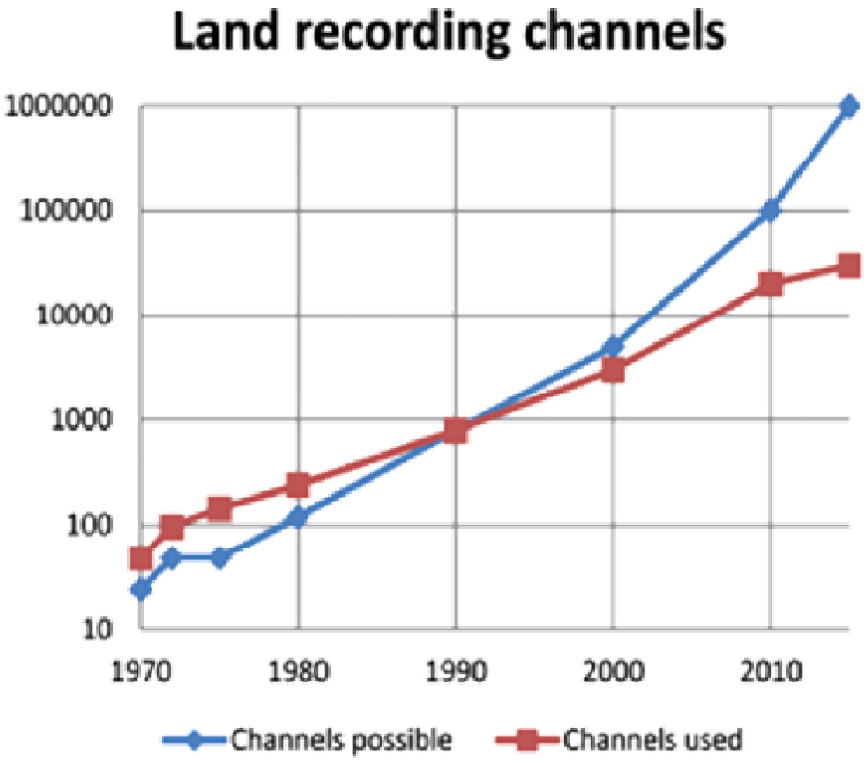

Figure 3.2: History of recording channels. (Courtesy of [3]).

The blue curve represents the number of channels that were available on majority of recording systems. The red curve depicts the number of channels that were being used. For many years when the red curve was above the blue curve, the industry was using more than one system in a master/ slave configuration [3].

3.2.1 Relevance of Spiral Architecture to Seismic Signals

The exponential increase in seismic data makes it necessary to go for an efficient approach. It is required by the sampling theorem to determine the minimum number of samples required in a lossless manner. The band region of 3D seismic data can be approximated by a region bounded by two cones as shown in Fig. 2.6. This signal is circularly band-limited in the k_y and k_x domains. Hence, hexagonally sampled seismic acquisition data is an ideal alternative to the regular approach as shown in Fig. 3.3 [8] [13]. It can be seen from Fig. 2.7, that a hexagon is most suitable for approximation of this seismic signal.

The hexagonal approach provides savings in processing time and data storage of seismic data. This is because the hexagonal sampling grid utilizes 13.4% lesser samples in comparison to the rectangular approach to represent a signal with the same level of accuracy [13]. Furthermore, the spiral architecture, offers advantages in data handling, as has been discussed in the previous chapter. As such, SA is the ideal choice for 3D seismic signal processing.

3.3 Digital Group Forming (DGF)

Digital group forming or the recording of seismic exploration data through point receivers instead of analogue receiver arrays has various advantages [9] [29]. The advantages include noise attenuation, bandwidth retention, velocity estimation and better statics solutions [9]. The output of an analogue array is achieved by averaging all the inputs. The shape of this array is approximately rectangular. Consequently the wavenumber response of this array is a wavenumber-independent 2D sinc function in the k_x-k_y domains. For seismic data, wavenumber/frequency-independent filters are not suitable to separate noise and signal because the ground-roll modes contain finite apparent velocity. The low frequency components of the ground roll may be passed, while the desired high frequency components of dipping seismic events may get attenuated. Consequently, optimal 3D digital filters need to be designed in order to explore the potential of DGF. This can be seen from the Fig. 3.4. In case of conventional approach, a lot of undesirable side lobes are present.

It is necessary to develop specific techniques to design 3D filters when dealing with hexagonal sampling. The objective is to compare the hexagonal SA 3D filter design using projections on convex sets(POCS) with the state of art hexagonal 3D filter with POCS but with the zero insertion method represented in [9]. In this research work, in order to design optimal 3D finite impulse response filters for DGF using the spiral architecture approach, a technique based on alternating projections onto convex sets (POCS) has been utilized.

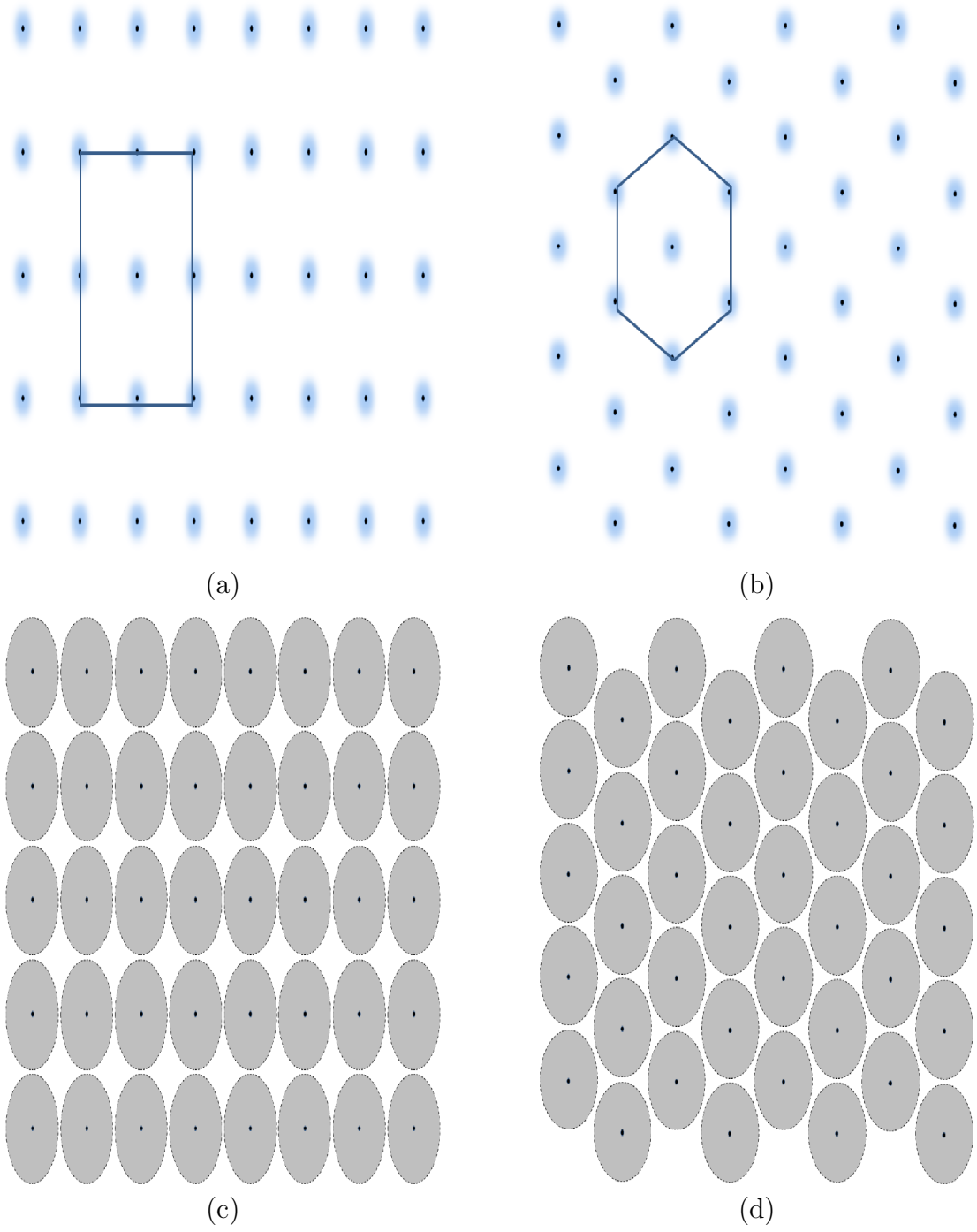

Figure 3.3: (a)Rectangular grid. (b) Hexagonal grid. (c) Spectral support of a rectangularly sampled signal. (d) Spectral support of a hexagonally sampled signal.

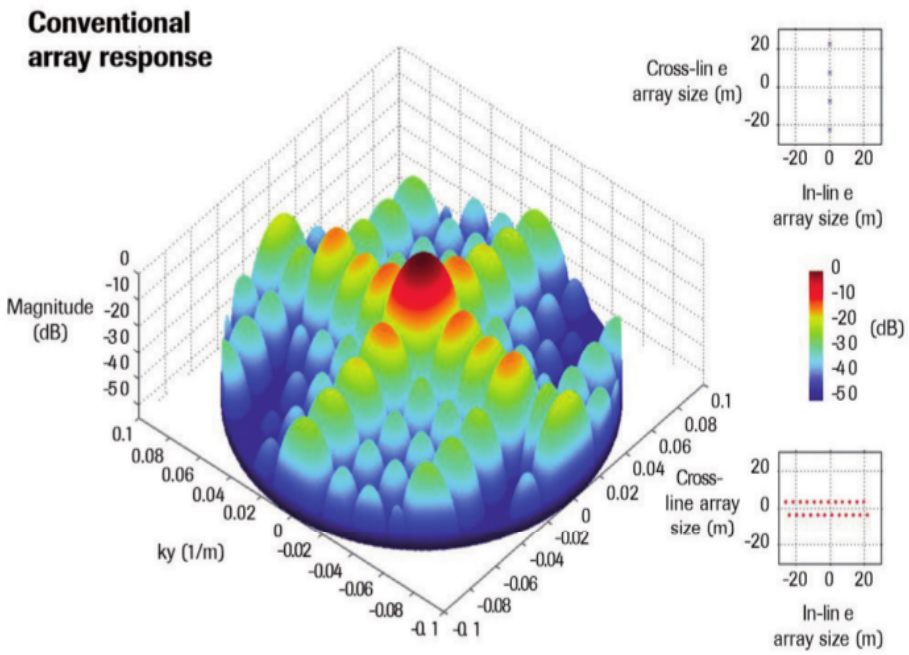

(a)

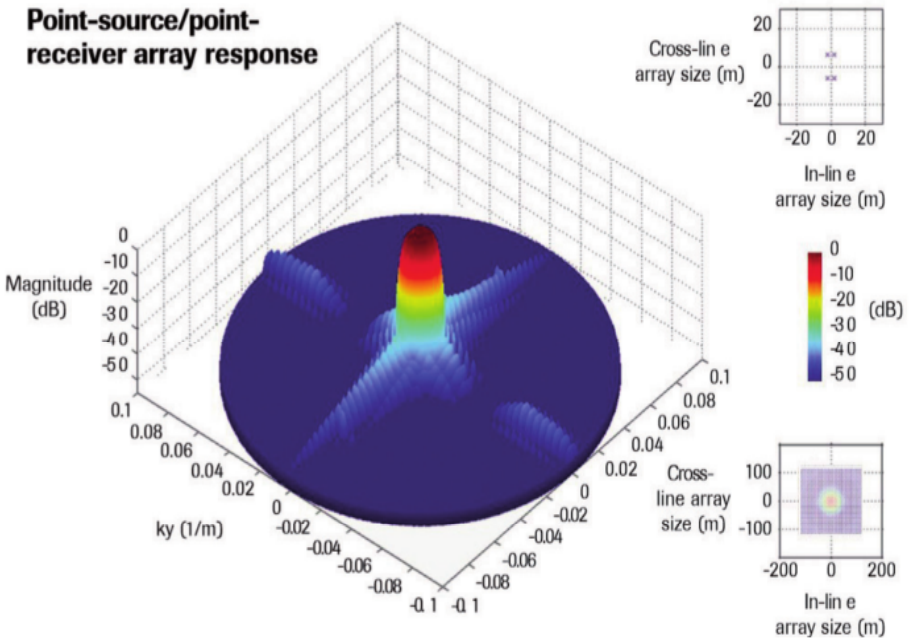

(b)

Figure 3.4: $k_x k_y$ Response plots. (a) Conventional source/receiver arrays . (b) Point-source/point-receiver digital spatial antialias filter (Courtesy of [29]).

3.3.1 Filter Design using POCS

There are several constrained optimization problems where the constraints are specified on different domains. These domains can be spatial or spectral. It is not always possible to apply these constraints to only one domain. If the constraints define convex sets in the set of square summable sequences, then applying alternating orthogonal projections onto these would converge to a feasible solution [9] [30]. This is known as projections onto convex sets. This method has been used to design zero-phase 3D FIR filters for the application of seismic DGF [31]. In this method, the filter design problem is formulated to alternatively fulfill time domain constraints on the impulse response support and frequency domain constraints on the magnitude response bounds.

In order to utilize POCS to design a 3D filter, it is required that the filter must be zero phase and its frequency response in the $f - k_x - k_y$ domain, $H(f, k_x, k_y)$ must be within tolerance ranges given by the following equation:

$$H_{id}\left(f, k_x, k_y\right) - E_d\left(f, k_x, k_y\right) \leq H_{id}\left(f, k_x, k_y\right) \leq H_{id}\left(f, k_x, k_y\right) + E_d\left(f, k_x, k_y\right) \tag{3.1}$$

In this equation, $H_{id}\left(f, k_x, k_y\right)$ is the ideal filter response, $E_d\left(f, k_x, k_y\right)$ is the desired maximum ripple level.

The ideal response and tolerance is given by Eq. (3.2) and Eq. (3.3) respectively. In the following equations, F_P and F_S represent the passband and stopband, σ_P and σ_S represent the tolerances.

$$H_{id}\left(f,k_x,k_y\right)=\begin{cases}1\ ,\ \text{if}\ \left(f,k_x,k_y\right)\ \epsilon F_P\\ 0\ ,\ \text{if}\ \left(f,k_x,k_y\right)\ \epsilon F_S\end{cases} \tag{3.2}$$

$$E_d\left(f,k_x,k_y\right)=\begin{cases}\sigma_P\ ,\ \text{if}\ \left(f,k_x,k_y\right)\epsilon F_P\\ \sigma_S\ ,\ \text{if}\ \left(f,k_x,k_y\right)\epsilon F_S\end{cases} \tag{3.3}$$

The filter must have a finite-extent support,I, in the t-x-y domain. In order to have a zero phase response requirement as mentioned earlier, I is a symmetric region around the origin. It is required by the time-domain space constraint that the values of filter coefficients must not be non zero outside the region I. We use the inverse Fourier transform of the ideal frequency response given by:

$$h_{id}=F^{-1}\left\{H_{id}\left(f,k_x,k_y\right)\right\} \tag{3.4}$$

The initial estimate is given as :

$$h_0\left(t,x,y\right)=\begin{cases}h_{id}\left(t,x,y\right)\ \ \text{if}\ \ \left(t,x,y\right)\epsilon I\\ \qquad 0\qquad \text{otherwise}\end{cases} \tag{3.5}$$

At each iteration of the algorithm, the frequency/wavenumber and time/space constraints are successively applied onto the current iterate.

The n^{th} iteration consists of the following steps:

- Compute the 3D Fourier transform $H_n(f, k_x, k_y)$ of the n^{th} iterate $h_n(t, x, y)$
- Apply the frequency/wavenumber domain constraints as given by:

$$G_n(f, k_x, k_y) = \begin{cases} H_{id}(f, k_x, k_y) + E_d(f, k_x, k_y), \\ \text{if } H_n(f, k_x, k_y) > H_{id}(f, k_x, k_y) + E_d(f, k_x, k_y), \\ H_{id}(f, k_x, k_y) - E_d(f, k_x, k_y), \\ \text{if } H_n(f, k_x, k_y) < H_{id}(f, k_x, k_y) - E_d(f, k_x, k_y), \\ H_n(f, k_x, k_y), \text{otherwise} \end{cases} \tag{3.6}$$

- Obtain the 3D inverse Fourier transform $g_n(t, x, y)$ of $G_n(f, k_x, k_y)$.
- As per the time-domain constraints, the values of $g_n(t, x, y)$ outside the region I need to be zeroed, to obtain $h_{n+1}(t, x, y)$ as given by:

$$h_{n+1}(t, x, y) = \begin{cases} g_n(t, x, y) \text{ if } (t, x, y) \epsilon I \\ 0, \quad \text{otherwise} \end{cases} \tag{3.7}$$

- Calculate the mean-squared error between the iterates $h_n(t, x, y)$ and $h_{n+1}(t, x, y)$. If this error is greater than a predefined threshold, then repeat the steps otherwise exit.

The flow diagram of the 3D POCS filter design algorithm can be seen in Fig. 3.5.

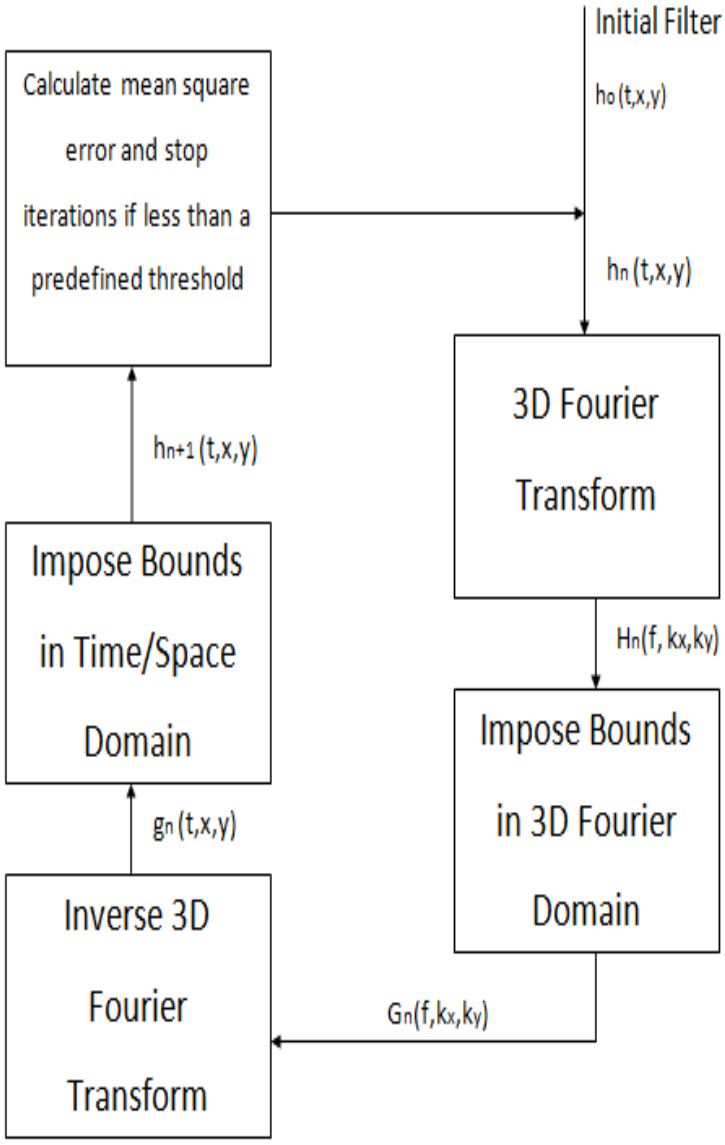

Figure 3.5: Flowchart of three dimensional FIR filter design algorithm using POCS.

It can be proven that the POCS approach is globally convergent under specific conditions. If the constraints in the spatial and frequency domains define convex sets in the set of square summable sequences, then the application of the constraints are the orthogonal projections onto these sets. Furthermore, if the sets are intersecting, the iterates converge to a member in the intersection set [9]. It must be noted that empirical results generated in [9] show that filters designed using POCS converge to equiriplle filters.

3.3.2 POCS for Hexagonally Sampled Seismic Data

The POCS algorithm has been applied to hexagonally grid by the insertion of zeros approach [9]. Unfortunately, this approach has a major problem; the insertion of zeros causes aliasing. The application of pure hexagonal approach, i.e., spiral architecture results in efficiently handling the data.

In order for SA to be applied instead of rectangular Fourier transform, hexagonal Fourier transform is used for the POCS algorithm. The hexagonal Fourier transform and its inverse is based on the SA arithmetic discussed in chapter 2. The use of pure hexagonal approach results in a filter design which avoids aliasing. (See chapter 2 for more detailed information regarding hexagonal sampling.)

3.3.3 Simulation Results

Consider the ideal FIR filter shown in Fig. 3.6. The features of the designed filter includes a slope of 3, passband F_P of 10 and the tolerance E_d as 0.02. These values are same as have been used previously for hexagonal grid using zero insertion approach. The size of filter is 5x5x6. The filter design using the rectangular approach is shown in Fig. 3.7. The filter design using the zero insertion approach for hexagonal sampled data is shown in Fig. 3.8. The filter design using the spiral architecture approach is shown in Fig. 3.9.

It is evident from the simulation results that spiral architecture approach is better as compared to the zero insertion approach. The zero insertion approach to hexagonal sampling introduces aliasing. This can be seen from Fig. 3.10. In case of zero insertion we can observe aliasing by the dark regions where aliasing is taking place. On the other hand, the SA hexagonal approach, is free from aliasing.

The computational power of SA for 3D data is an added feature of SA which is very important when dealing with huge amounts of seismic data. The added power is based on the lesser samples required. Another reason for decreased computational requirement for seismic signal processing is because of SA's unique data handling capability causing a reduction in number of loops.

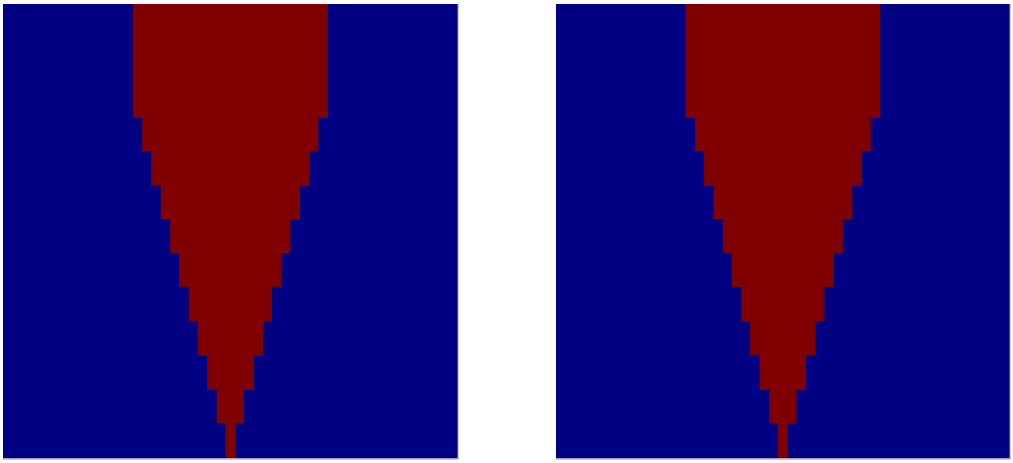

(a) (b)

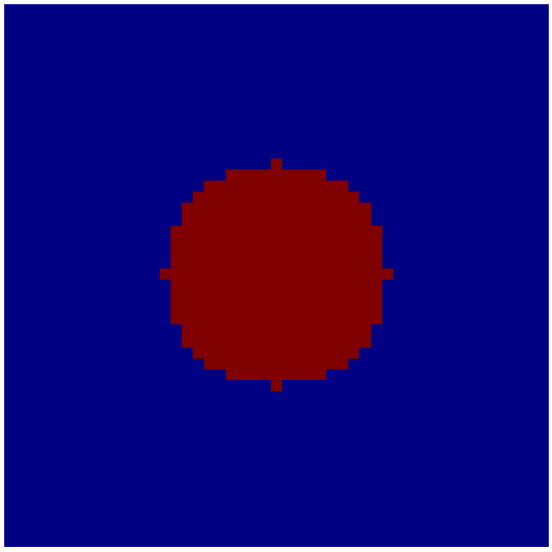

(c)

Figure 3.6: Ideal 3D rectangular filter in $f-k_x-k_y$ domain with passband F_P of 10, tolerance E_d as 0.02 and slope as 3. (a) The response slice for k_x=0. (b) The response slice for k_y=0. (c) The response slice for f=40 Hz.

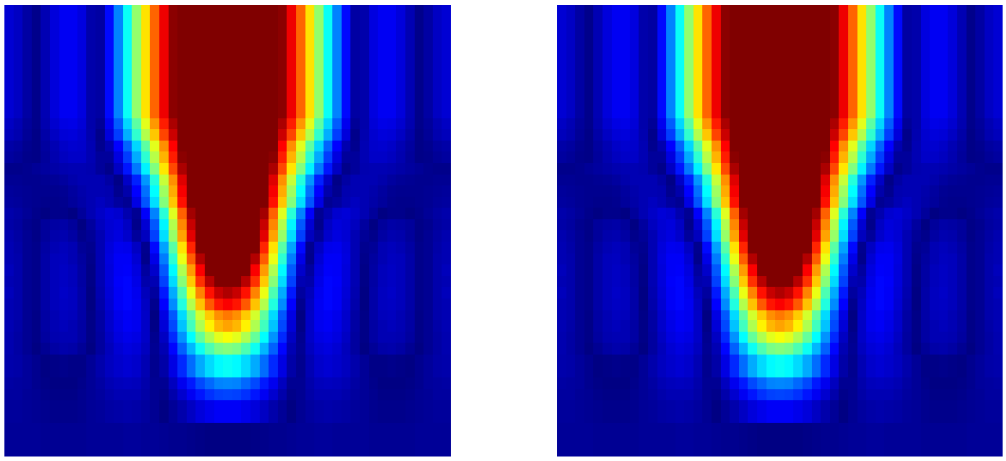

(a) (b)

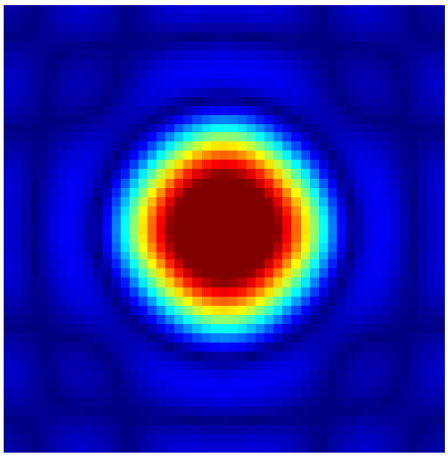

(c)

Figure 3.7: Rectangular 3D filter in $f - k_x - k_y$ domain with E_d as 0.02 and slope as 3. (a) The response slice for k_x=0. (b) The response slice for k_y=0. (c) The response slice for f=40 Hz.

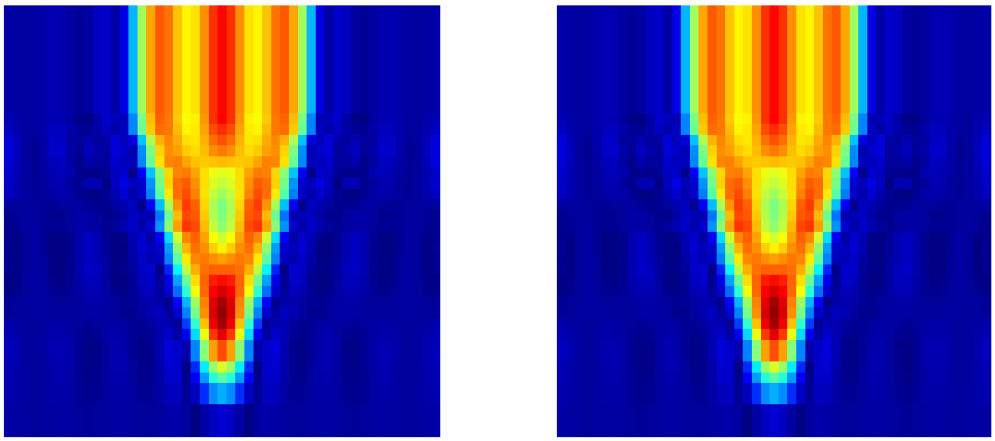

(a) (b)

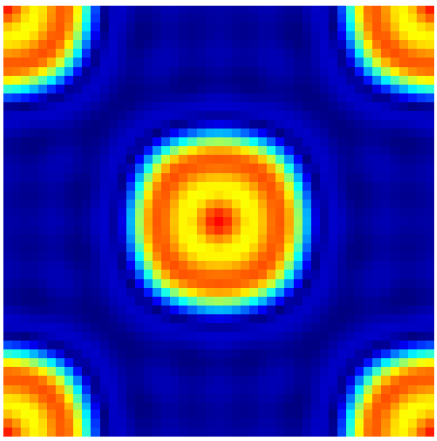

(c)

Figure 3.8: Zero insertion hexagonal 3D filter in $f - k_x - k_y$ domain with passband F_P of 10, tolerance E_d as 0.02 and slope as 3. (a) The response slice for k_x=0. (b) The response slice for k_y=0. (c) The response slice for f=40 Hz.

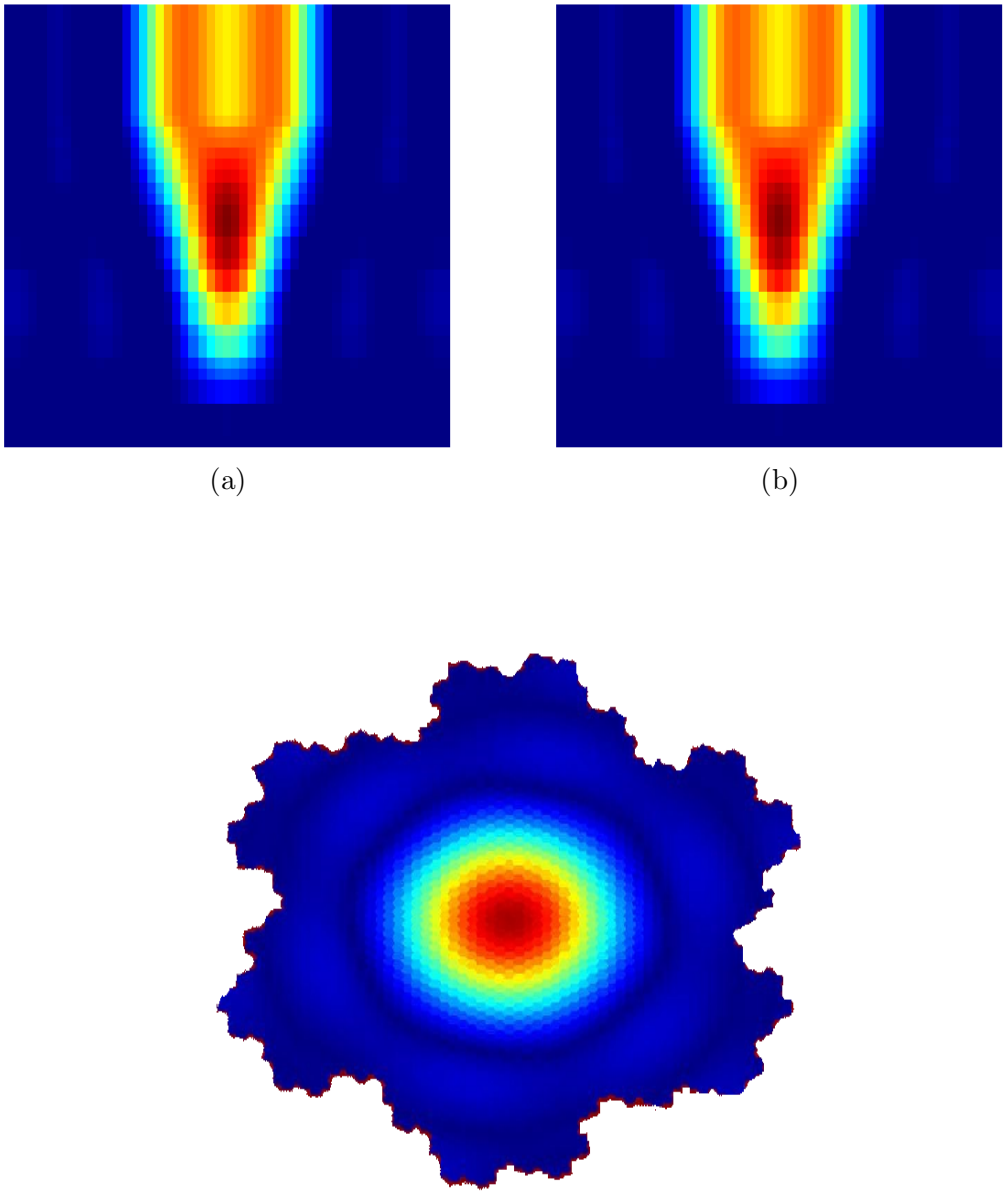

Figure 3.9: SA Hexagonal 3D filter in $f - k_x - k_y$ domain with passband F_P of 10, tolerance E_d as 0.02 and slope as 3. (a) The response slice for k_x=0. (b) The response slice for k_y=0. (c) The response slice for f=40 Hz.

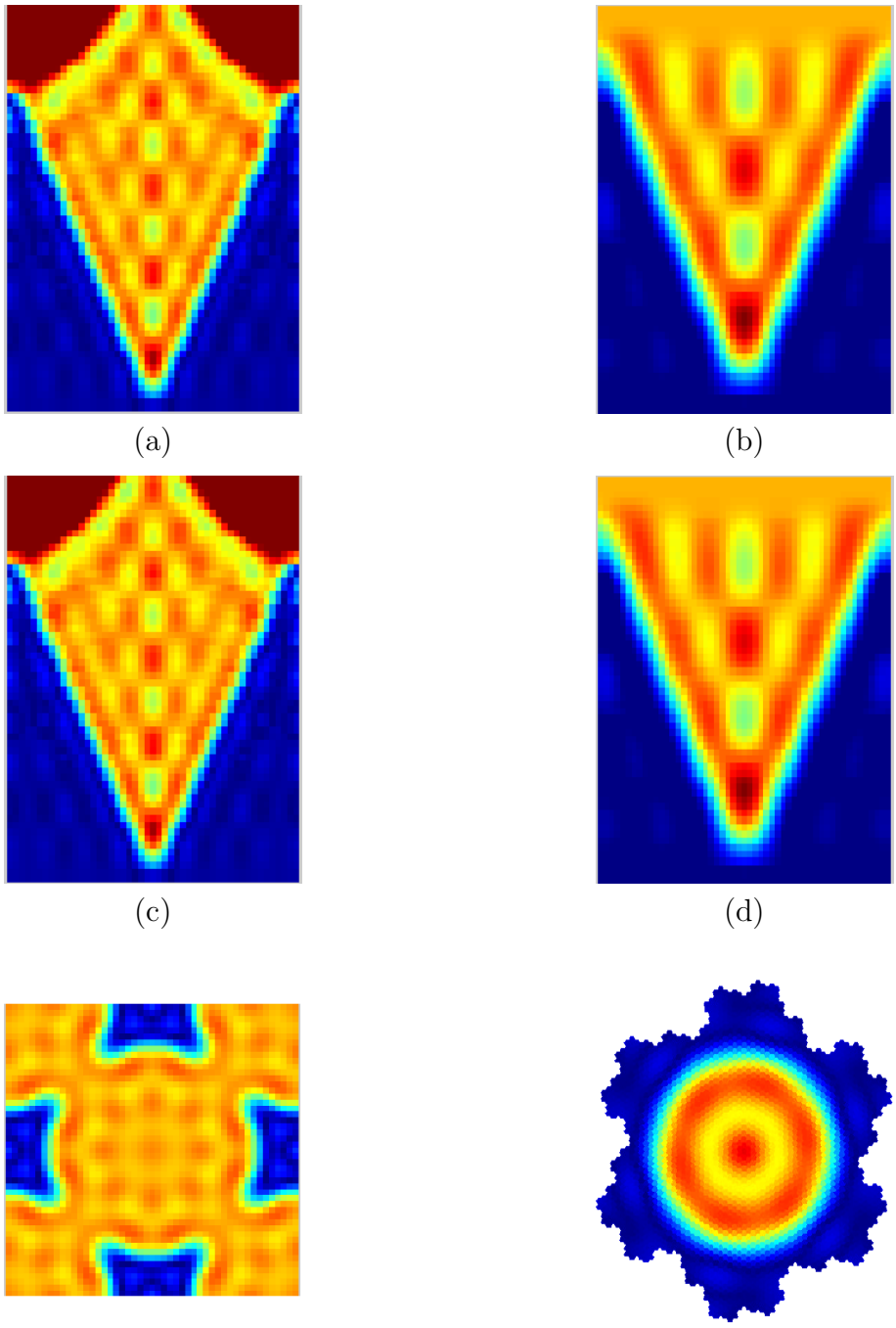

Figure 3.10: Comparison of aliasing in hexagonal approach with passband F_P of 20, tolerance E_d as 0.02 and slope of 2. (a) The response slice for k_x=0 in zero insertion approach. (c) The response slice for k_y=0 in zero insertion approach. (e) The response slice for f=34 Hz in zero insertion approach. (b) The response slice for k_x=0 in SA approach. (d) The response slice for k_y=0 in SA approach. (f) The response slice for f=34 Hz in SA approach.

3.4 Conclusion

The increase in seismic exploration data and relevance of hexagonal approach to this increasing data is important to consider. The advantage of point receiver technology/ digital group forming over conventional analog acquisition systems is of no question. The usage of hexagonal SA approach has proved to be efficient as compared to the zero insertion approach. The zero insertion approach increases the data samples by 100% owing to the extra zeros. On the other hand, hexagonal case using the spiral architecture reduces the required number of samples by 13.4% as compared to the rectangular approach.

Since previous attempts to this problem were not hexagonal in true sense, the attempts introduced certain problems. The zero insertion approach not only leads to increased data size and consequently increased processing time, but also results in aliasing. The attempt to employ SA for hexagonally sampled seismic data has successfully reduced the number of samples while simultaneously avoiding aliasing.

CHAPTER 4

EFFICIENT EDGE DETECTION ATTRIBUTES OF HEXAGONALLY SAMPLED 3D SEISMIC DATA

4.1 Introduction

The automatic detection of geological features such as faults and channels is a challenging problem in today's industry. Edge detection filters are generally applied for the purpose of locating features. Till now, edge detection has been carried out on rectangularly sampled seismic data. In this chapter, for the first time an attempt has been made to detect edges in hexagonally sampled seismic data. As discussed before, hexagonal approach is an efficient method of sampling

with greater symmetry as compared to the rectangular approach. In this chapter a comparison of edge detection on both rectangular and hexagonally sampled seismic data is carried out. The data used was provided by Saudi Aramco. It is shown that hexagonal processing results in well defined edges with fewer computations, while simultaneously improving the quality of the results.

4.2 Seismic Interpretation

Seismic interpretation is greatly dependent on data visualization. The interpreter has to select and highlight the main features [32]. Delicate geological features often appear as sharp edges and are not so easily detected. These features such as channels and faults are located with the application of edge detection algorithms [32], [33], [34]. The detection of these geological features is imperative for seismic interpretation. In order to understand the geological system, the location of faults is important. A precise knowledge of the features results in an accurate modeling. Consequently, a well defined planning of drilling targets is achieved [34].

Convolution kernels can be used to process seismic data. Most of the current image processing tools are two-dimensional (2D). In applications where the correlation of depth/time is irrelevant, 2D kernels can be employed. However, for scenarios which are correlated vertically, three dimensional (3D) kernels must be considered [32].

The Sobel filter is a famous edge detecting filter. It has been widely used in the field of computer vision and image processing. It has also been employed for medical imaging and processing of astronomical data [35]. Sobel attribute has been employed on seismic data by many researchers [34], [36], [37]. The Sobel attribute has been applied in several combinations such as separable/non-separable, 2D/3D and with various operator size. So far Sobel filter has not been applied on hexagonally sampled seismic data.

Spiral architecture was introduced for machine vision as handling structure of hexagonally sampled signals. The data sample is of a hexagonal shape in SA. Application of SA on image processing has been performed several times but no work has been carried out for the application of SA on seismic data which will not only reduce the number of samples required for the same resolution but will also assist in treating with a 3D problem as a 2D problem. Only 2D Sobel filters have been designed for the SA [38].For the first time, in this work, 3D edged detection Sobel filters for SA have been derived and applied on seismic data.

4.3 Hexagonal Sampling for Seismic Interpretation

With rectangular sampling, a band-limited function of two independent variables is sampled at evenly spaced values of each of those variables [12]. It has been the

method of choice for virtually all signal processing applications for a variety of reasons as have been mentioned earlier:

- Algorithms for processing signals which have been rectangularly sampled can be easily generalized from the 1D case.
- The resulting expressions can be readily understood and implemented in software.
- Hardware to perform the sampling (scanning) is straightforward to build.

In fact, both researchers and industry have become so comfortable with rectangularly sampled arrays that the alternatives are rarely considered [11]. The fundamental advantage of hexagonal sampling lattice is its great strength:

- A regular hexagon is 50 percent more symmetric than a square.
- Hexagon exhibits a 12 fold as opposed to 8 fold symmetry

It is evident that a hexagon has more symmetry than a square. Refer to chapter 2 for more details.

The increased symmetry of a hexagon forms the basis of the efficiency of hexagonal sampling technique [11], [14], [15]. Each sample location in a rectangular raster has four nearest neighbors (horizontal and vertical) and four diagonal neighbors, which are located at a greater distance. Each sample location in a hexagonal raster, however, has six nearest neighbors, each of which is the same distance away [15]. This can be a convenience for certain image processing problems involving edge detection, cluster separation, boundary tracing, etc. Thus, the application

of hexagonal sampling to seismic data can help in not only increasing the processing speed owing to 13.4% less data but also the quality of results obtained even at the interpretation stage are better defined because of greater neighborhood connectivity of a hexagon.

4.4 Edge Detection

Research in hexagonal sampled images has increased in the recent past, mainly, due to the inherent property of the hexagonal pixels to represent curvatures in a better manner than the typical case of rectangularly sampled images [39]. Another advantage of hexagonal sampling is the equidistant nature of all immediate neighbors of a hexagonal sample [19]. This symmetric nature of neighborhood, which is nonexistent in rectangular case, is helpful in the application of circular symmetric kernels. These kernels are linked with an increased accuracy when detecting straight and curved edges [40].

Edge detection is regularly employed as a basic but a highly fundamental operation for correctly identifying and measuring features. In a gray level image an area where gray level value moves from a high value to a low value or vice versa is considered an edge. Edges are indicative of a boundary between an object and a background or amongst two objects. Consequently, edge detection is imperative for locating objects and determining their shapes and sizes [41].

4.4.1 Sobel Filter

The Sobel filter for edge detection is a discrete differentiation kernel, extensively employed in image processing of seismic data for the detection of faults automatically. First order intensity gradients are used by the Sobel algorithm for edge detection [36]. These gradients are either in x, y or z direction. These individual gradients are used to find the overall resultant output of the Sobel algorithm.

Sobel operators have been designed and applied on 2D/3D rectangular data as 2D/3D filters. Work has also been done on the application of Sobel operators for hexagonally sampled seismic 2D data images using SA [42]. In this chapter, a 3D Sobel filter for hexagonally sampled seismic data has been introduced.

The Sobel filters for x and y direction for 2D rectangular data are $G2_x$ and $G2_y$ [43] shown respectively as:

$$G2_x = \begin{bmatrix} -1 & -2 & -1 \\ 0 & 0 & 0 \\ 1 & 2 & 1 \end{bmatrix}. \tag{4.1}$$

$$G2_y = \begin{bmatrix} -1 & 0 & 1 \\ -2 & 0 & 2 \\ -1 & 0 & 1 \end{bmatrix}. \tag{4.2}$$

Similarly, the 3D Sobel filters for x, y and z gradients namely $G3_x$, $G3_y$ and $G3_z$ are represented as:

$$G3_x = \begin{bmatrix} -1 & -2 & -1 \\ 0 & 0 & 0 \\ 1 & 2 & 1 \end{bmatrix} \begin{bmatrix} -2 & -4 & -2 \\ 0 & 0 & 0 \\ 2 & 4 & 2 \end{bmatrix} \begin{bmatrix} -1 & -2 & -1 \\ 0 & 0 & 0 \\ 1 & 2 & 1 \end{bmatrix}. \tag{4.3}$$

$$G3_y = \begin{bmatrix} -1 & 0 & 1 \\ -2 & 0 & 2 \\ -1 & 0 & 1 \end{bmatrix} \begin{bmatrix} -2 & 0 & 2 \\ -4 & 0 & 4 \\ -2 & 0 & 2 \end{bmatrix} \begin{bmatrix} -1 & 0 & 1 \\ -2 & 0 & 2 \\ -1 & 0 & 1 \end{bmatrix}. \tag{4.4}$$

$$G3_z = \begin{bmatrix} -1 & -2 & -1 \\ -2 & -4 & -2 \\ -1 & -2 & -1 \end{bmatrix} \begin{bmatrix} 0 & 0 & 0 \\ 0 & 0 & 0 \\ 0 & 0 & 0 \end{bmatrix} \begin{bmatrix} 1 & 2 & 1 \\ 2 & 4 & 2 \\ 1 & 2 & 1 \end{bmatrix}. \tag{4.5}$$

Similarly, Sobel filters can be designed for the hexagonal domain. 2D SA Sobel filters have been implemented [42]. The Sobel filters for 2D case can be given as $H2_x$ and $H2_y$ as follows:

$$H2_x = \begin{bmatrix} 0 & 2 & 1 & -1 & -2 & -1 & 1 \end{bmatrix}. \tag{4.6}$$

$$H2_y = \begin{bmatrix} 0 & 0 & -1 & -1 & 0 & 1 & 1 \end{bmatrix}. \tag{4.7}$$

Based on the Sobel filters for square domain, shown before and the 2D Sobel filters for SA [42], an attempt has been made to design 3D SA Sobel filters given by $H3_x$, $H3_y$ and $H3_z$.

$$H3_x = \begin{bmatrix} 0 & 2 & 1 & -1 & -2 & -1 & 1 \\ 0 & 4 & 2 & -2 & -4 & -2 & 2 \\ 0 & 2 & 1 & -1 & -2 & -1 & 1 \end{bmatrix} \tag{4.8}$$

$$H3_y = \begin{bmatrix} 0 & 0 & -1 & -1 & 0 & 1 & 1 \\ 0 & 0 & -2 & -2 & 0 & 2 & 2 \\ 0 & 0 & -1 & -1 & 0 & 1 & 1 \end{bmatrix} \tag{4.9}$$

$$H3_y = \begin{bmatrix} 6 & 1 & 1 & 1 & 1 & 1 & 1 \\ 0 & 0 & 0 & 0 & 0 & 0 & 0 \\ -6 & -1 & -1 & -1 & -1 & -1 & -1 \end{bmatrix} \tag{4.10}$$

The magnitude of Sobel operators for 2D and 3D are calculated as:

$$G2 = \sqrt{G2_x^2 + G2_y^2}. \tag{4.11}$$

$$G3 = \sqrt{G3_x^2 + G3_y^2 + G3_z^2}. \tag{4.12}$$

Similarly, for hexagonal processing, the magnitude is calculated as:

$$H2 = \sqrt{H2_x^2 + H2_y^2}. \tag{4.13}$$

$$H3 = \sqrt{H3_x^2 + H3_y^2 + H3_z^2}. \tag{4.14}$$

4.5 Sobel Edge Detection on 2D Seismic Data

The objective of this section is to test the 2D Sobel filter for hexagonally sampled seismic data and show the effectiveness, efficiency and robustness. In this section, the filters will be tested on both synthetic and real seismic data.

4.5.1 Synthetic Data for 2D Edge Detection

The hexagonal and rectangular test images are shown in Fig. 4.1. The slice contains two lines, one vertical and one diagonal line. The size of both the images is equal. The hexagonal is of length 7^5 while the rectangular test size is 129 x 130. The application of 2D Sobel filter is can be seen in Fig. 4.1. The edges are detected perfectly in this noiseless scenario.

To test the robustness of the 2D Sobel filter, on a noisy test case containing 10% noise, it can be observed that the edge detection ability remains intact despite this level of noise as can be seen from Fig. 4.2.

Consider the test case containing 30% noise, it can be observed that the edges are detected perfectly despite increased levels of noise. These test slices containing noise and the results of Sobel edge detection are shown in Fig. 4.3.

In the test case shown in Fig. 4.4 containing 50% noise, it can be seen that the noise is significantly increased. These test slices containing noise and the results of Sobel edge detection are shown in Fig. 4.4. Despite the high levels of noise, it is evident that the Sobel edge detection is able to detect the edges in both rectangular as well as hexagonal approaches.

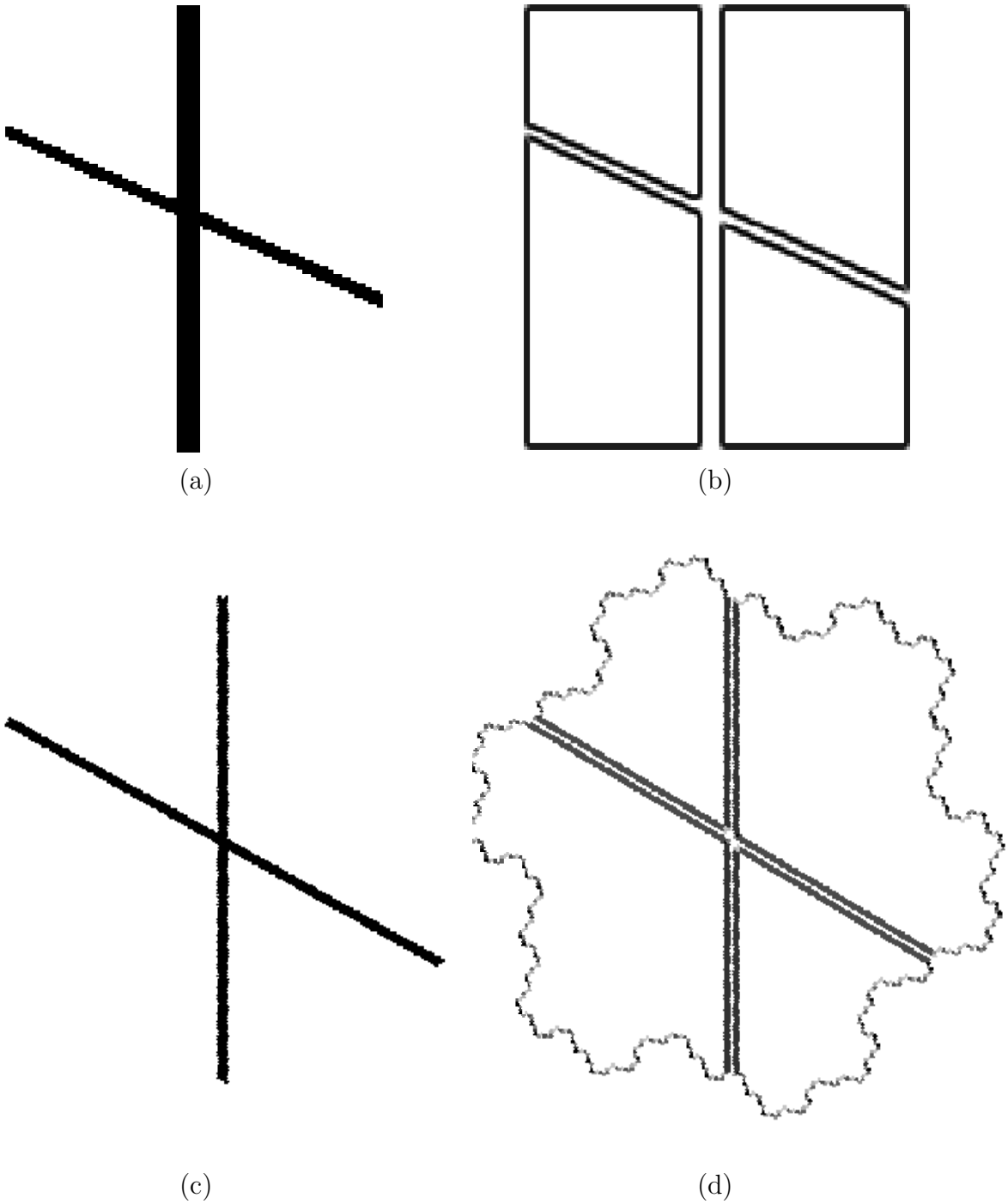

Figure 4.1: (a) Synthetic rectangular data. (b) 2D Sobel on synthetic rectangular data. (c) Synthetic hexagonal data. (d) 2D Sobel on synthetic hexagonal data.

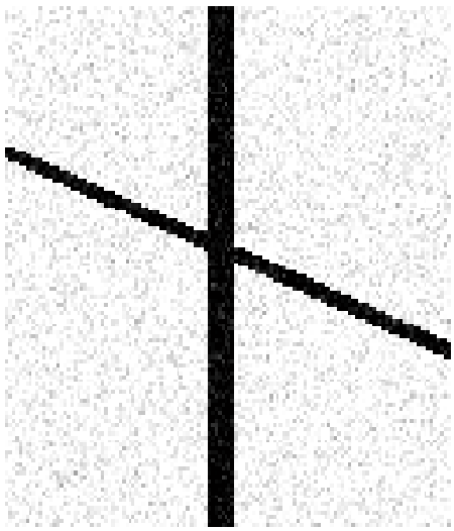

(a)

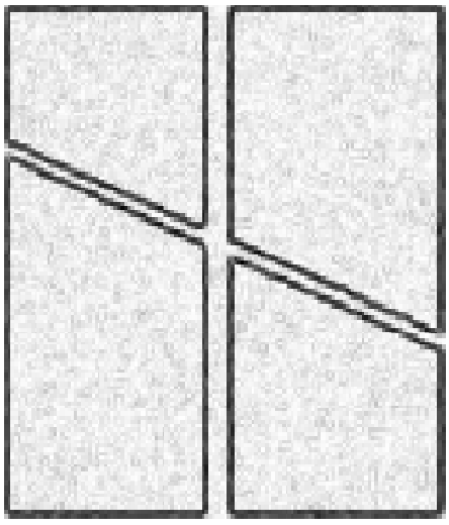

(b)

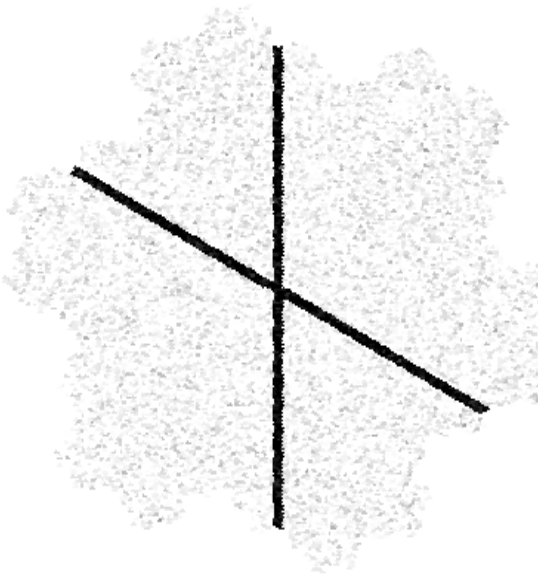

(c)

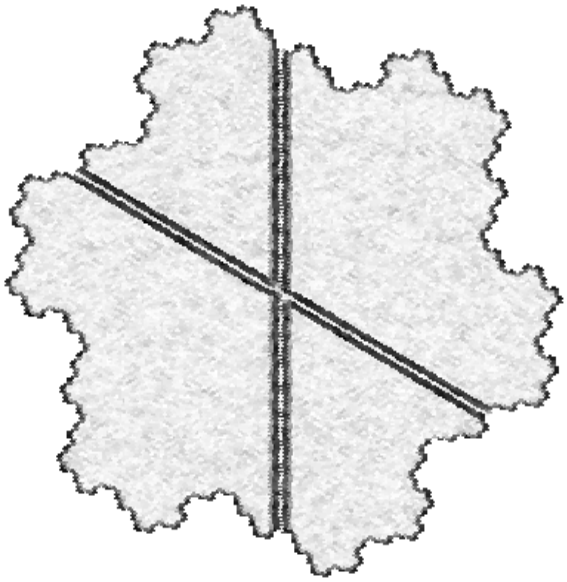

(d)

Figure 4.2: (a) Synthetic rectangular data with 10% noise. (b) 2D Sobel on synthetic rectangular data with 10% noise. (c) Synthetic hexagonal data with 10% noise. (d) 2D Sobel on synthetic hexagonal data with 10% noise.

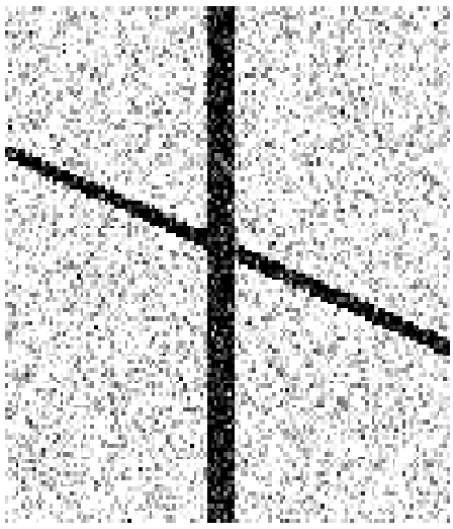

(a)

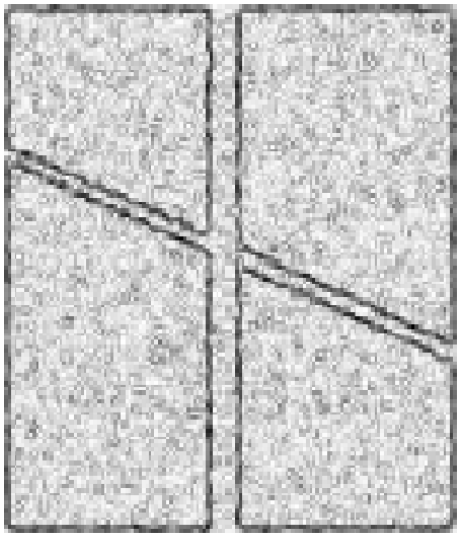

(b)

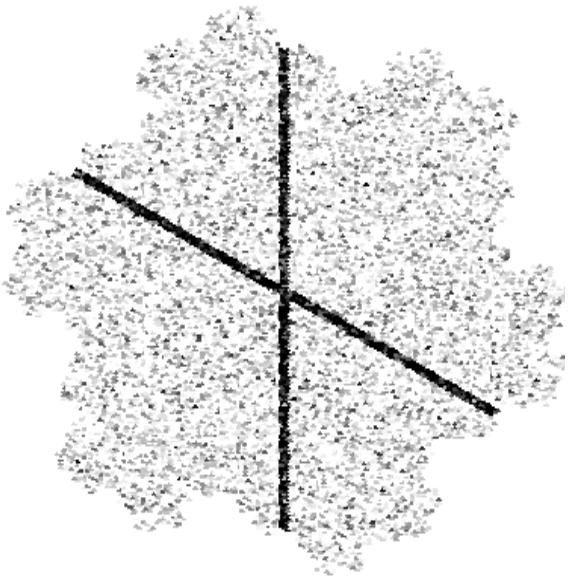

(c)

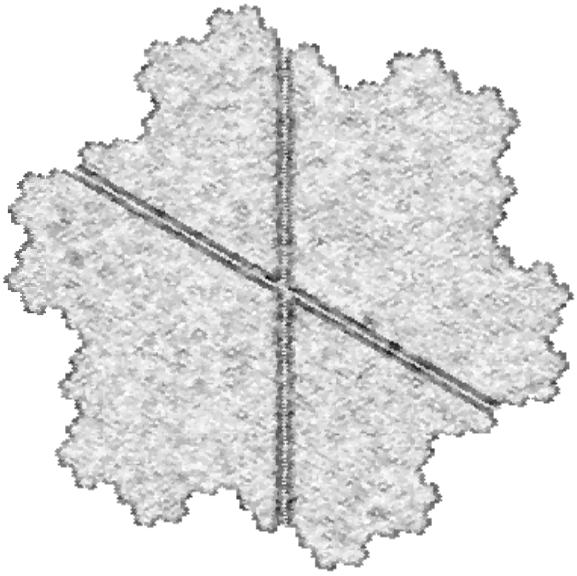

(d)

Figure 4.3: (a) Synthetic rectangular data with 30% noise. (b) 2D Sobel on synthetic rectangular data with 30% noise. (c) Synthetic hexagonal data with 30% noise. (d) 2D Sobel on synthetic hexagonal data with 30% noise.

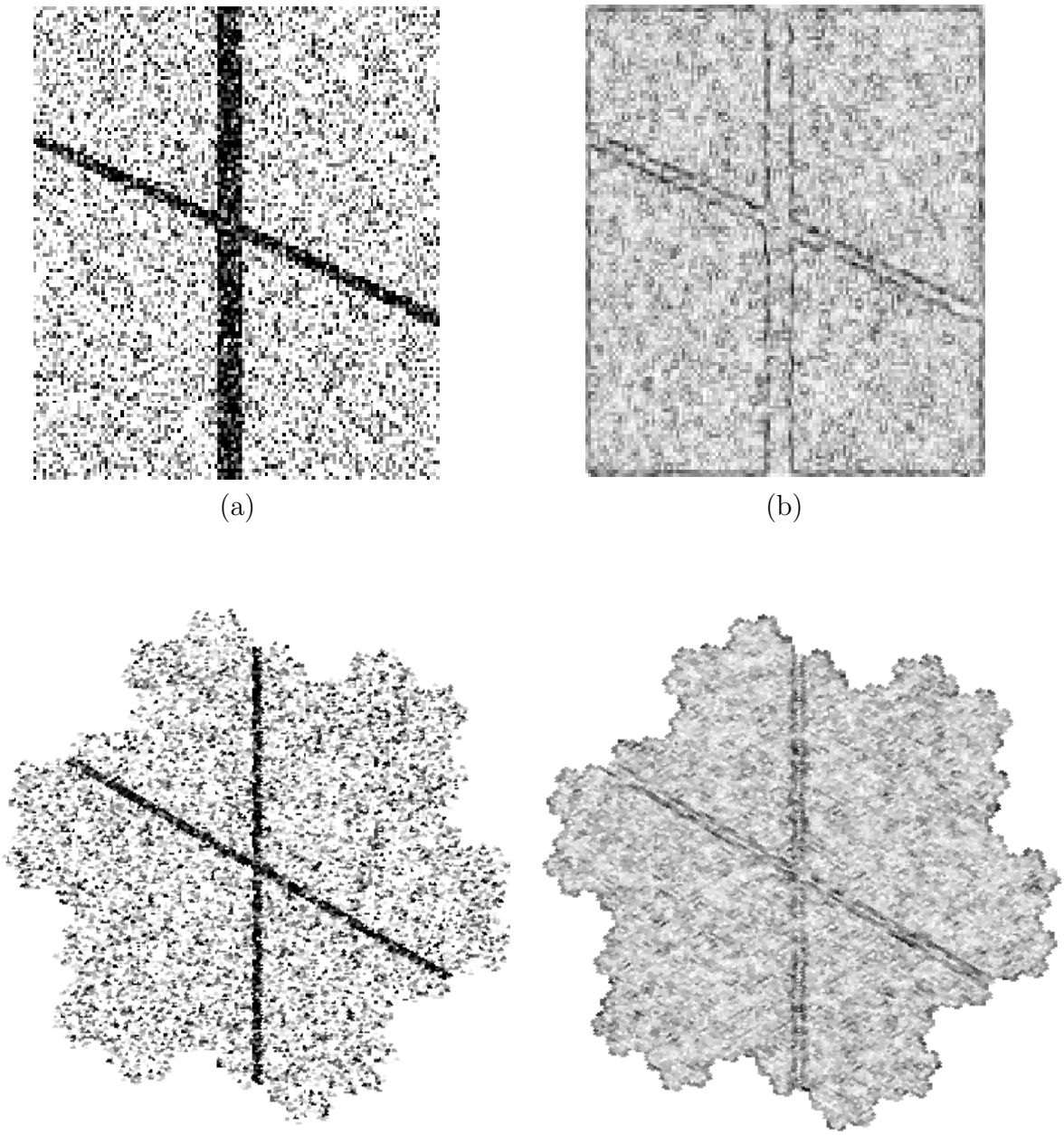

Figure 4.4: (a) Synthetic rectangular data with 50% noise. (b) 2D Sobel on synthetic rectangular data with 50% noise. (c) Synthetic hexagonal data with 50% noise. (d) 2D Sobel on synthetic hexagonal data with 50% noise.

4.5.2 Hexagonal Sampling of Seismic Data

3D seismic data sets have been provided by Saudi Aramco in the rectangular domain. One data set contains a channel. The second data set contains faults. These data sets are first converted to the hexagonal format. Ideally, the best case scenario would have been if the data was initially in the hexagonal format. The test slice of channel data set in the rectangular domain is shown in the Fig. 4.5.

The size of this rectangular image is 350 x 340. The hexagonal sampled version of this test slice is a 1D vector of length 117649 corresponding to a rectangular image of size 343 x 343 obtained using the designed toolbox. The hexagonal equivalent image is shown in Fig. 4.6.

The second data set containing faults is shown in Fig. 4.7 and Fig. 4.8. The seismic data shown in Fig. 4.5, Fig. 4.6, Fig. 4.7 and Fig. 4.8 is used in this chapter to check the effectiveness of spiral architecture in the seismic domain.

4.5.3 Seismic Data for 2D Edge Detection

In this section 2d Sobel operator has been applied on seismic data provided by Saudi Aramco. Consider the section of rectangular test slice and the hexagonal resampled section shown in Fig. 4.9.

The Sobel operator on these test slices is shown in Fig. 4.10. The 2D Sobel operator perfectly follows the edge in both cases. The curves are represented more precisely in SA owing to higher symmetry of hexagons.

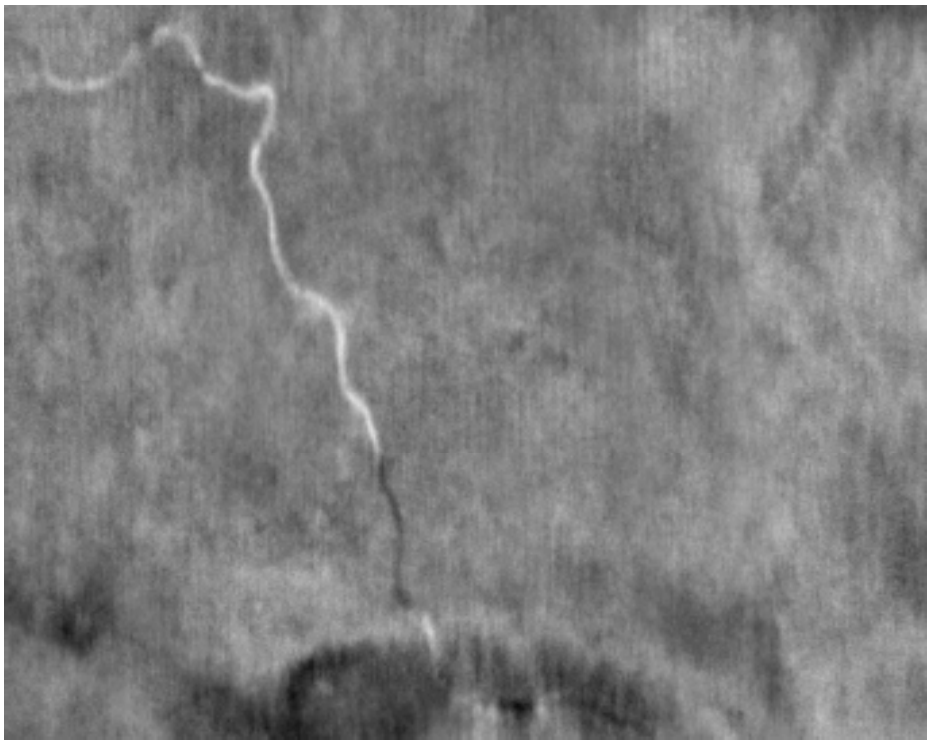

Figure 4.5: Rectangularly sampled data from the seismic data set containing channel. (Courtesy of Saudi Aramco)

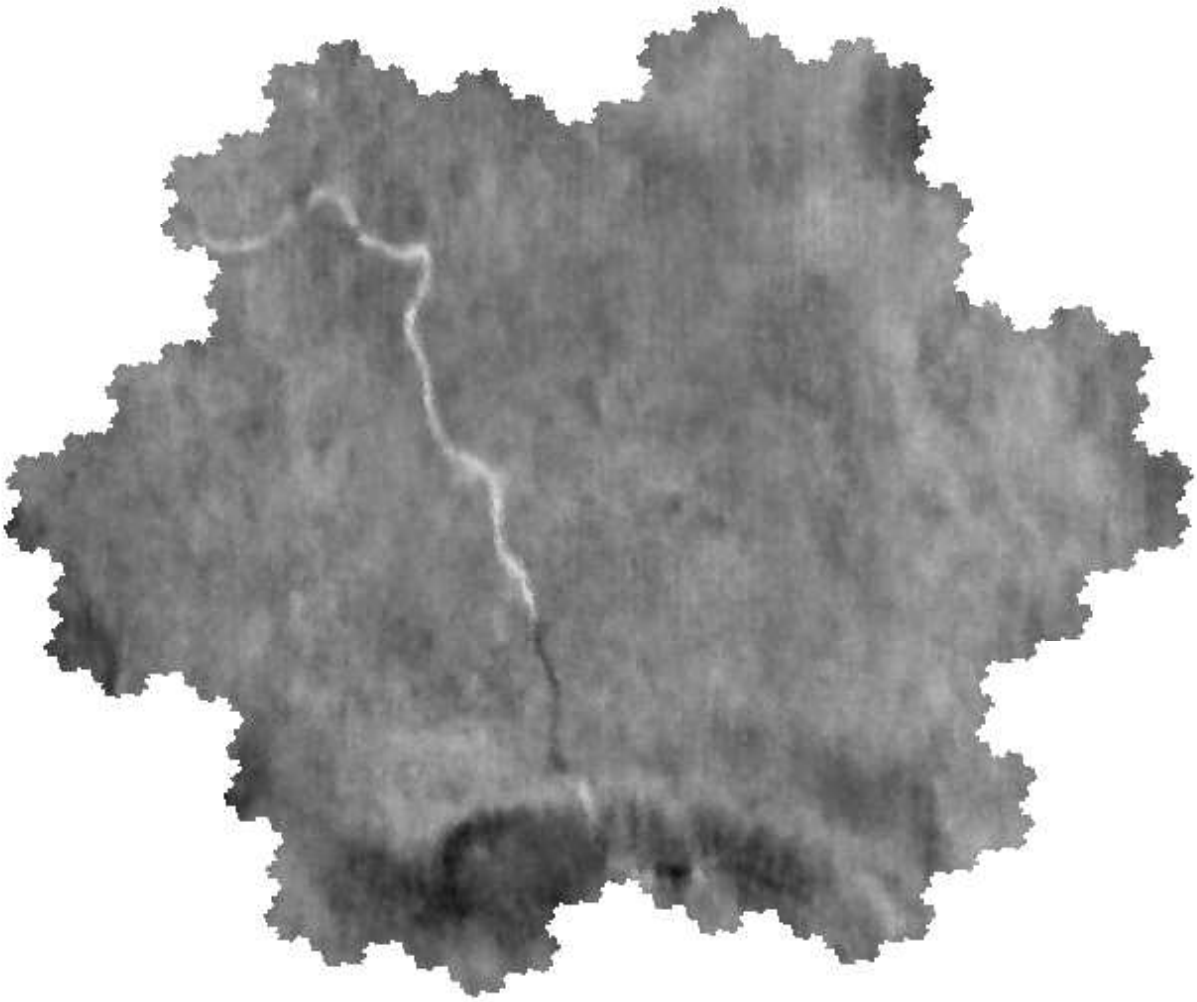

Figure 4.6: Hexagonally resampled data from the seismic data set containing channel.

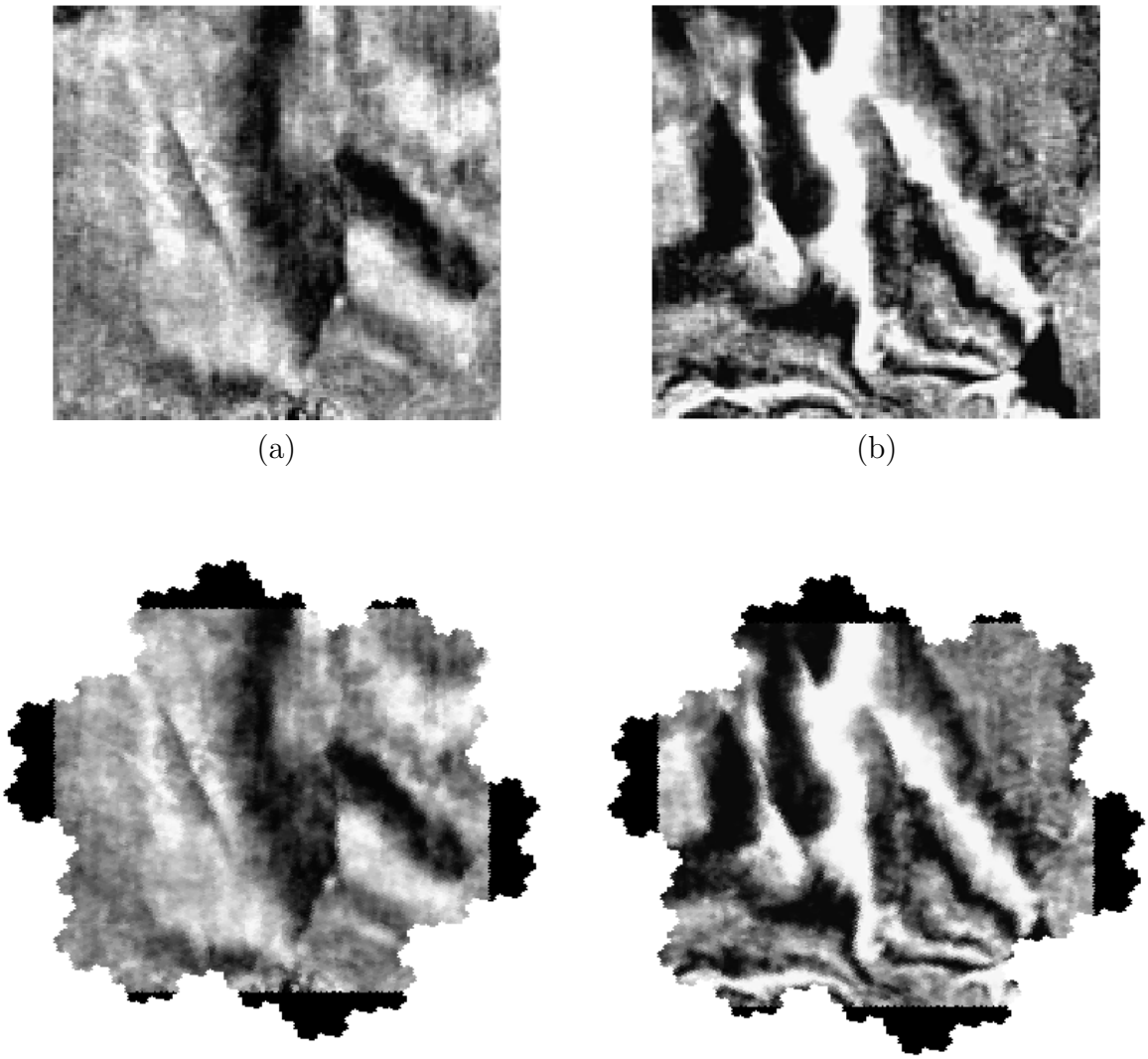

Figure 4.7: Seismic data set containing faults. (a) Rectangularly sampled slice 1. (b) Rectangularly sampled slice 2. (c) Hexagonally resampled slice 1. (d) Hexagonally resampled slice 2. (Courtesy of Saudi Aramco.)

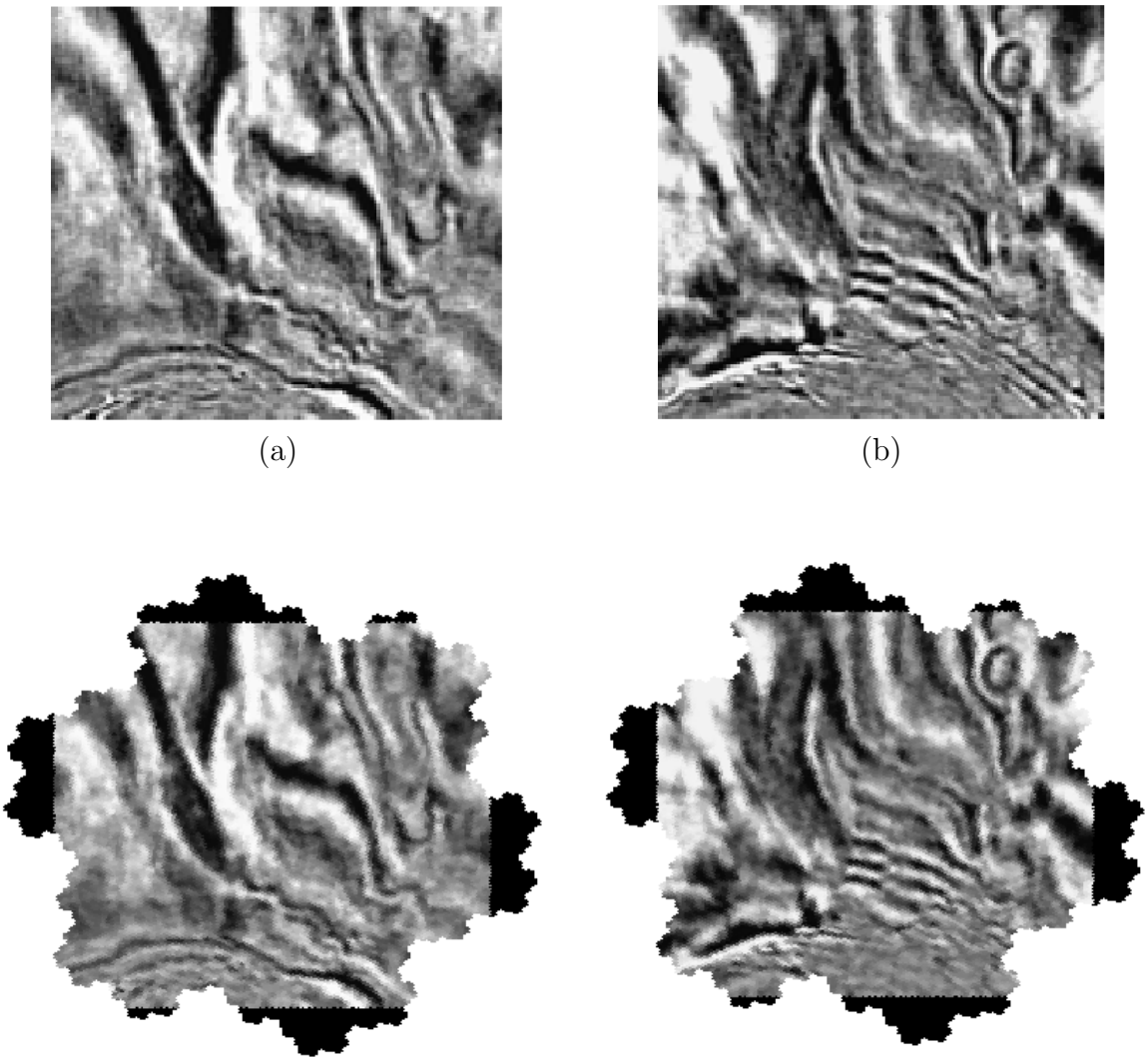

Figure 4.8: Seismic data set containing faults. (a) Rectangularly sampled slice 3. (b) Rectangularly sampled slice 4. (c) Hexagonally resampled slice 3. (d) Hexagonally resampled slice 4. (Courtesy of Saudi Aramco.)

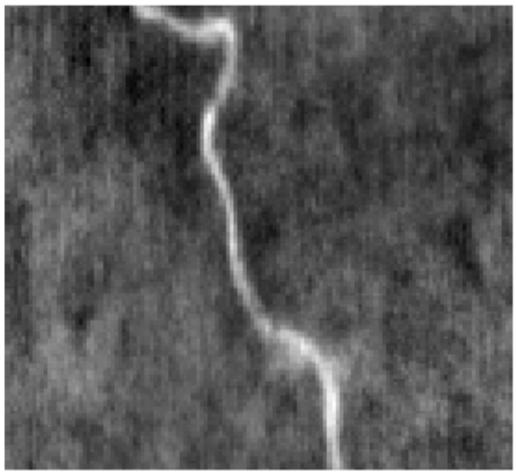

(a)

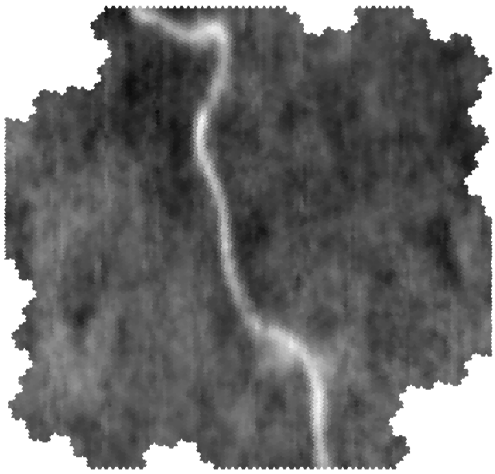

(b)

Figure 4.9: (a) Rectangularly sampled seismic data for 2D Sobel edge detection. (b) Hexagonally sampled seismic data for 2D Sobel edge detection.

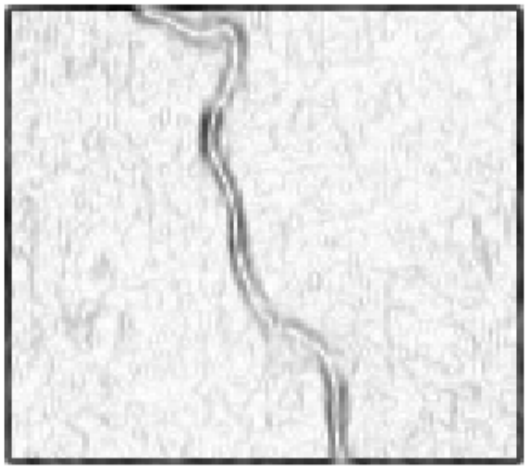

(a)

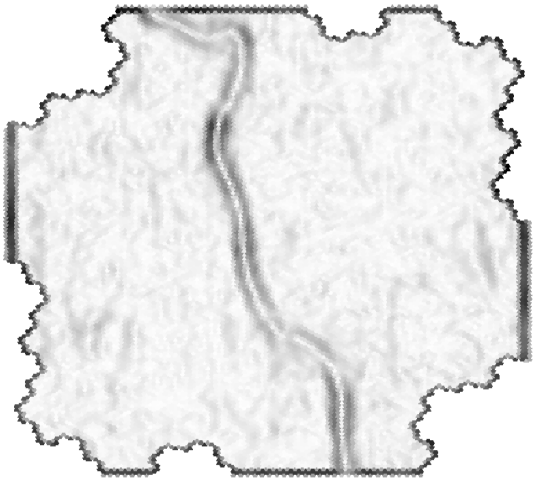

(b)

Figure 4.10: (a) 2D Sobel edge detection on section of rectangularly sampled seismic data. (b) 2D Sobel edge detection on section of hexagonally sampled seismic data.

4.6 Edge Detection of 3D Seismic Data

In this section the application of edge detection Sobel filters for hexagonally sampled seismic data is discussed. The test slices are Fig. 4.5, Fig. 4.6, Fig. 4.7 and Fig. 4.8. The application of rectangular Sobel operator $G3$ generates the output shown in Fig. 4.11. Equivalently, the output of the hexagonal operator $H3$ is shown in Fig. 4.12. Similarly, the application of 3D Sobel filter on data set containing faults is shown in Fig. 4.13 and Fig. 4.14.

4.7 Analysis

4.7.1 Qualitative Analysis

The qualitative comparison reveals that the hexagonal approach is visibly better for detection of curves. It is due to the inherent increased symmetric nature of a hexagon as compared to that of a square. In case of rectangular approach, curves are portrayed as stair case, whereas in case of hexagons, the curves are smoother. The comparison of two approaches can be seen in Fig. 4.15. In the red blocks we can see that the hexagonal case represents the curve in smoother fashion as compared to the rectangular approach. In the typical approach we can clearly observe that a stair case pattern exists in the centre of the red block.

On the other hand, in the hexagonal approach, we observe a very well defined representation of the slight curve. Furthermore, the rectangular case gives a highly pixilated view. Similarly, in the green blocks of Fig. 4.15 we see yet

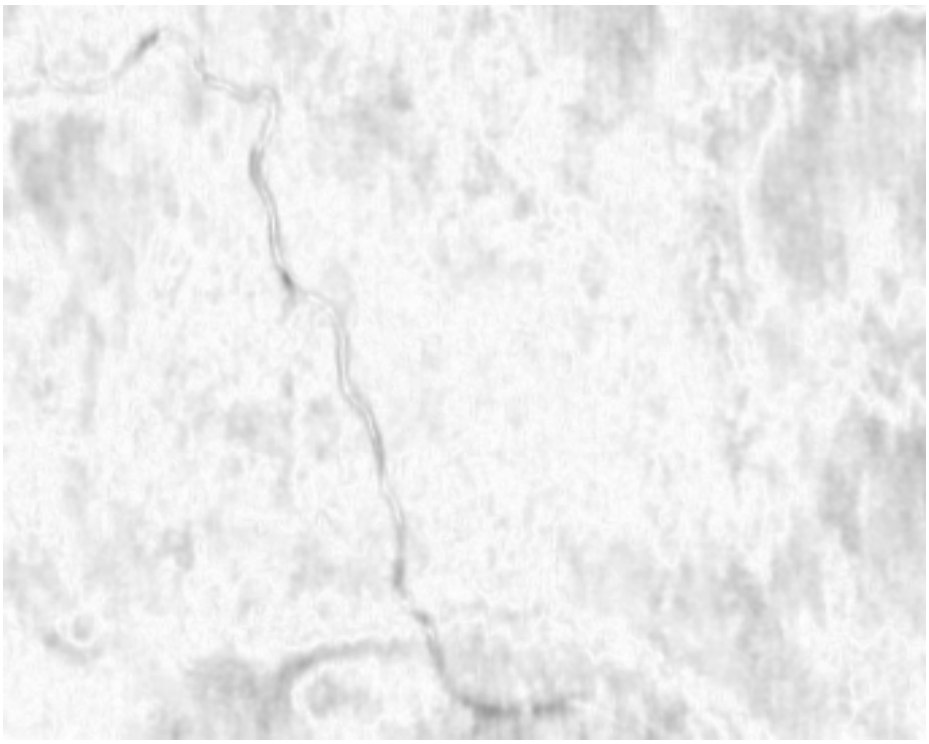

Figure 4.11: Rectangular Sobel filter magnitude of slice number 180 of the seismic data set containing channel.

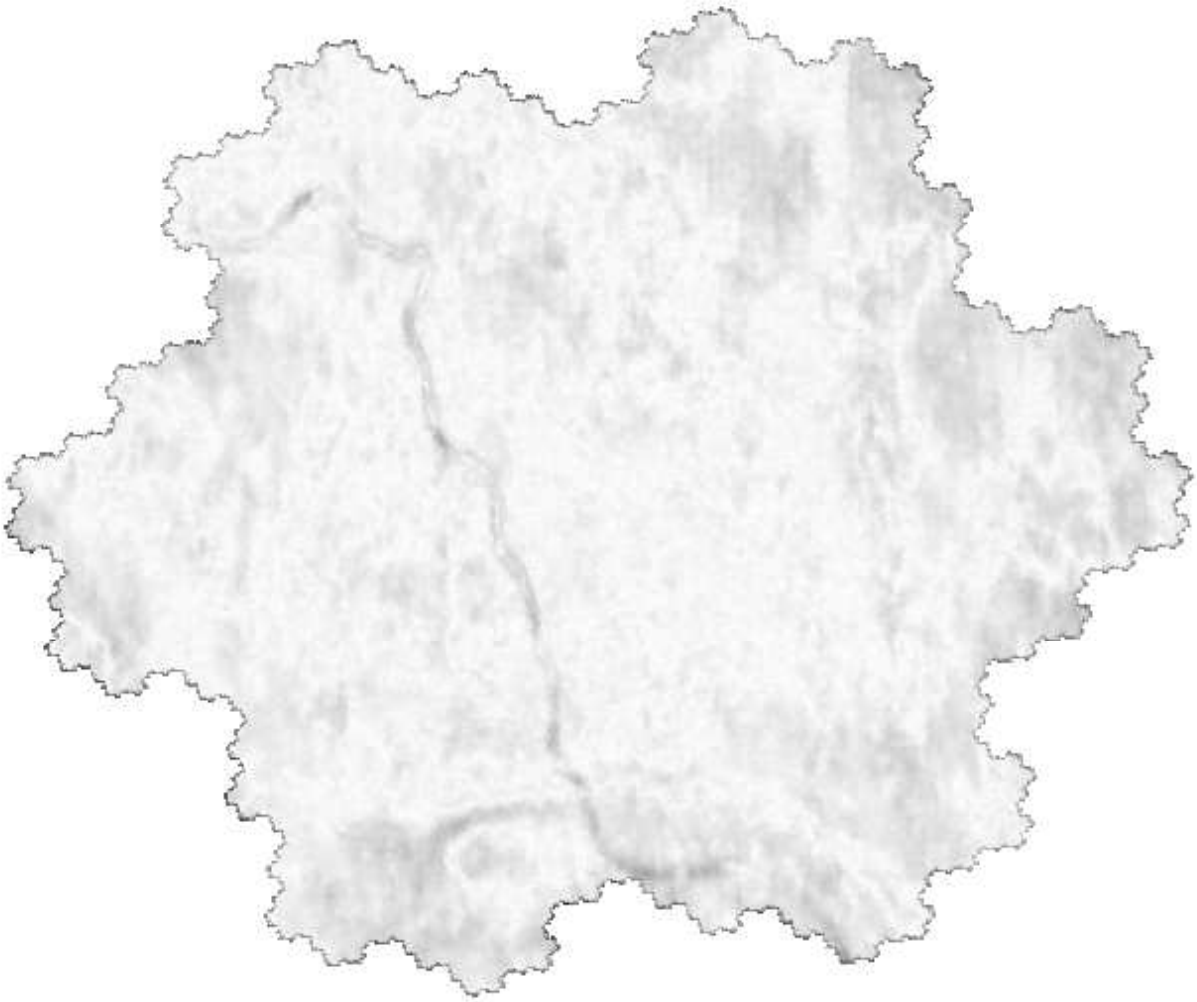

Figure 4.12: Hexagonal Sobel filter magnitude of slice number 180 of the seismic data set containing channel.

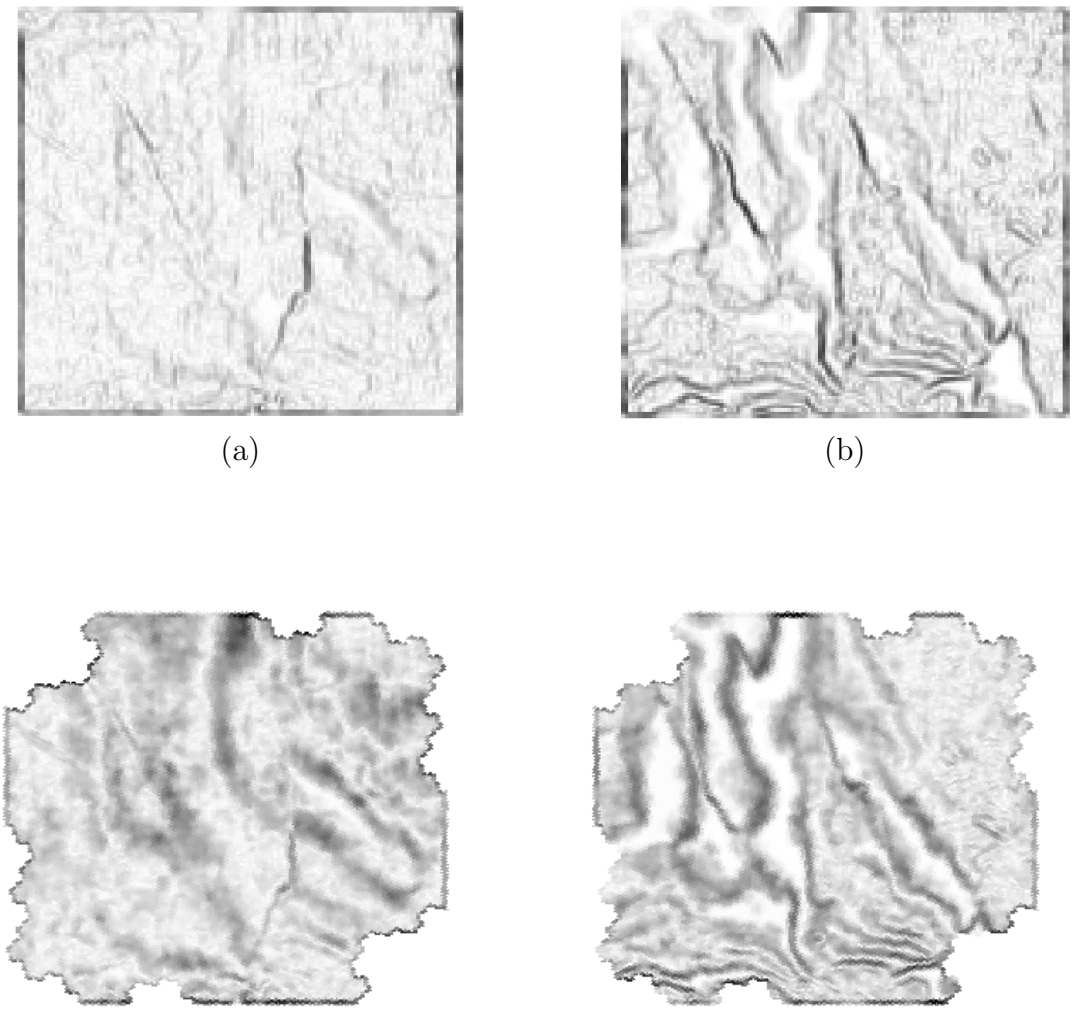

Figure 4.13: 3D Sobel filter edge detection of seismic data set containing faults. (a) Rectangularly sampled slice 1. (b) Rectangularly sampled slice 2. (c) Hexagonally resampled slice 1. (d) Hexagonally resampled slice 2.

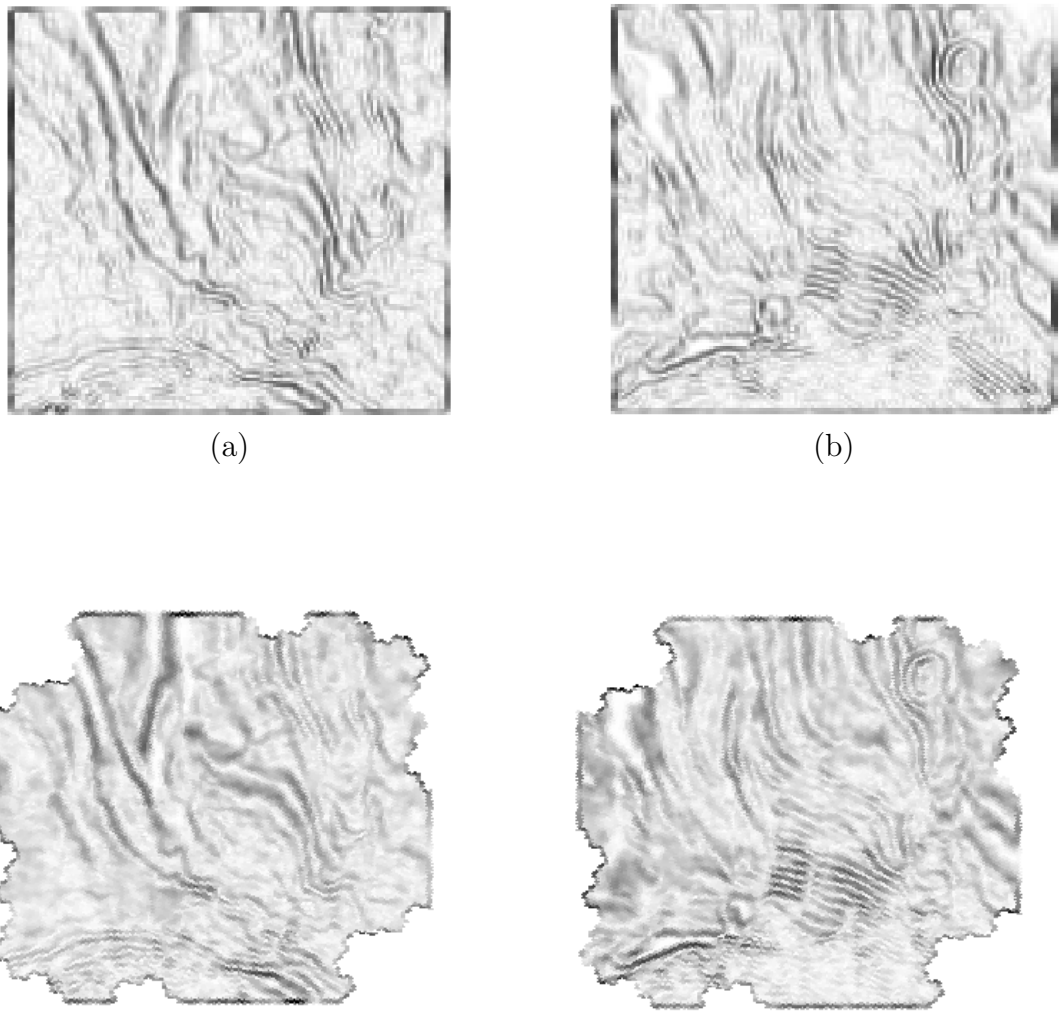

Figure 4.14: 3D Sobel filter edge detection of seismic data set containing faults. (a) Rectangularly sampled slice 3. (b) Rectangularly sampled slice 4. (c) Hexagonally resampled slice 3. (d) Hexagonally resampled slice 4.

another near vertical edge being represented in a crisp manner in the hexagonal approach.

As in the previous case, the rectangular approach, results in a stair case representation of the edges. The hexagonal approach gives relatively better curve detection. Another area of test slices under consideration is shown in Fig. 4.16. We can see that visually the hexagonal Sobel operator gives a well defined curve whereas in case of the regular rectangular sampling approach, the curves are represented in a step wise manner. We can observe that the edge at approximately 120 degrees is defined in a highly continuous manner in case of hexagonal case. In the rectangular Sobel output, we can observe a stepwise/stair case representation for this 120 degree edge.

Another section of the slice can be seen in Fig. 4.17. This region consists of curves in addition to vertical, horizontal and diagonal lines. The arrow points to blurring of edge in rectangular case. The hexagonal approach preserves this edge as evident from Fig. 4.17. In case of rectangular approach we observe staircase effects whereas the hexagonal sampling yields relatively smooth curve following. The edges are fine in SA in comparison to rectangular sampled approach. The arrows point to a region blurred in rectangular case. It is visible that hexagonal approach results in relatively sharper edge detection.

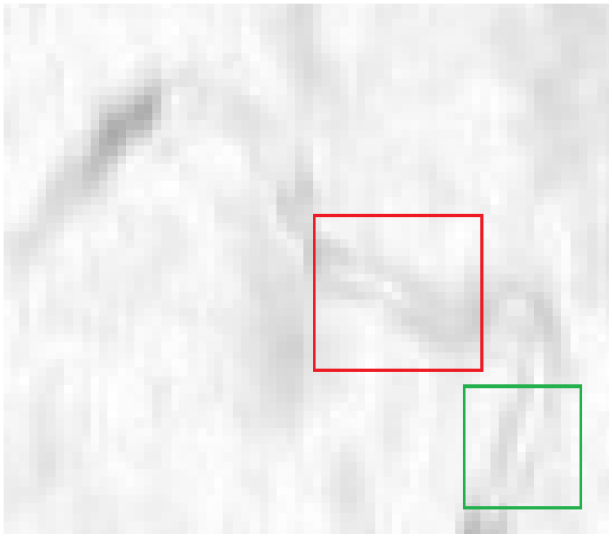

(a)

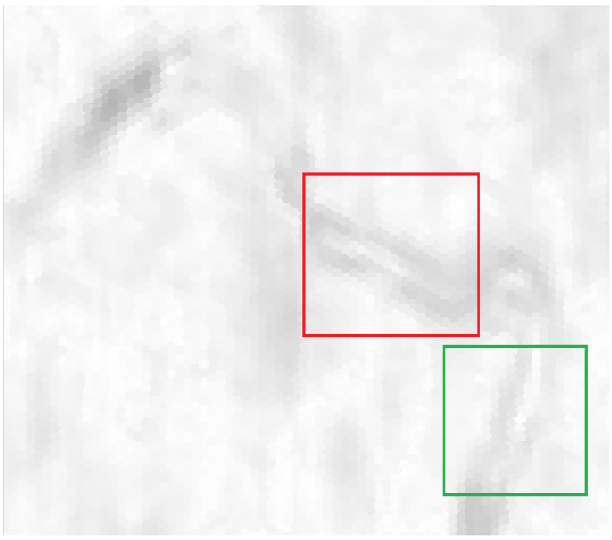

(b)

Figure 4.15: Zoomed sections of slice number 180 of the seismic data set containig channel. (a) Rectangularly sampled. (b) Hexagonally sampled.

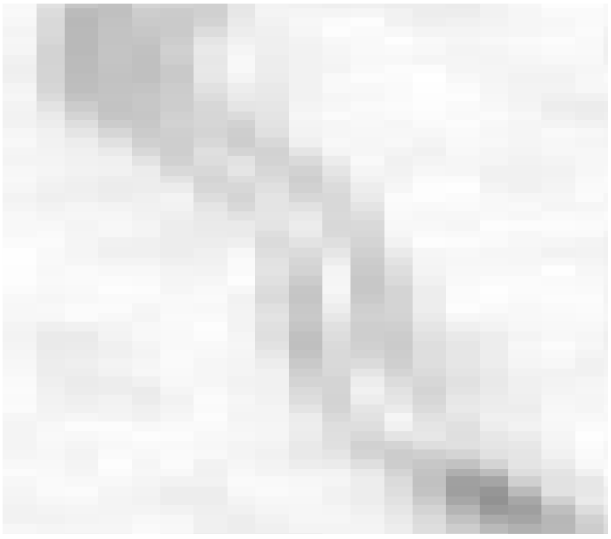

(a)

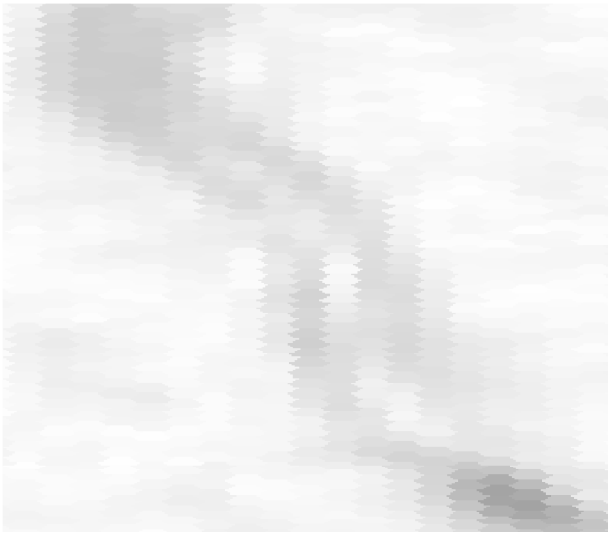

(b)

Figure 4.16: Staircase edge representation of a diagonal line. (a) In rectangularly sampled seismic data (b) In hexagonally sampled seismic data.

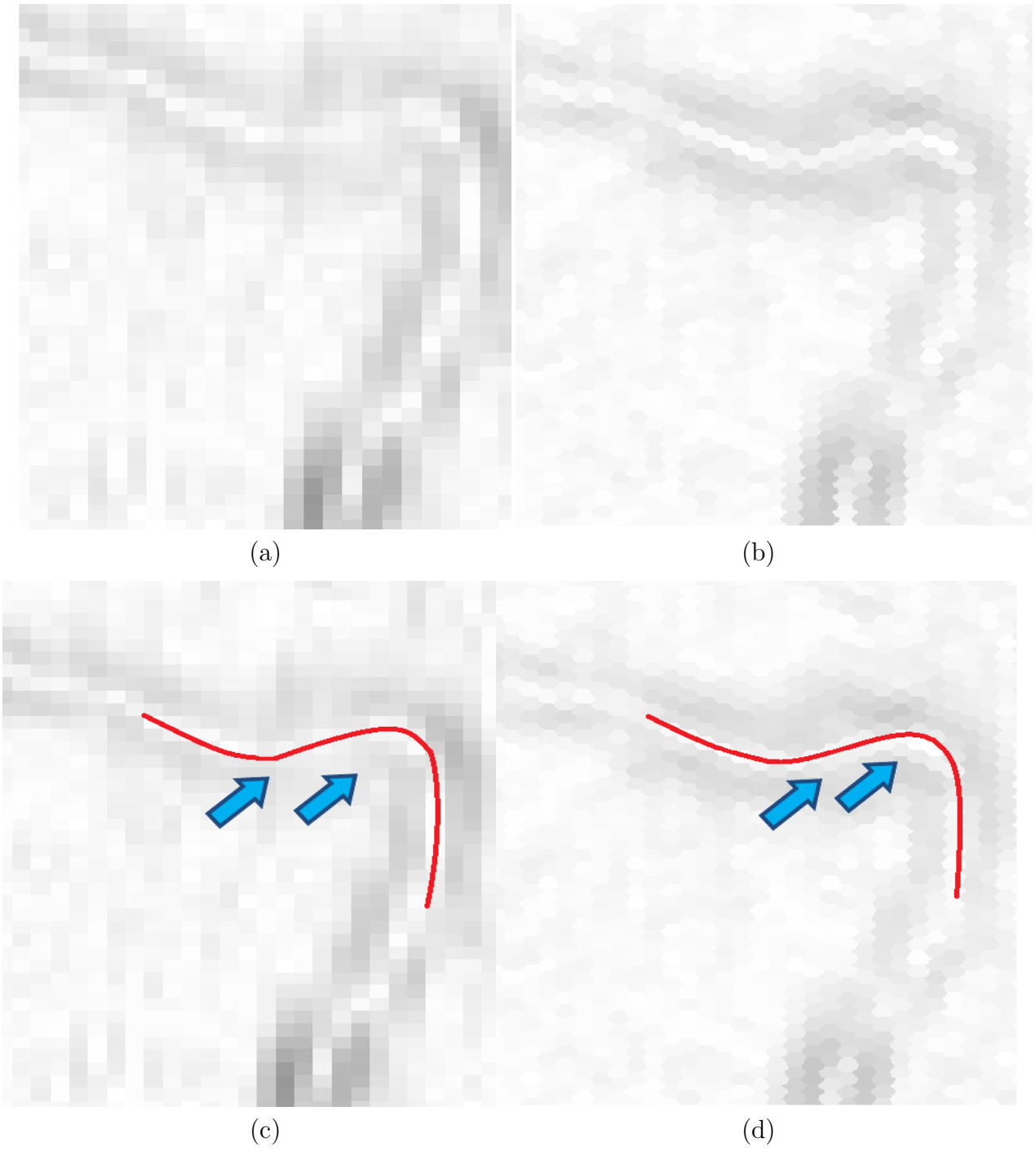

Figure 4.17: Edge blurring. (a) In rectangularly sampled seismic data. (b) In hexagonally sampled seismic data (c) Highlighted curve and blurred region in rectangular approach. (d) Highlighted curve in hexagonal approach.

4.7.2 Computational Analysis

The data handling advantage of the SA has been mentioned before. The ability of SA to handle 3D data as 2D data is computationally a significant advantage. Also, the fact that 13.4% lesser samples are required as compared to the typical rectangular approach results in lesser data thus increased processing efficiency. Similarly, the size of the convolution kernel is 28.57% more in case of a rectangular filter. Overall, the number of multiplications and additions for 3D convolution in case of rectangular sampling is 47% more as compared to the SA scenario.

Owing to all the benefits mentioned above, the computational time is exponentially reduced. Another major reason for a significant reduction in time is the fact that the number of nested loops is 50% less in case of 2D convolution. The savings of loops is 33% in case of 3D operations. Consequently, the processing time for a data of size 369x369x25 on a core i5 2.4 GHz processor system with a 2 GB RAM, is 9.6 seconds for hexagonal approach and 200 times more i.e., 1960 seconds for the rectangular approach. For the purpose of comparing the processing time with the rectangular approach, nested for loops have been used as they are being used in SA approach. This computational saving is a significant factor when considering huge 3D data sets. The computational efficiency is evident from the Table 4.1. The size of the data is 117649 data samples per slice in hexagonal case while $368x368$ per slice in the rectangular domain.

Table 4.1: Computational comparison to calculate $G3$ & $H3$ for data size of 369x369

Sampling approach	Time for 25 slices in seconds	Time for 50 slices in seconds	Time for 75 slices in seconds	Time for 150 slices in seconds
Rectangular approach	1958	3909	6379	11600
Hexagonal approach	9.6	11.02	14.13	30.08
Efficiency of hexagonal approach	204 times faster	355 times faster	451 times faster	385 times faster

4.8 Conclusion

It has been proven before that hexagonal sampling is an efficient alternative to rectangular sampling since the size of data is reduced. In this chapter, we have successfully proven this efficiency for the 3D seismic data processing. The qualitative superiority of hexagonal approach lies in the increased equidistant neighbors of a hexagon and the greater symmetry it provides as compared to a square. Consequently in case of hexagons, there are six neighbours with shared edges thus leading to much better curve following than the rectangular case. This makes the hexagonal approach an ideal choice for edge detection.

In comparison to the rectangular approach, commonly used 3D Sobel edge detection, the results of the hexagonal SA Sobel filter are not only slightly improved but computationally offer a significant advantage over the typical approach. Even, if we suppose that the data is originally in rectangular domain and needs to be resampled, the resampling time and the hexagonal convolution time is still nearly half in comparison to the rectangular convolution time.

It must also be mentioned that seismic interpretation does not include a single operation, e.g., Sobel edge detection. In seismic interpretation, several processes are needed to successfully locate geological features. Thus even if the seismic data acquisition and later imaging processes are in rectangular domain, interpretation can be efficiently managed by hexagonal resampling since 2D and 3D SA convolutions are exponentially better suited than rectangular case and the resampling of data will be carried out only once.

CHAPTER 5

EFFICIENT AND ACCURATE EDGE PRESERVING SMOOTHING FOR 3D HEXAGONALLY SAMPLED SEISMIC DATA

5.1 Introduction

It is of critical importance to suppress random noise before the application of edge detection algorithms such as Sobel filters. The reflection data near fractures/faults generally contains relatively more noise than other areas. In general the seismic edge detection algorithms are sensitive to the effects of noise [44]. A

very common approach for reducing noise before edge detection is to apply a low pass or averaging filter. The disadvantage of this type of noise removal is that it results in blurred sharp edges.

The edge preserving smoothing (EPS) algorithm was introduced in 1979 [23]. The EPS results in significant reduction of noise in the image without fading the sharpness of edges. This also plays a part in sharpening the edges which are blurred initially [23] [45] [46].

In this chapter, EPS algorithm has been modified to be used for hexagonally sampled seismic data but by using spiral architecture. This provides the advantages of lesser samples and efficient processing associated with SA in addition to qualitatively better results when compared to rectangular case.

5.2 Edge Preserving Smoothing

EPS initially locates the homogenous neighborhood around every data sample. Once the most uniform neighborhood region is determined, the average of that particular neighborhood is calculated. This average value replaces the value of data sample under consideration.

The first step is the selection of neighborhood. There are many options available for rectangular domain [47]. Researchers have generally used 4, 5 and 9 neighborhoods for EPS. The fundamental requirement of these neighborhood definitions is that the data samples of these various neighborhoods are connected and the data sample under consideration is a part of these neighborhoods. One such

neighborhood definition is shown in Fig. 5.1, in this case the window size is 5x5 and 9 neighborhoods are defined. This is one approach of neighborhood selection, there can be other type of neighborhoods based on the window size and the shape of individual neighborhood within the window [47] .

For the hexagonal case we have six direct neighbors instead of eight rectangular neighbors, four diagonal and four on the horizontal and vertical axes. In case of spiral architecture, the immediate neighbors are six. For distance level 2, the number of neighbors is 19. In rectangular case the number of neighbors, for distance 2, is 25. These 25 neighbors are not all equidistant as opposed to the hexagonal case. One possible neighborhood, that we propose definition for EPS in SA can be shown as Fig. 5.2. Similarly another possibility of neighborhood selection for SA is shown in Fig. 5.3.

In this chapter, the nine rectangular neighborhoods, shown by Fig. 5.1 and the seven hexagonal neighborhoods, shown by Fig. 5.3 have been used. It must be remembered that the size of neighborhood window must be chosen as per the expected size of edges that are to be determined. If the width of an edge is smaller than the window size, than the edge might be considered noise and removed by EPS [44].

Maintaining a balance between noise removal and preservation of sharp edges demands that the averaging must not take place in an area which consists of edges. Consequently, the most uniform neighborhood is required to be determined. If an area contains an edge, the variance of that neighborhood will be high as compared

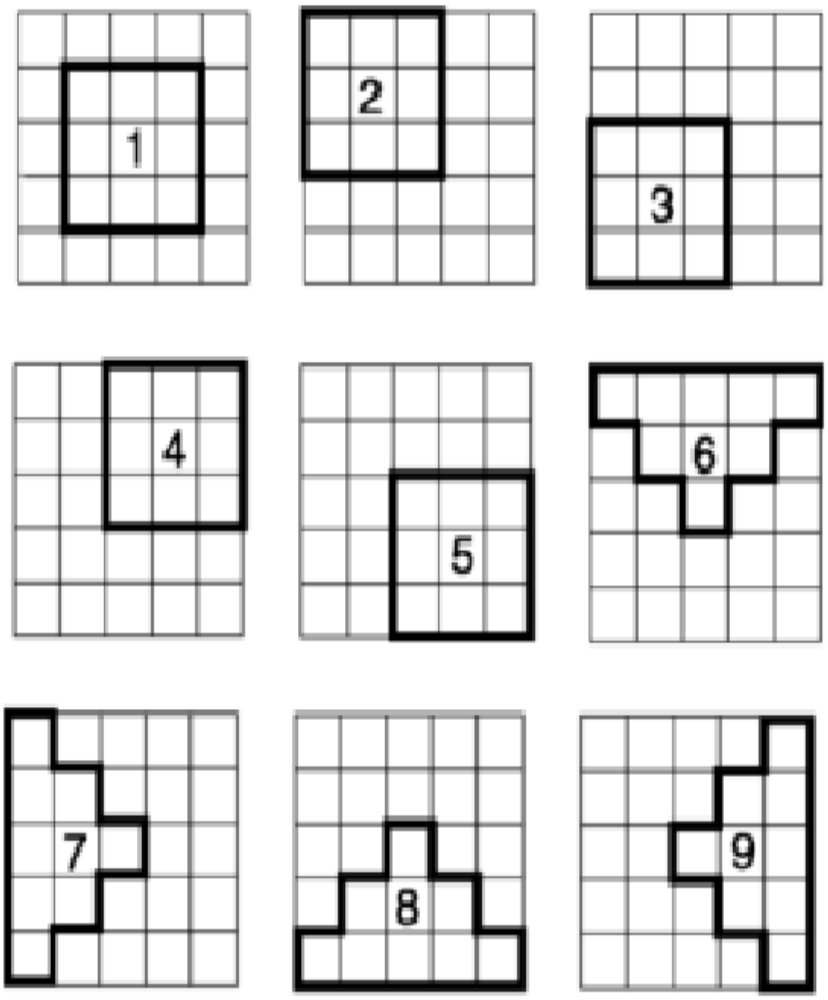

Figure 5.1: Nine possible rectangular neighborhoods used for 2D EPS. (Courtesy of [47]).

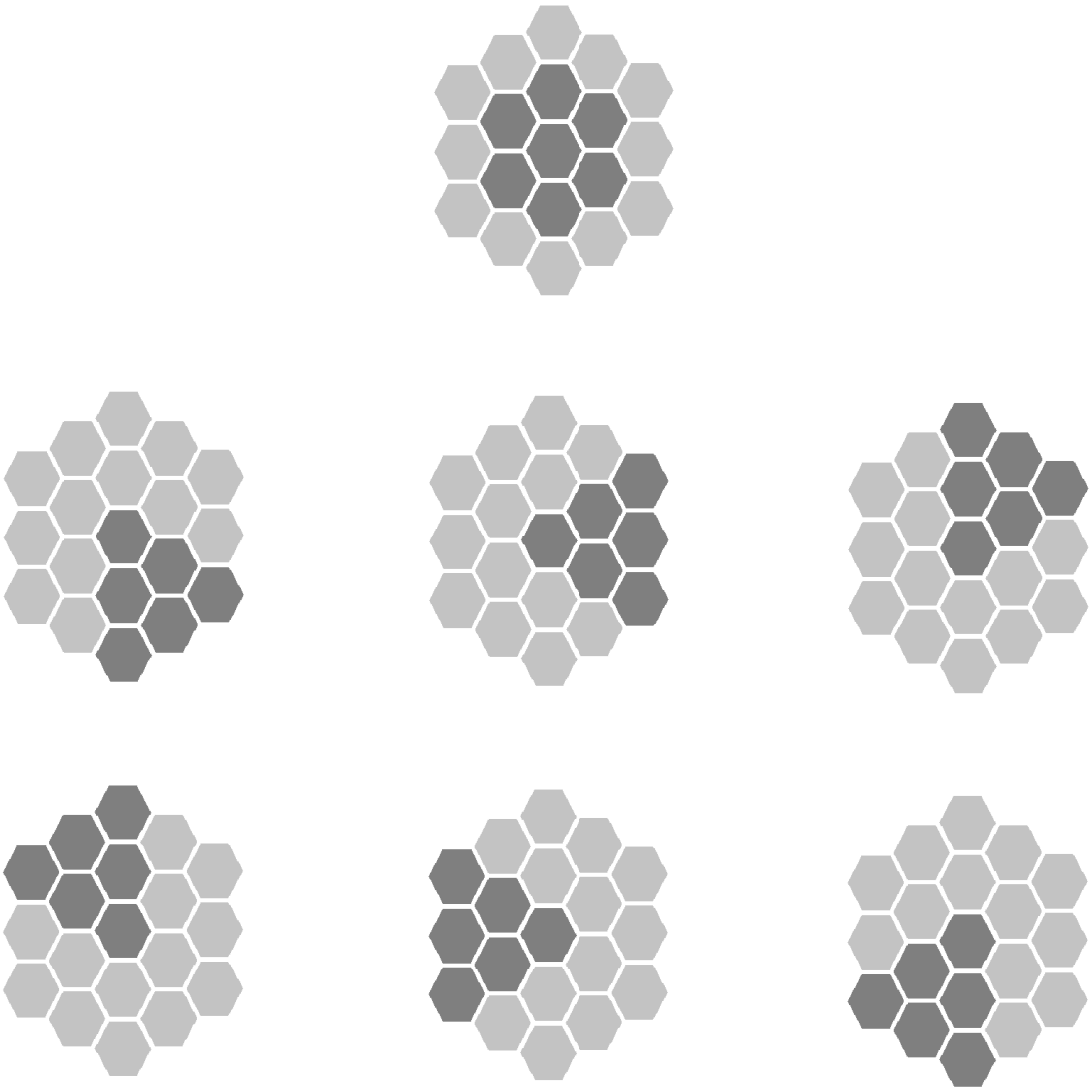

Figure 5.2: Seven possible hexagonal neighborhoods alternative 1.

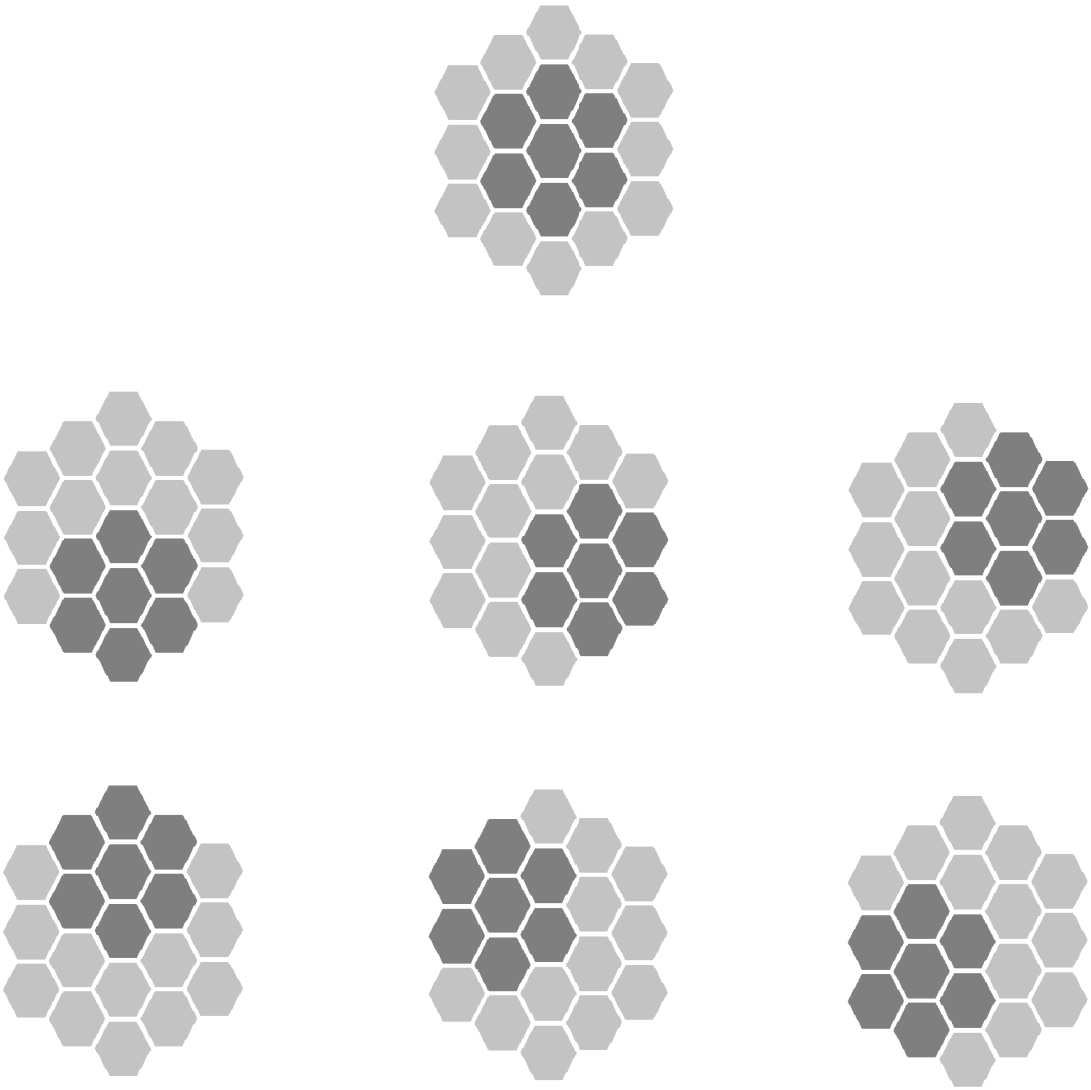

Figure 5.3: Seven possible hexagonal neighborhoods alternative 2.

to a homogenous region. As such variance is an ideal choice to save edges. The average of the most homogenous neighborhood is calculated. Finally, the value of data sample under evaluation is replaced by the average value of the most uniform neighborhood.

5.3 Simulation Results

The objective of this section is to test the EPS algorithm on hexagonally sampled seismic data and show the effectiveness, efficiency and robustness of the spiral architecture. The tests will be carried out on both synthetic and real seismic data.

5.3.1 EPS on Synthetic Data

In this section, EPS has been applied to a synthetic hexagonally sampled data and its comparison with similar rectangular sampled data is shown. The synthetic data for rectangular section has been generated similar to the hexagonal case consisting of one vertical line and one diagonal line. The hexagonal data has a length of 7^4 and the rectangular data is 7^2 x 7^2. The Fig. 5.4 shows the EPS applied on a noise less data containing two lines. It is evident that the EPS has no effect on the edges and the sharpness of the edges is maintained in both sampling approaches.

The introduction of noise proves that EPS successfully suppresses it while maintaining the crispness of the edges. This can be seen from Fig. 5.5, Fig. 5.6 and Fig. 5.7. The noise suppression is visibly improved in hexagonal case.

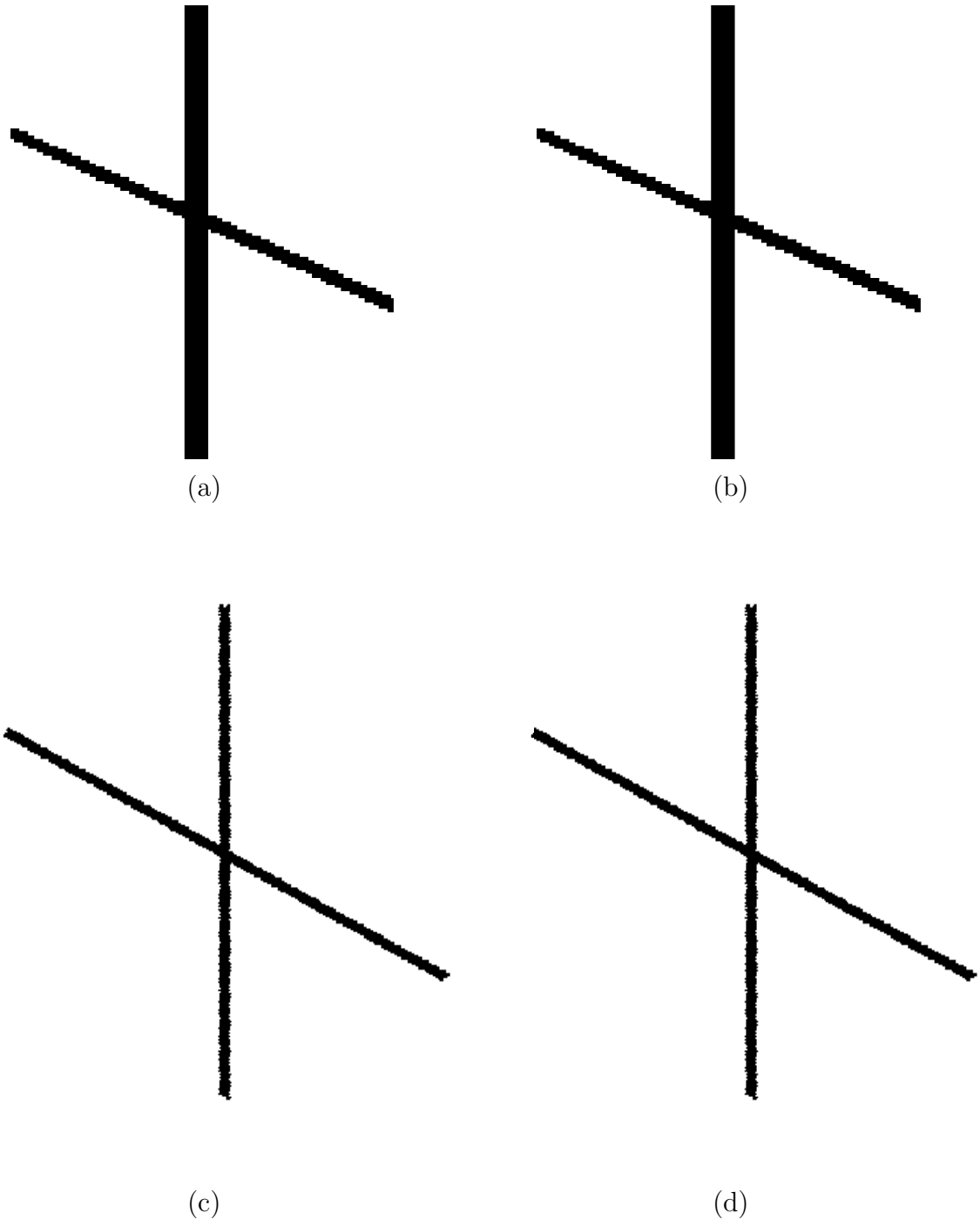

Figure 5.4: Noiseless synthetic data. (a) Rectangular sampled data. (b) EPS on rectangular data. (c) Hexagonally sampled data. (d) EPS on hexagonal data.

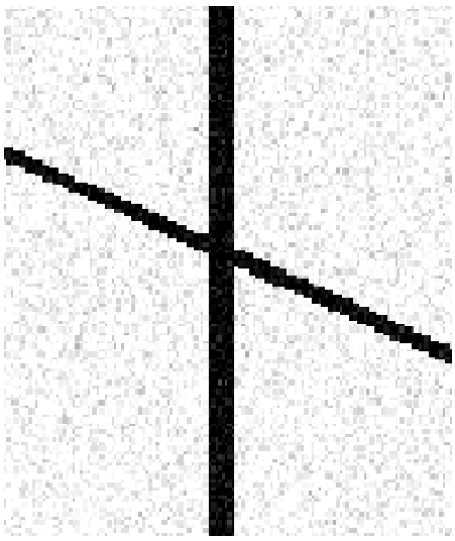

(a)

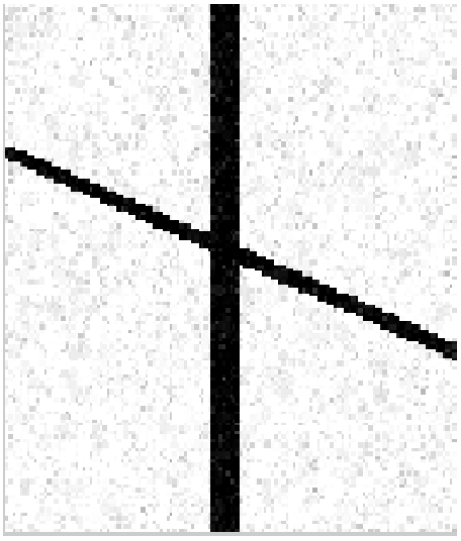

(b)

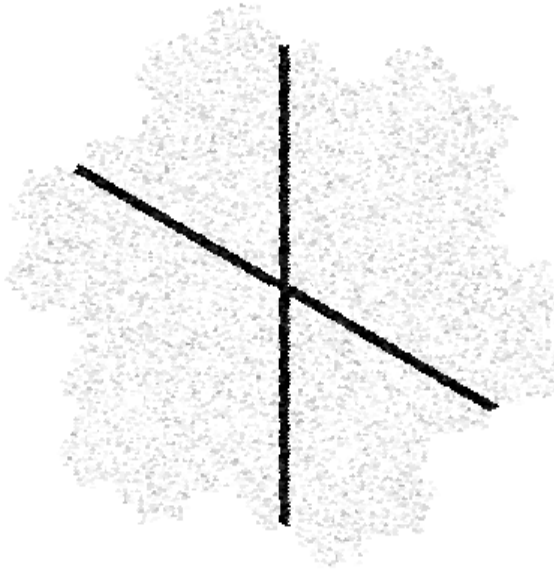

(c)

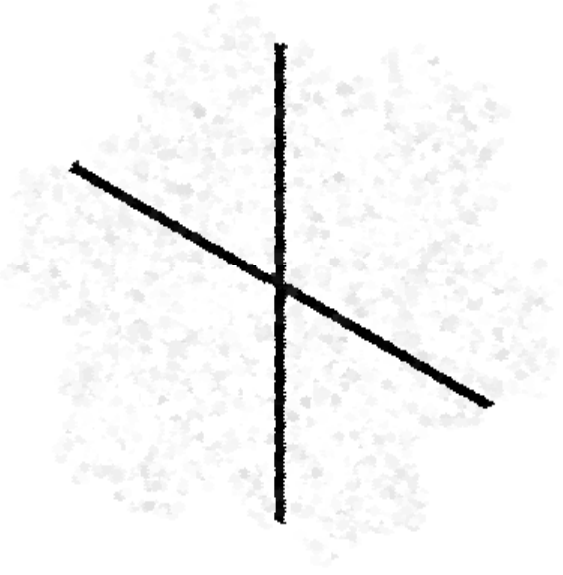

(d)

Figure 5.5: Synthetic data with 10% noise. (a) Rectangular sampled data. (b) EPS on rectangular data. (c) Hexagonally sampled data. (d) EPS on hexagonal data.

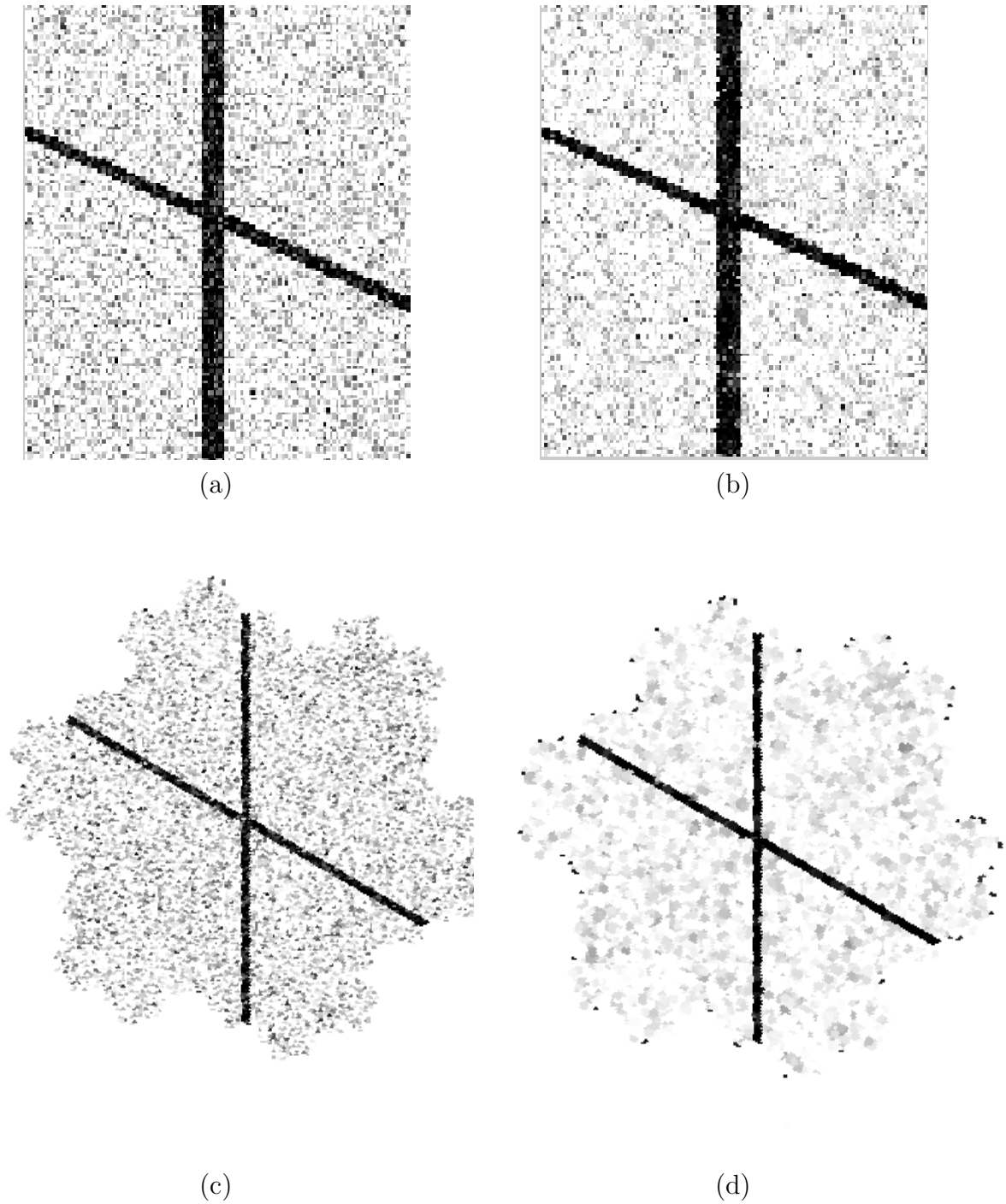

Figure 5.6: Synthetic data with 30% noise. (a) Rectangular sampled data. (b) EPS on rectangular data. (c) Hexagonally sampled data. (d) EPS on hexagonal data.

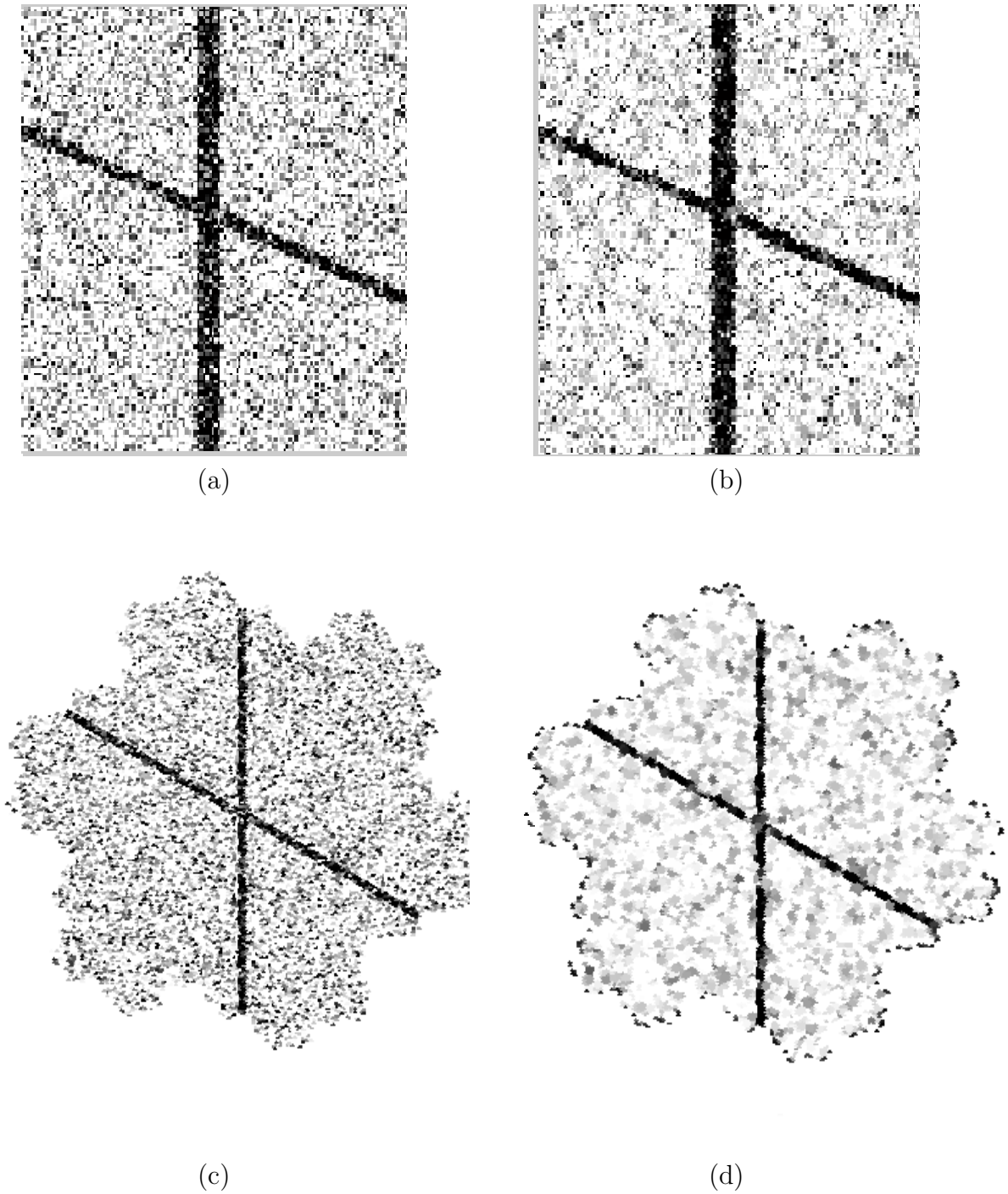

Figure 5.7: Synthetic data with 50% noise. (a) Rectangular sampled data. (b) EPS on rectangular data. (c) Hexagonally sampled data. (d) EPS on hexagonal data.

5.3.2 EPS on Seismic Data

EPS has been applied on real seismic data provided by Saudi Aramco. The application of EPS before edge detection results in sharper edges in the output and enhanced noise suppression. To compare both hexagonal and rectangular cases, same slices have been used in both cases. Let us consider the test slice 1 as shown in Fig. 5.8. The EPS on the test slice 1 is shown in Fig. 5.9. The noisy areas of the test slice have been smoothed while maintaining the edge sharpness.

It is evident from applying EPS on test slice 1, that the noise suppression is overall improved in case of Sobel with EPS. Similarly, in case of test slice 2, shown in Fig. 5.10, EPS results in smoothing of the small level of noise prevalent in this data. EPS gives a well defined sharp edge on a relatively smooth background as shown in Fig. 5.11.

5.3.3 Edge Detection with EPS on Seismic Data

The application of Sobel edge detection with EPS results in edge preservation as well as suppression of overall noise level. Furthermore, some smaller edges also become visible with the help of EPS. In Fig. 5.12, 3D Sobel filter has been applied on test slice 1 shown earlier. Despite the fact that edges have been detected, but the background noise is significantly present.

The application of EPS as a preprocessing step before Sobel edge detection leads to sharper edges and suppression of overall noise levels in the output. The

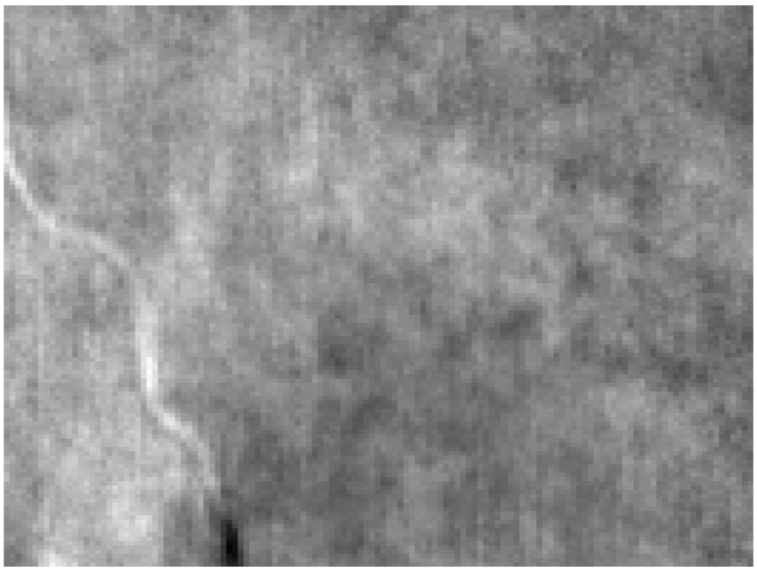

(a)

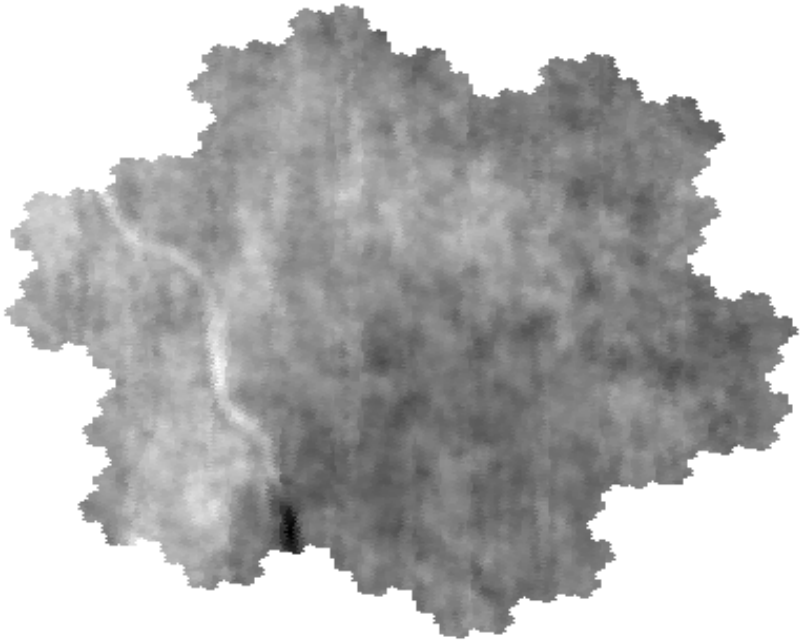

(b)

Figure 5.8: (a) Rectangular test slice 1. (Courtesy of Saudi Aramco.) (b) Hexagonal test slice 1.

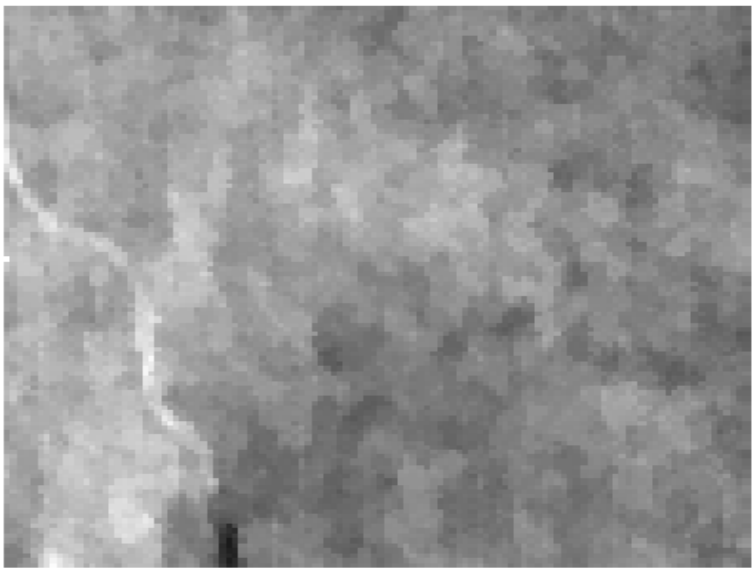

(a)

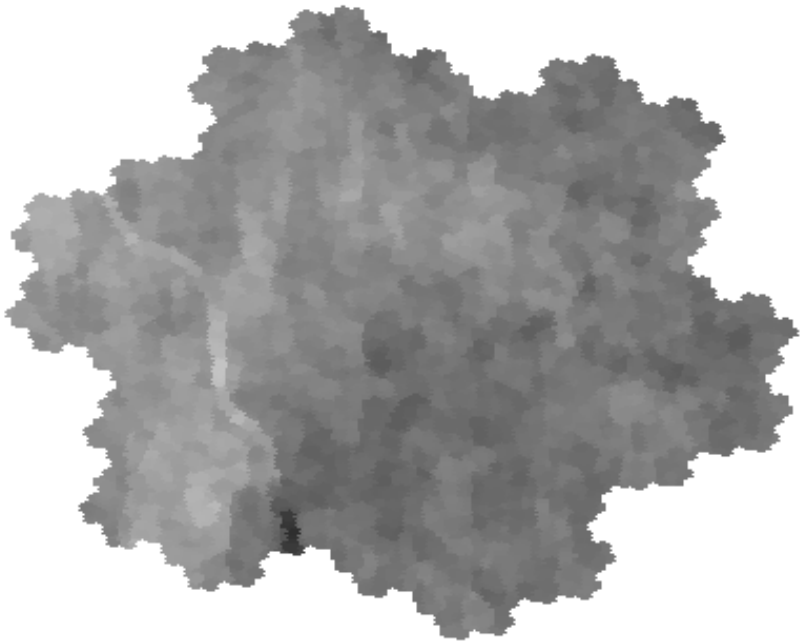

(b)

Figure 5.9: (a) EPS on rectangular test slice 1. (b) EPS on hexagonal test slice 1.

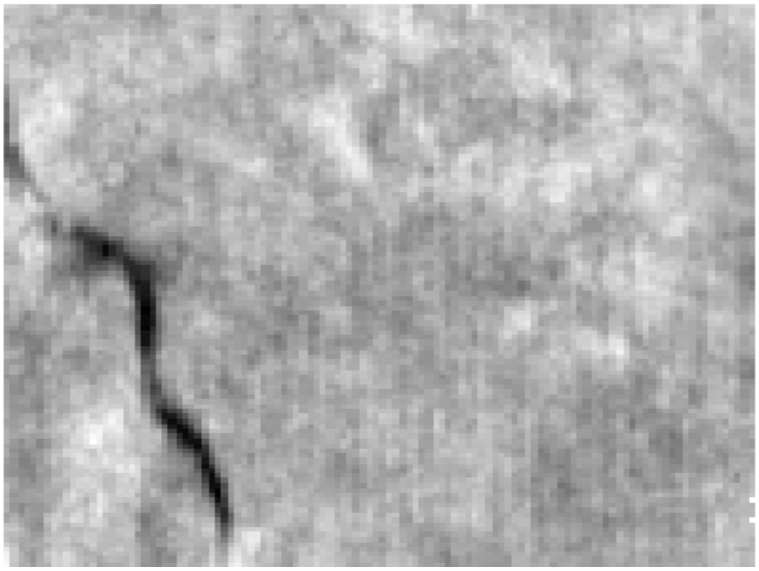

(a)

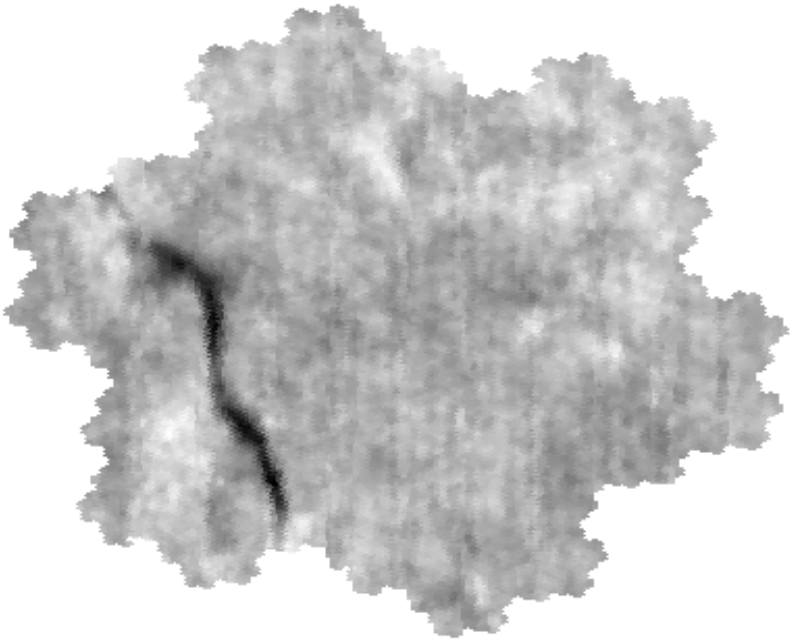

(b)

Figure 5.10: (a) Rectangular test slice 2. (Courtesy of Saudi Aramco.) (b) Hexagonal test slice 2.

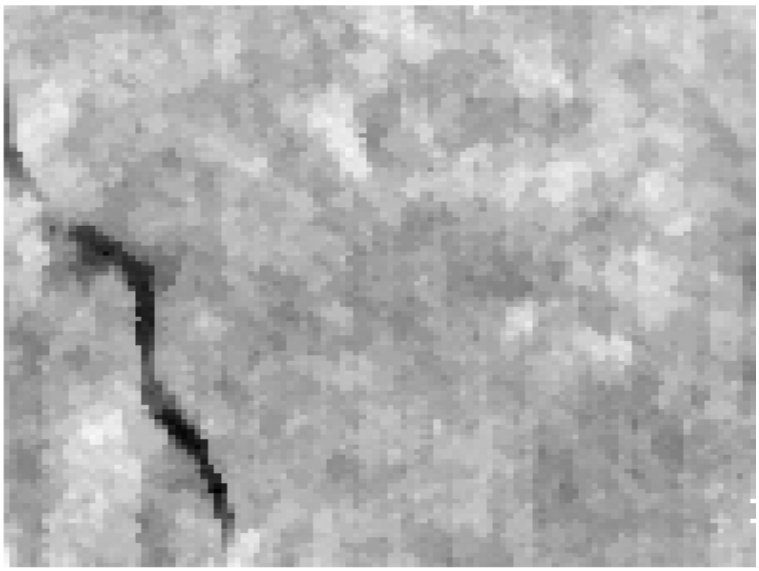

(a)

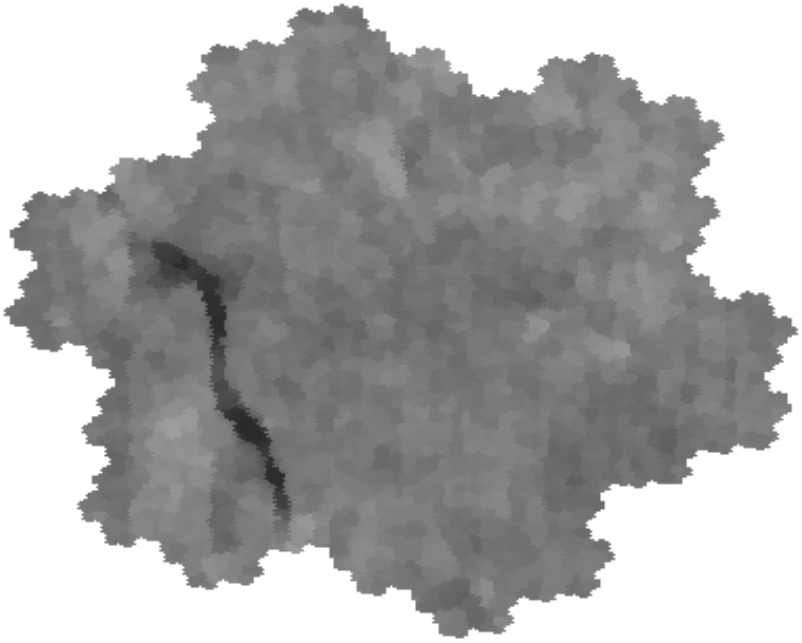

(b)

Figure 5.11: (a) EPS on rectangular test slice 2. (b) EPS on hexagonal test slice 2.

effect of EPS on edge detection can be seen in Fig. 5.13. It is evident that the noise levels have been suppressed significantly in case of EPS. The noise suppression is more effective in hexagonal sampled data.

Furthermore, the prominent edge on the lower left side of test slice 1 is much more pronounced in case of EPS. Moreover, several smaller edges have also been highlighted from the use of EPS with Sobel, which otherwise seemed noise in case of simple Sobel edge detection. As has been observed earlier, EPS has more pronounced effect in case of hexagonal approach, it is evident from this case, that the edge restoration and noise suppression is much less in rectangular case.

Similarly, in Fig. 5.14 the effects of Sobel edge detection on test slice 2 can be seen. We observe that the edges are perfectly detected in both sampling cases. The application of EPS on test slice 2 results in even sharper edge detection shown in Fig. 5.15. It is evident from this that EPS results in significantly sharper edges.

Moreover, EPS has also been applied on seismic data set containing faults. As per the previous case, it is evident, that EPS gives sharper images with a reduction in noise levels. The Sobel edge detection with EPS can be seen in Fig. 5.16, Fig. 5.17, Fig. 5.18 and Fig. 5.19. The backgrounds of edges are relatively smoother in the hexagonally sampled data.

(a)

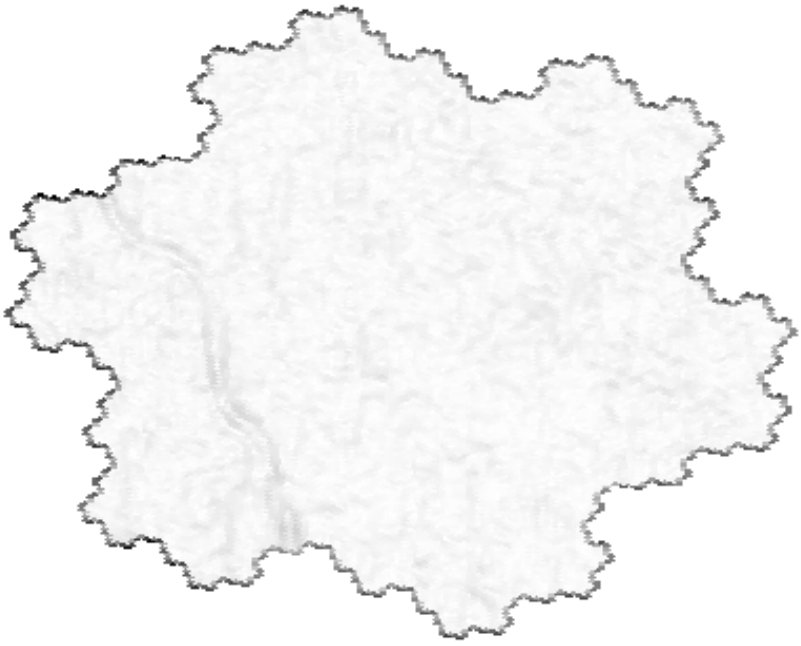

(b)

Figure 5.12: (a) Sobel edge detection on rectangular sampled test slice 1. (b) Sobel edge detection on hexagonal sampled test slice 1.

(a)

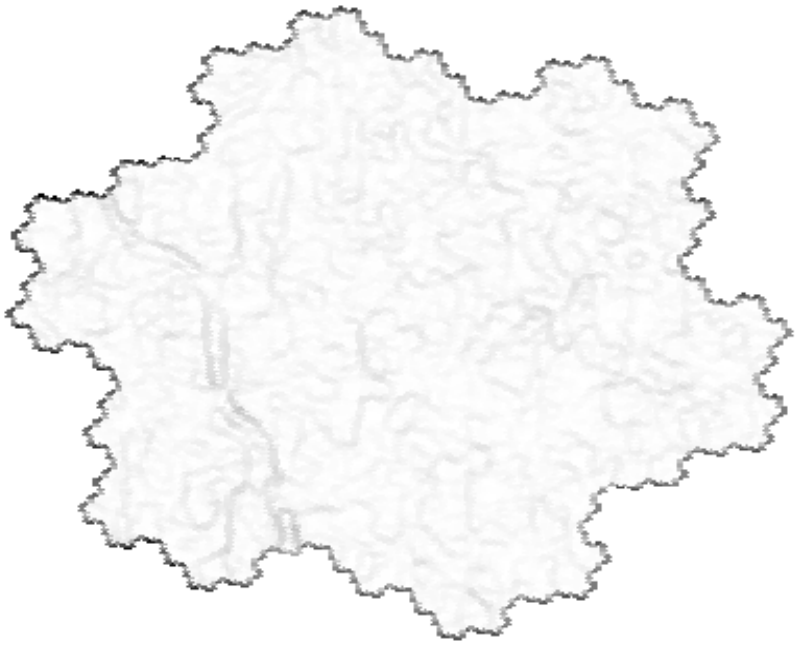

(b)

Figure 5.13: (a) Sobel edge detection with EPS on rectangular test slice 1. (b) Sobel edge detection with EPS on hexagonal test slice 1.

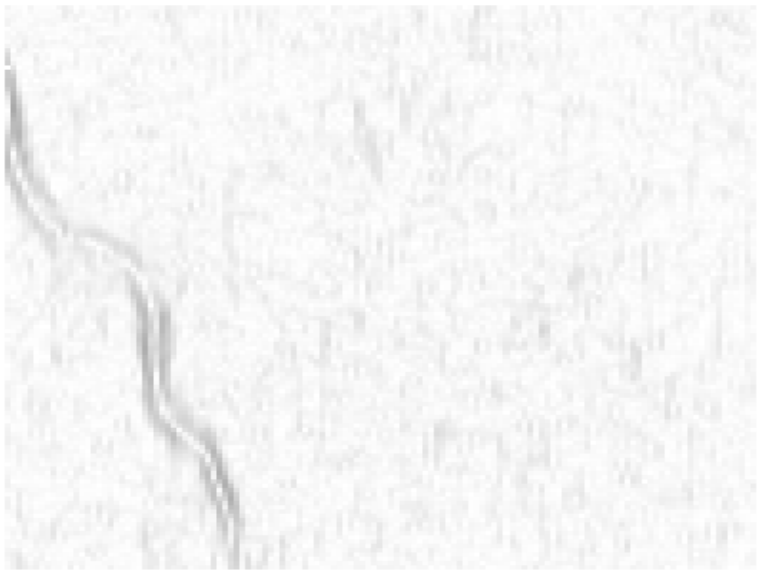

(a)

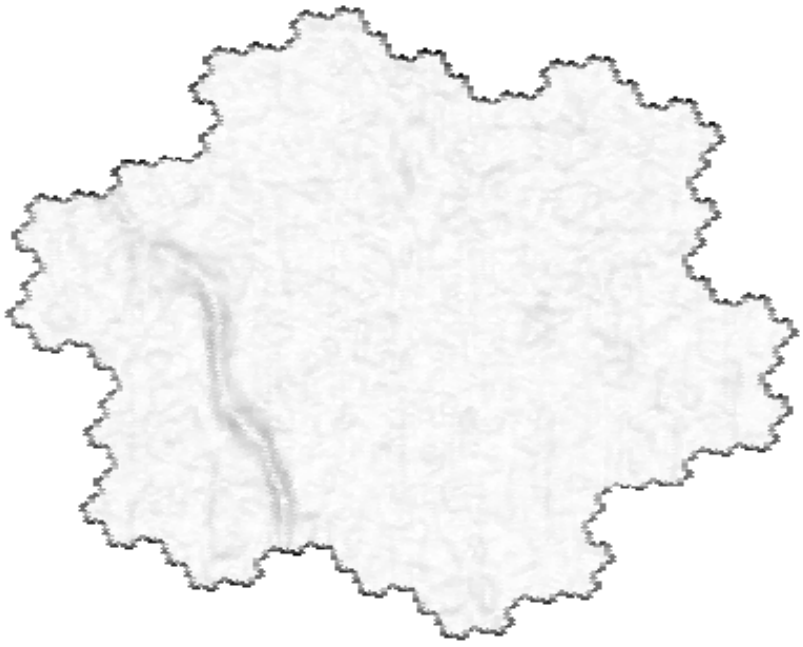

(b)

Figure 5.14: (a) Sobel edge detection on rectangular sampled test slice 2. (b) Sobel edge detection on hexagonal sampled test slice 2.

(a)

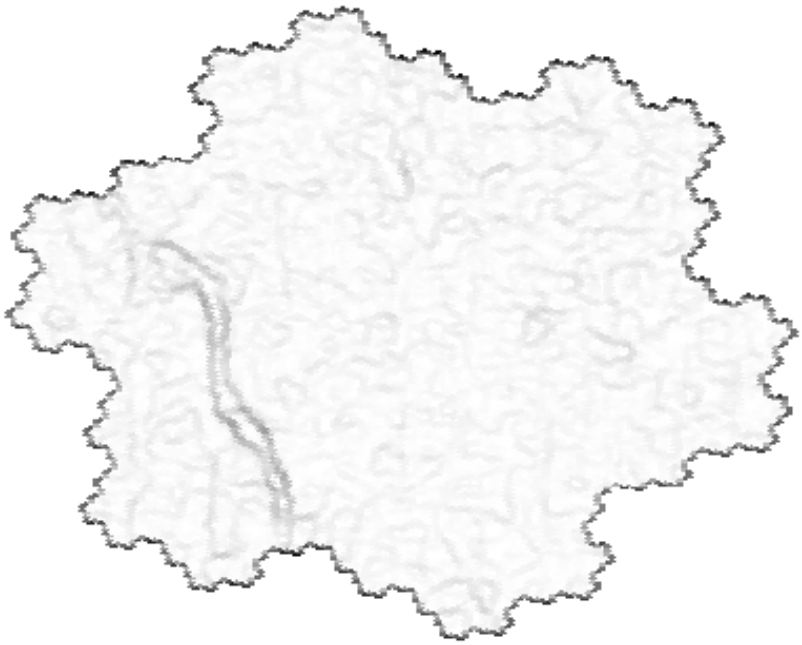

(b)

Figure 5.15: (a) Sobel edge detection with EPS on rectangular test slice 2. (b) Sobel edge detection with EPS on hexagonal test slice 2.

By comparing the results of Sobel with EPS of seismic fault slices to the edge detection without EPS results of previous chapter (see Fig. 4.7, Fig. 4.7, Fig. 4.7 and Fig. 4.7), it is visible that the edge sharpness is better and noise levels have been suppressed.

The comparison of SA EPS with regular rectangular EPS displays considerable crispness of edges as can be seen from Fig. 5.20. This section of test slice 2 contains vertical, diagonal and horizontal edges in addition to a curvature. It is evident that SA Sobel with EPS results in much sharper and accurate edge detection as compared to other three approaches. The SA Sobel results in smoother edge following as compared to the rectangular edge detection.

Moreover, the noise suppression is exceptionally well, owing to EPS. The noise reduction is more in case of hexagonal approach in this section. SA edge preserving and detection ability is exponentially better than the rectangular case because of the inherent increased symmetry associated with a hexagon.

Furthermore it must be kept in mind that the processing time of SA EPS is nearly 2 times better than rectangular EPS. The EPS code was run on core i5 2.4 GHz computer. This time saving is due to the unique data handling capability associated with SA and the lesser number of overall neighbors.

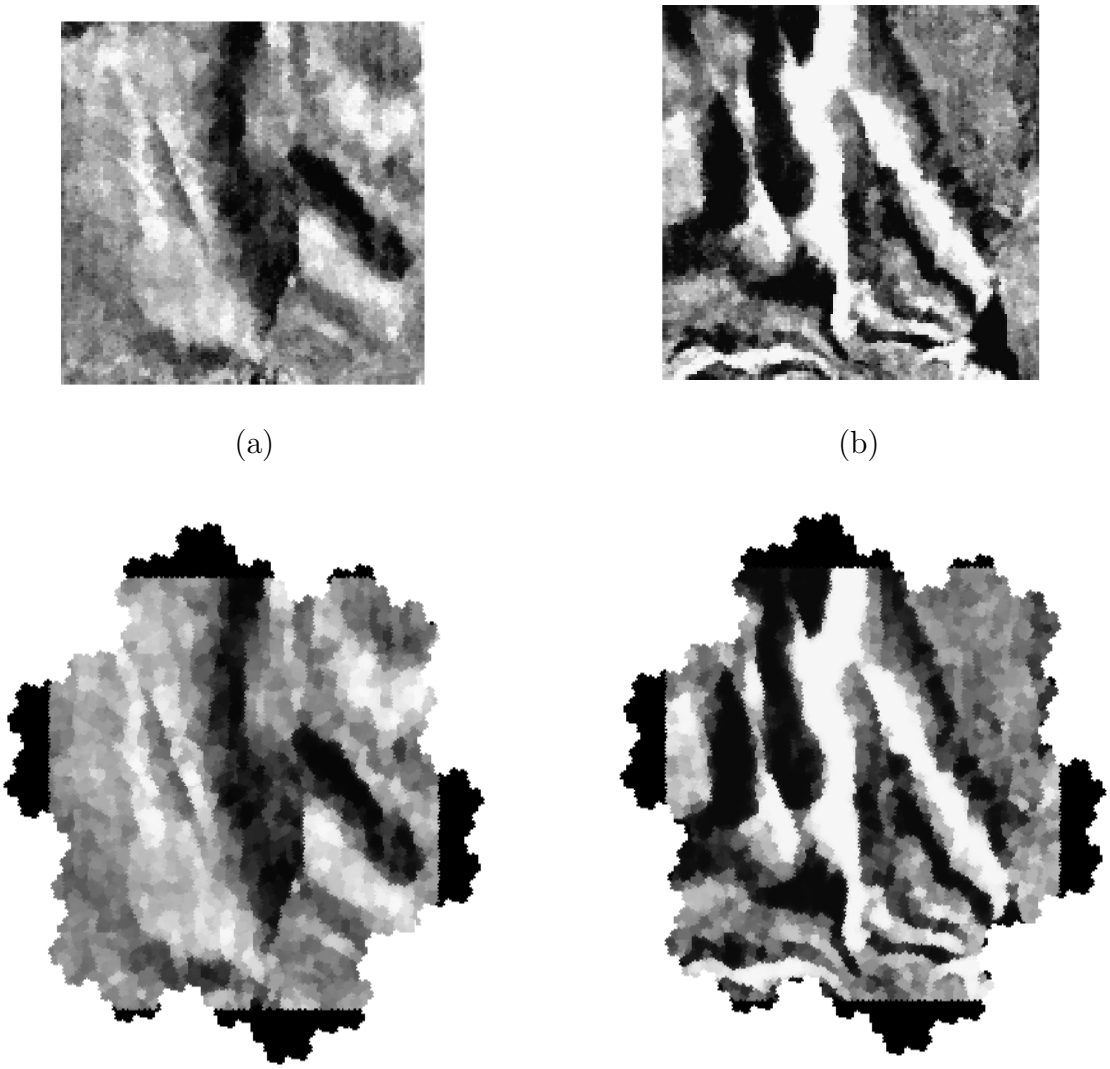

Figure 5.16: EPS on seismic data set containing faults. (a) Rectangularly sampled slice 1. (b) Rectangularly sampled slice 2. (c) Hexagonally resampled slice 1. (d) Hexagonally resampled slice 2.

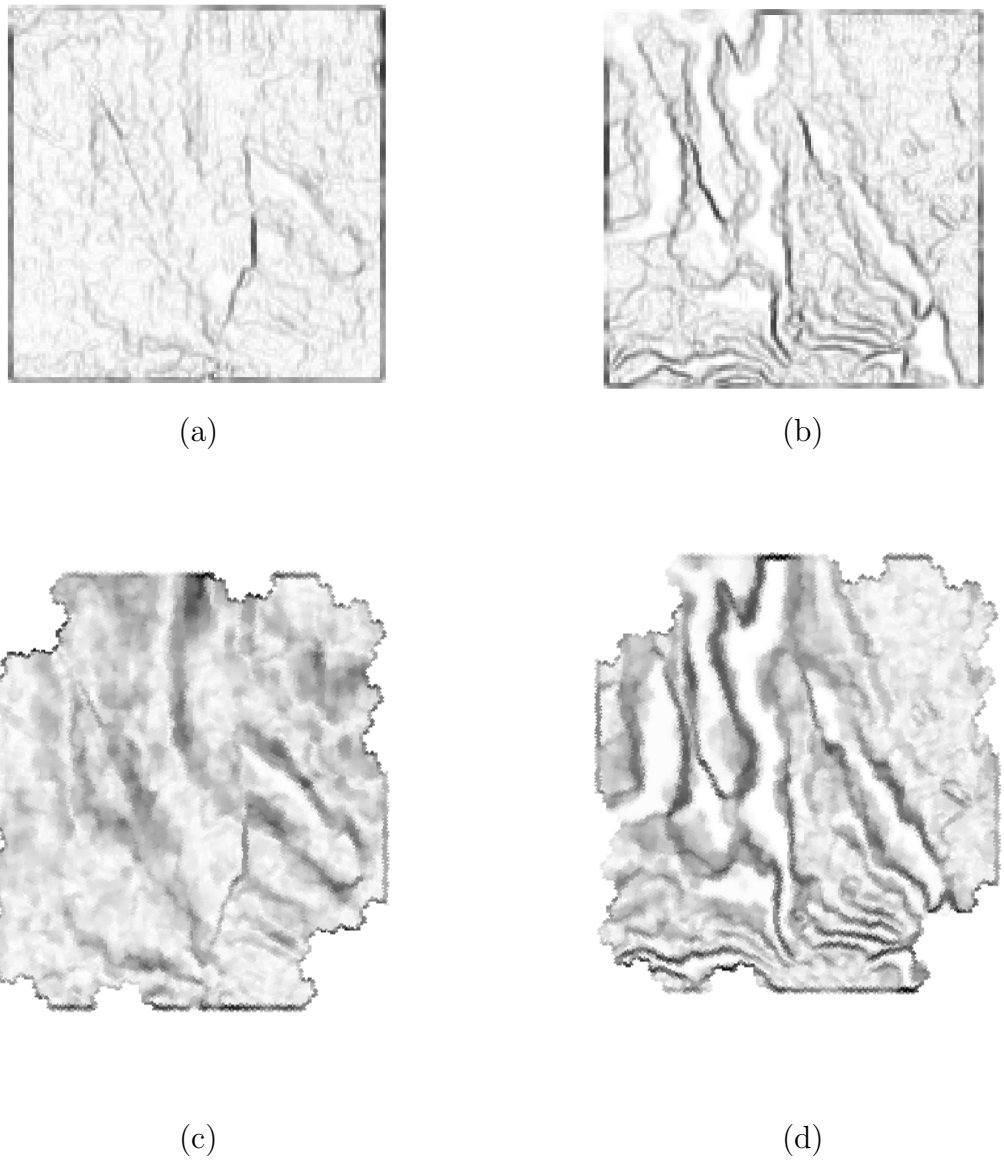

Figure 5.17: 3D Sobel filter with EPS for edge detection of seismic data set containing faults. (a) Rectangularly sampled slice 1. (b) Rectangularly sampled slice 2. (c) Hexagonally resampled slice 1. (d) Hexagonally resampled slice 2.

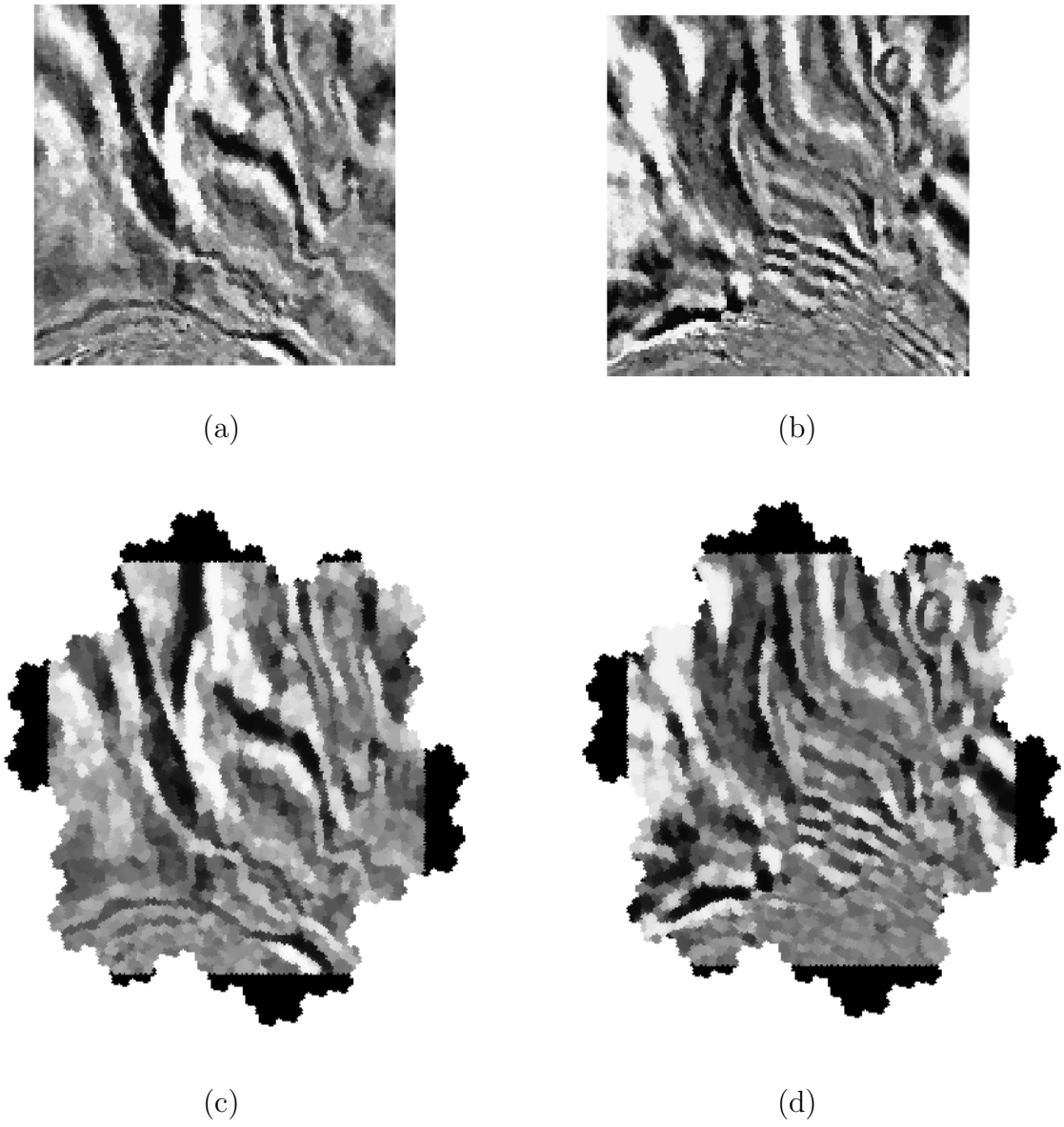

Figure 5.18: EPS on seismic data set containing faults. (a) Rectangularly sampled slice 3. (b) Rectangularly sampled slice 4. (c) Hexagonally resampled slice 3. (d) Hexagonally resampled slice 4.

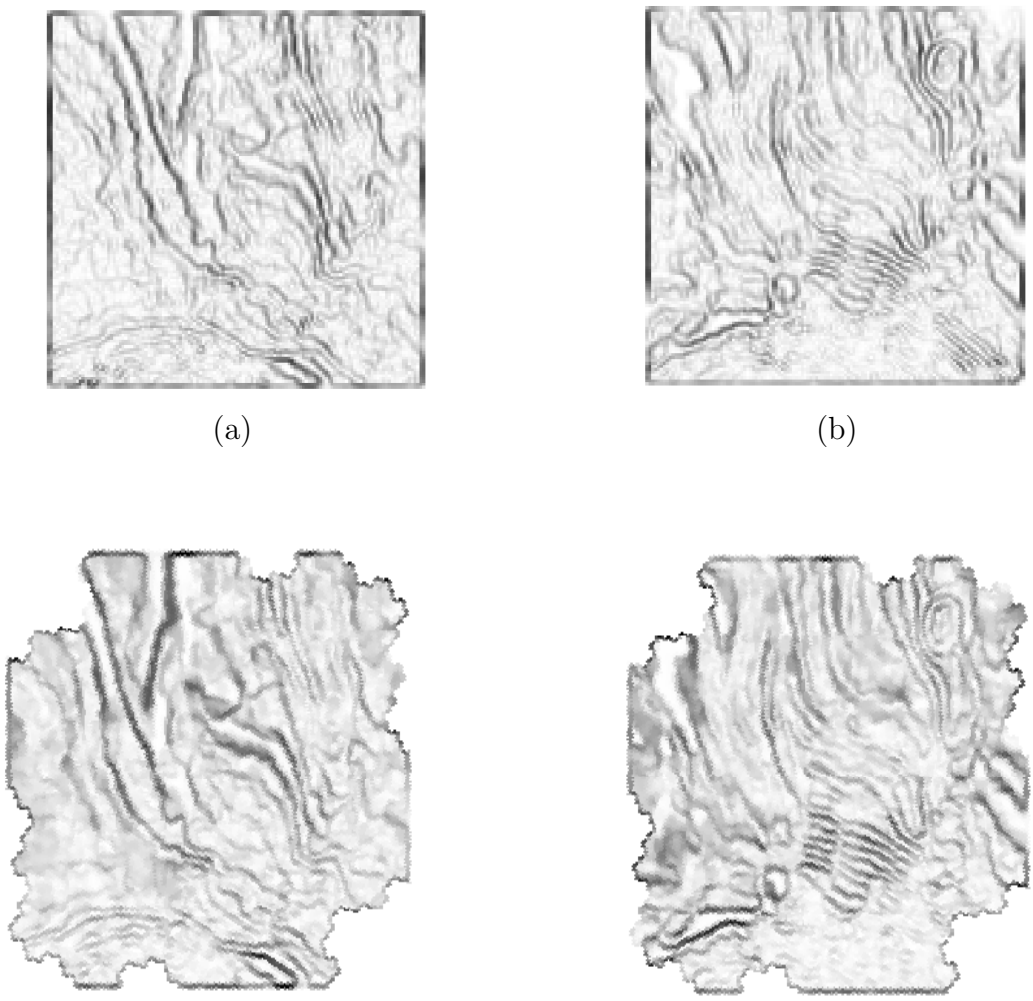

Figure 5.19: 3D Sobel filter with EPS for edge detection of seismic data set containing faults. (a) Rectangularly sampled slice 3. (b) Rectangularly sampled slice 4. (c) Hexagonally resampled slice 3. (d) Hexagonally resampled slice 4.

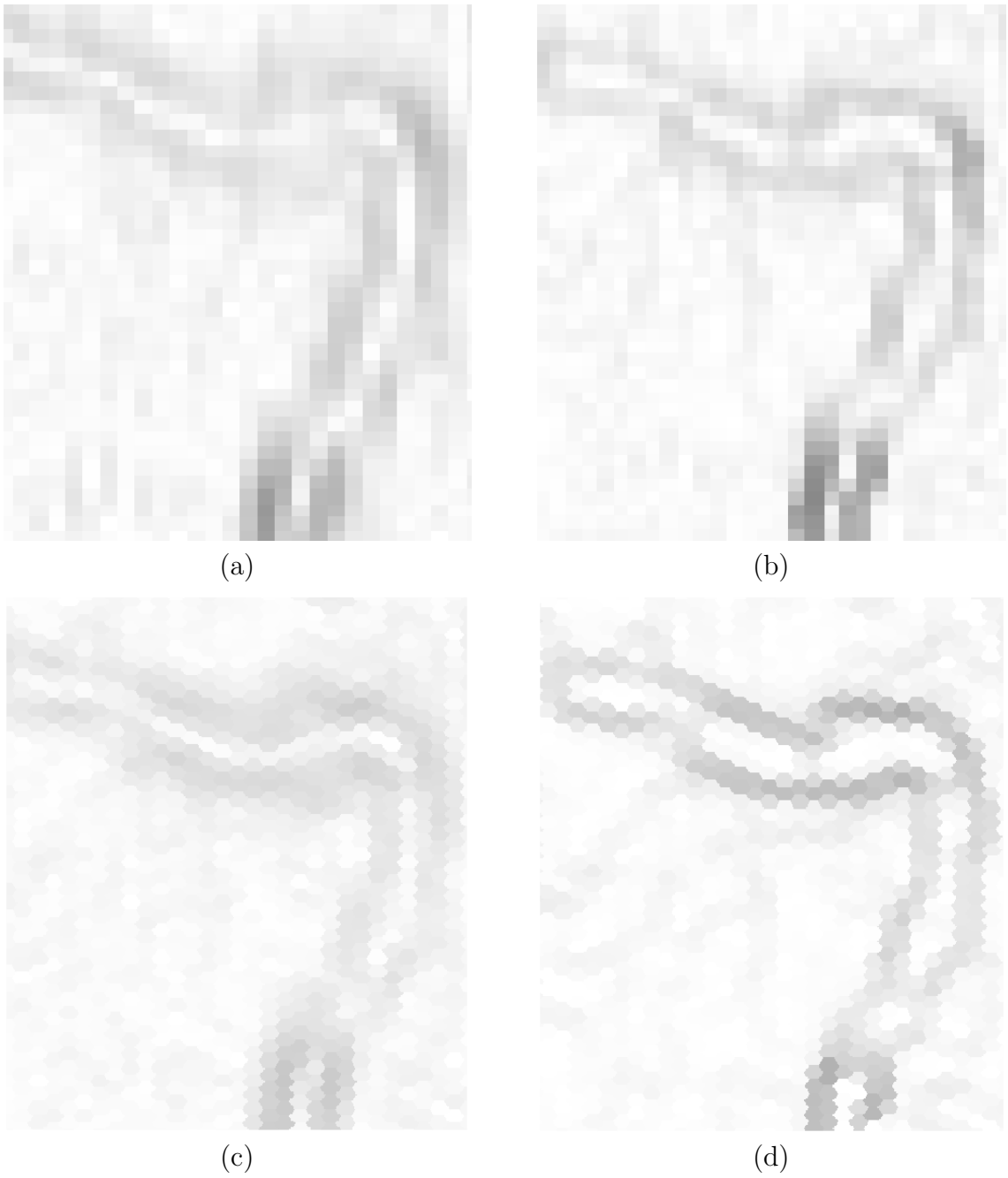

Figure 5.20: Edge detection comparison. (a) Sobel edge detection on rectangular sampled data. (b) Sobel edge detection with EPS on rectangular sampled data. (c) Sobel edge detection on hexagonal sampled data. (d) Sobel edge detection with EPS on hexagonal sampled data.

The comparison of 2D EPS with 3D EPS can be seen on Fig.5.21. It must be noted that in case of 3D EPS, the same 2D neighbourhoods shown earlier have been extended to three dimensions. The 2D and 3D EPS on the test slice are shown in Fig.5.22. The edge detection can be seen in Fig.5.23. The zoomed in version in Fig.5.24 shows that 3D EPS reveals hidden edges which were otherwise undetected by 2D EPS.

5.4 Conclusion

The edge preserving smoothing algorithm has been successfully modified to the spiral architecture domain. The SA EPS has worked exceptionally well with even high levels of noise. The processing efficiency of SA domain is an added benefit. Moreover on real data, EPS has been tested and it has verified its efficiency of maintaining edge sharpness while simultaneously suppressing noise unlike simple averaging or low pass filters. The edge sharpness and noise suppression is visibly better in SA hexagonal approach in comparison to rectangular approach.

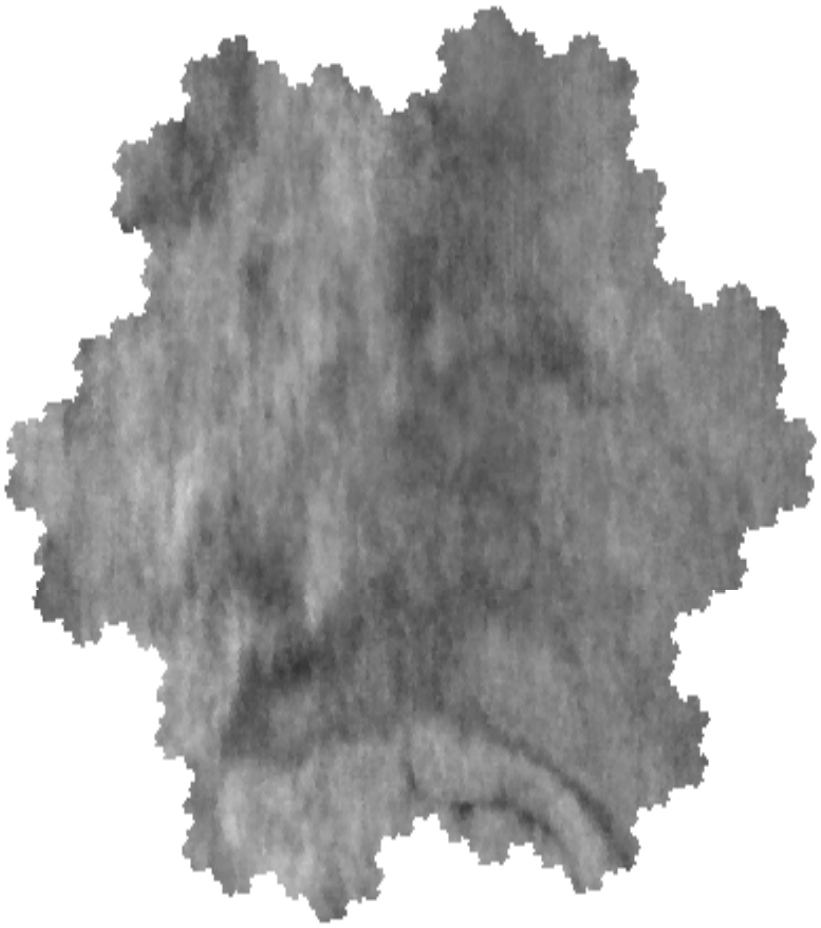

Figure 5.21: Test slice for comparison of 2D EPS with 3D EPS.

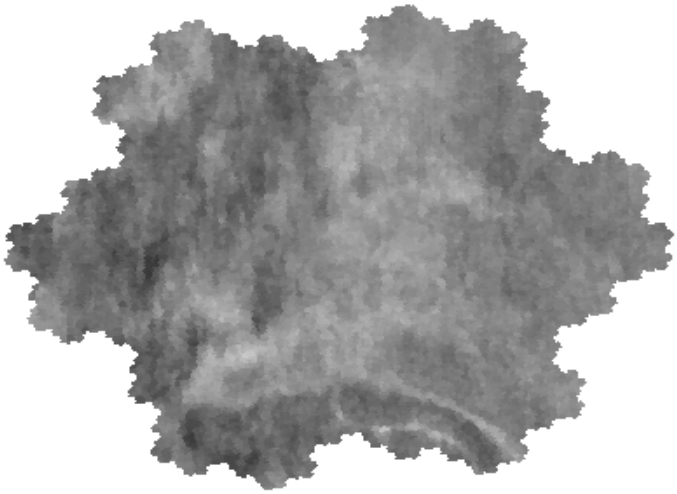

(a)

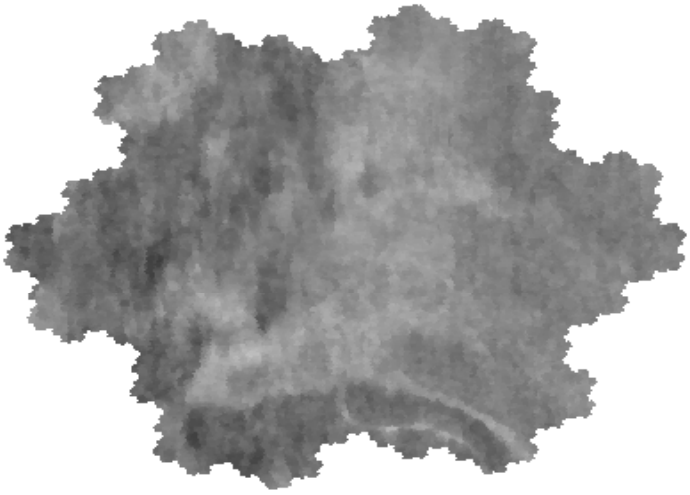

(b)

Figure 5.22: (a) 2D EPS. (b) 3D EPS.

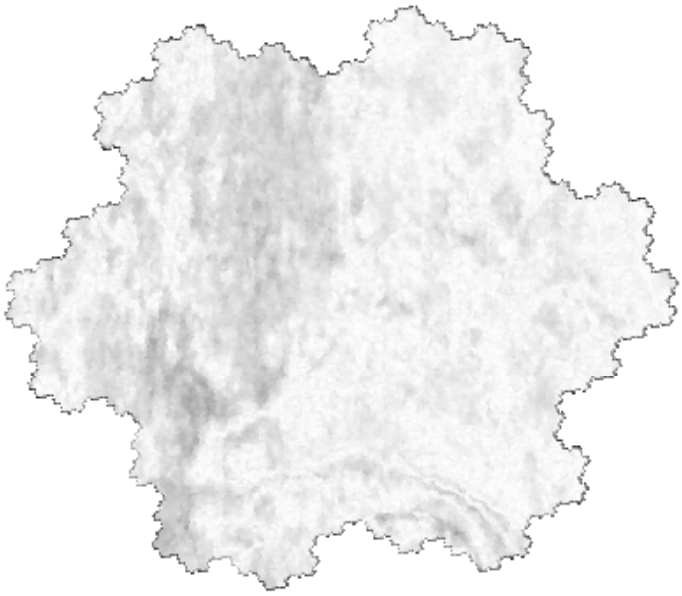

(a)

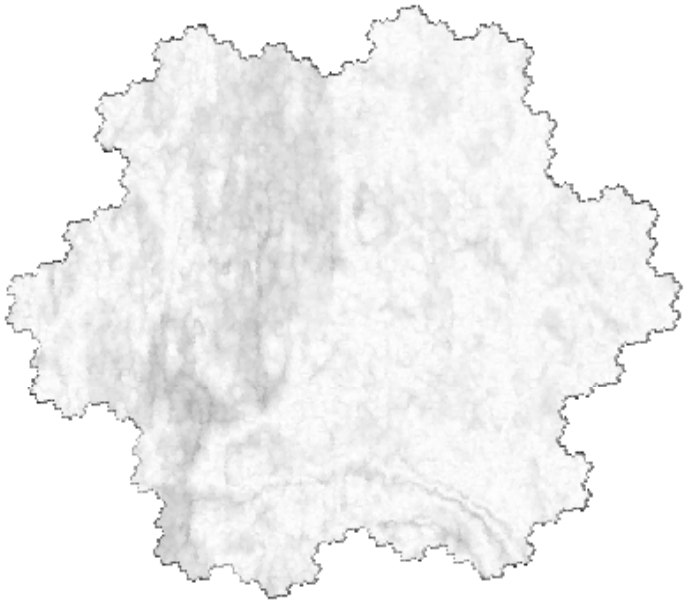

(b)

Figure 5.23: (a) Sobel on 2D EPS. (b) Sobel on 3D EPS.

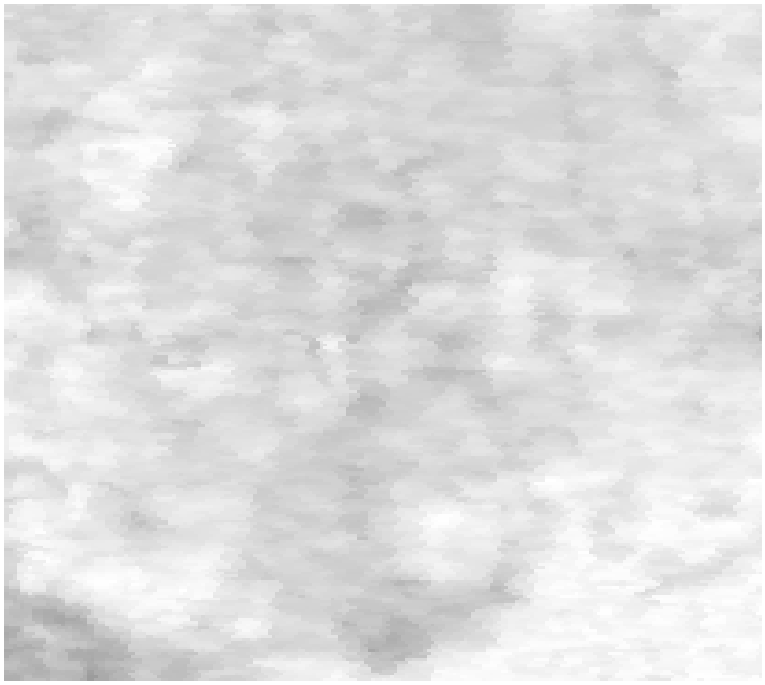

(a)

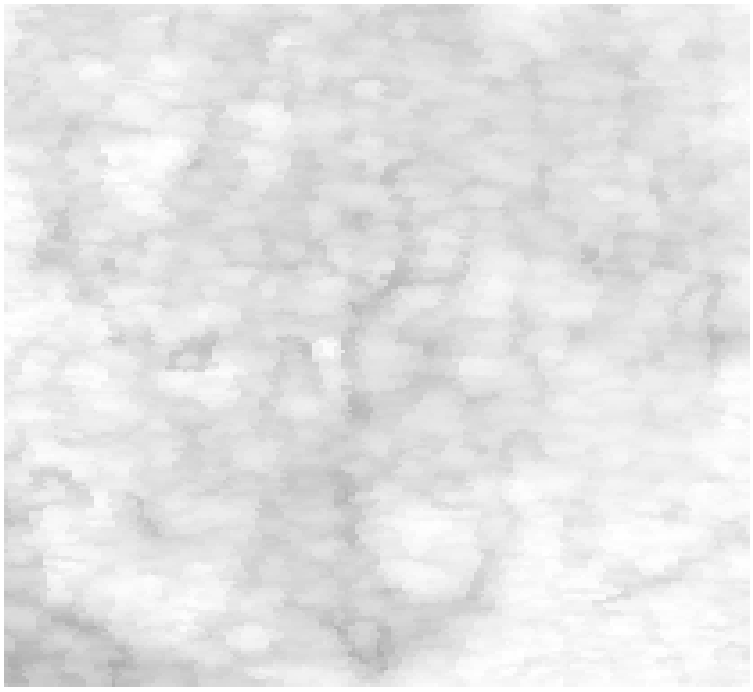

(b)

Figure 5.24: (a) Magnified section of sobel on 2D EPS. (b) Magnified section of sobel on 3D EPS.

CHAPTER 6

CONCLUSIONS

In this research work, a novel approach was applied on the problems associated with huge amounts of seismic data encountered in the seismic signal processing. In this research work, hexagonal sampling, the most optimum method to sample circularly band limited signals due to closer approximation and reduced number of samples, has proven its efficiency, extending the early work of 2D spiral architecture handling method to the case of 3D seismic data. It has been shown that, with the help of a dedicated hexagonal toolbox, existing algorithms for various seismic processes can be easily converted to the spiral architecture domain. Once these processes have been modified as per the spiral architecture, the advantages of hexagonal sampling can be easily extracted.

It has been shown that spiral approach for filter design is efficient than the zero insertion approach for filter design using POCS. The zero insertion method introduces aliasing, whereas the spiral method is computationally efficient and

free of any aliasing due to zero insertion (when zero insertion is used to represent hexagonally sampled seismic data). This is because the true hexagonal arithmetic has been used rather than rectangular methods to deal with hexagonally sampled data. Furthermore, the data requirement is far less in SA approach than rectangular or zero insertion approach.

Similarly, in the field of seismic interpretation, no work had been carried out regarding the application of SA for edge detection in 3D data. In this work, we have shown that spatial filters can be easily designed in the spiral domain as well. 3D edge detection filters have been designed and tested on real data. The SA based Sobel edge detection has been able to detect edges perfectly.

Moreover, the edge preserving smoothing algorithm has also been applied to the hexagonal data as a pre processing step for edge detection. The results have been compared with existing rectangular methods. It can be easily seen that curve following ability in hexagonally sampled data is much better than that of the rectangular Sobel filter. The noise suppression is better in case of SA due to increased symmetry of spiral neighbourhood. Furthermore, the multidimensional data handling ability of the spiral architecture assists in significantly reducing the processing time.

The reduction in size of data, superior quality of results and exponential de-

crease in computational time makes it ideal for the oil and gas industry. The application of spiral architecture to seismic data can lead to higher resolution of seismic data. This higher resolution is pivotal for accurate determination of oil and gas. As such, the adoption of spiral architecture based algorithms can significantly enhance the resolution of seismic data by simultaneously reducing the time and resources required by the industry for seismic signal processing.

6.1 Future Work and Suggestions

In this research work, fundamentally, a proof of concept has been presented that hexagonally sampled seismic exploration data can be processed efficiently based on the SA. Only the basic spatial and spectral operations of the existing algorithms need to be converted into the spiral domain operations. These spiral domain operations have already been created and tested as evident from this research work. As such, all of the basic operations carried out in industry for seismic exploration can be converted to the spiral domain.

The spiral domain toolbox that has been created can be further improved by re writing the codes in a low level language like C, C++ and FORTRAN to increase the computational efficiency of the spiral architecture. A low level language based spiral toolbox will be much more efficient and practical from an industrial point of view to carry out various processes on seismic data. Such a toolbox can be used to develop a complete set of seismic data processing set of algorithms for 3D hexagonally sampled data.

APPENDIX

A.1 Data Resampling & Basic Operations

The MATLAB toolbox is capable of resampling rectangularly sampled data to hexagonal domain. This step is crucial since the data available is generally rectangularly sampled and needs to be converted to hexagonal domain. The process of converting an image sampled on one lattice to another is termed resampling. There are two types of resampling of interest here. They are resampling an image from a square to a hexagonal lattice and, from a hexagonal to a square lattice. The first type of resampling serves as a solution for acquisition of hexagonal images given a square image source such as a camera or a processed image. This is of interest in implementing either a complete hexagonal image processing system or a mixed system. The second type of resampling is useful when further processing is desired to be done using square images. This is not relevant to this research work.

In devising solutions for hexagonal image acquisition through resampling, one can use an exact or an approximate solution. In the exact solution, resampling can be done such that the output samples are on a true (regular) hexagonal grid. Consequently, the acquired image will have regular hexagon shaped pixels. A discrete image, $f(m, n)$, has an associated lattice L defined as:

$$L = \{m\mathbf{b_1} + n\mathbf{b_2} : m, n \in \mathbb{Z}\}$$

The vectors $\mathbf{b_1}$ and $\mathbf{b_2}$ are basis vectors which generate the lattice. Different lattices hence have different basis vector sets as generators. The basis vector set $\mathrm{B} = \mathbf{b_1}\ ,\mathbf{b_2}$ corresponding to the square lattice L_s is given by:

$$\mathbf{B_s} = \left\{ \begin{bmatrix} 1 \\ 0 \end{bmatrix}, \quad \begin{bmatrix} 0 \\ 1 \end{bmatrix} \right\}$$

Similarly, the basis vector set B corresponding to the hexagonal lattice L_h is given by:

$$\mathbf{B_h} = \left\{ \begin{bmatrix} 1 \\ 0 \end{bmatrix}, \quad \frac{1}{2} \begin{bmatrix} -1 \\ \sqrt{3} \end{bmatrix} \right\}$$

These lattices together with the generating basis vectors are shown in the following figure

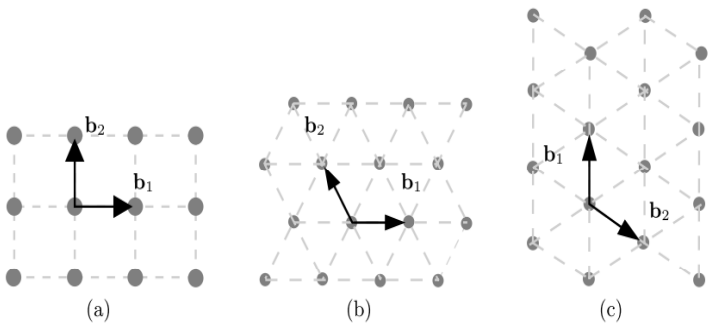

Figure. A.1 Basis vectors for (a) square (b) horizontally aligned hexagonal lattice (c) vertically aligned hexagonal lattice. Courtesy of [15].

In the process of resampling, the change in the lattice (original to desired) is effected by first reconstructing a continuous image from the original image samples via interpolation. This reconstructed image is then resampled with the desired

lattice. These steps are illustrated in the following figure.

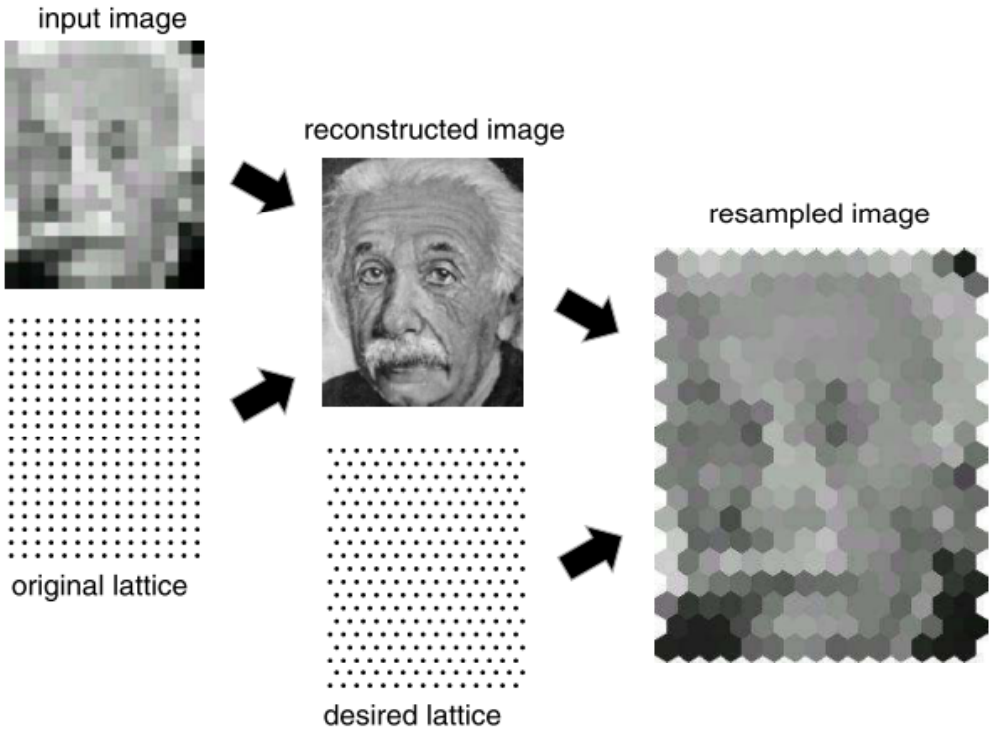

Figure. A.2 Image resampling on a hexagonal lattice. Courtesy of [15].

Since, only samples at points on the desired lattice are of interest, the reconstruction and resampling with the desired lattice can be combined. Hence, given an image $f_s(m,n)$ defined on a square lattice with $M \times N$ points, the desired hexagonal image, $f_h(x,y)$ is found as:

$$f_h(x,y) = \sum_{m=0}^{M-1} \sum_{n=0}^{N-1} f_s(m,n)\, h(x-m, y-n)$$

where, h is the interpolating kernel for the reconstruction scheme and (m,n) and (x,y) are sample points in the original square and the desired hexagonal

images, respectively. There are two major issues in this resampling procedure and these are the choice of the hexagonal lattice and the interpolating kernel. Two different hexagonal sampling lattices shown can be used for resampling. The lattice in Figure A.1(c) is obtained by rotating the one in Figure A.1(b) clockwise, by 30 degrees. These two basis vectors can be labelled as $\mathbf{B_{h1}}$ for Figure A.1(b) and $\mathbf{B_{h2}}$ for Figure A.1(c). Note that, $\mathbf{B_{h1}}$ and $\mathbf{B_{h2}}$ are also rotated versions of each other.

Both $\mathbf{B_{h1}}$ and $\mathbf{B_{h2}}$ differ from $\mathbf{B_s}$ only by a single basis vector as a result of which $\mathbf{B_{h1}}$ and $\mathbf{B_s}$ have the same horizontal spacing and $\mathbf{B_{h2}}$ and $\mathbf{B}_s$ have the same vertical spacing. Consequently, the samples are more densely packed in a hexagonal lattice in the direction in which its basis vector differs from the square lattice. It is possible to pick either of these lattices to provide a uniform fit in either the horizontal or vertical directions. Now, if an image is to be resampled from an $M \times M$ square image then the choice of $\mathbf{B_{h1}}$ will result in one of two possibilities: horizontal lattice spacing is fixed or vertical lattice spacing is fixed. If the horizontal lattice spacing is fixed to give M points, this will result in 15% extra vertical points due to its closer packing ($\sqrt{3}/2$ versus 1). This can lead to vertically elongated images if a simple approach (with uniform sized tiles) is used for visualisation. Alternatively, if the vertical lattice spacing is fixed so as to yield M points, an image with 15% fewer horizontal points will be produced. Once again, using a simple approach for visualisation will result in an image with an

inappropriate aspect ratio. These points are illustrated in Figure A.3. Note that using a fixed vertical spacing results in a coarser overall image. These problems also occur, though in reverse, if $\mathbf{B_{h2}}$ is the choice for the resampling lattice.

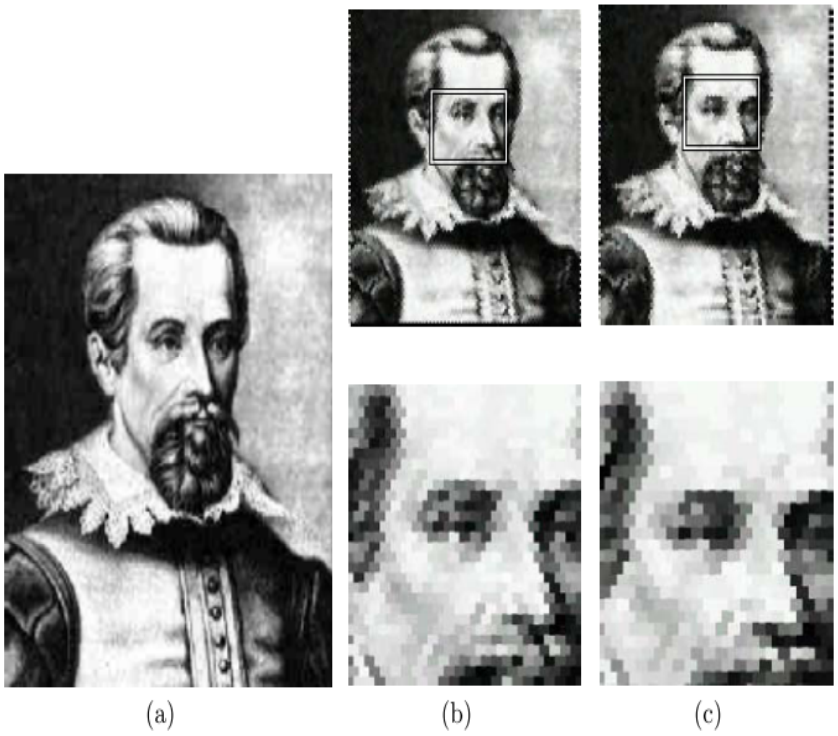

Figure. A.3 Two options in resampling onto a hexagonal lattice:
(a) Original image (b) and (c) resampled images (top row)
with fixed horizontal and vertical spacing respectively,
with magnified portions (bottom row) Courtesy of [15].

The final issue in resampling is the interpolating kernel. The accuracy and computational cost of resampling are determined by the type of interpolation used. For computational efficiency, we will consider only separable kernels of the form:

$$h\left(x,y\right)=h_1\left(x\right)h_2\left(y\right).$$

The simplest form of interpolation that can be used is the nearest neighbour method. Here, each interpolated output pixel is assigned the value of the nearest sample point in the input image. The corresponding 1D kernel is given as:

$$h(x) = \begin{cases} 1 \ if \ 0 \leq |x| \leq \frac{1}{2} \\ \\ 0 \ if \ \ |x| \geq \frac{1}{2} \end{cases}$$

This method requires no direct computation and only copying of values from the input to output images. There exist more advanced choices for the resampling kernel [15]. However, these are more computationally intensive. Once the data is in hexagonal domain, all the algorithms of SA can be tested. Consider the rectangular and resampled hexagonal test image shown in the test figure.

The apparent difference between rectangular and hexagonal test slices is not visible. In order to understand the difference it is better to zoom in at a certain section and view the shape of the pixels closely. Consider the region in the red box of hexagonal test image. It is evident that even the shape of the pixel is a hexagon in this toolbox. The hexagonal sampling renders the regular (rectangular) image into a hexagonally sampled image by changing the shape of the underlying pixel shape.

(a)

(b)

Figure. A.4 Test image. (a) Rectangularly sampled. (b) Hexagonally sampled.

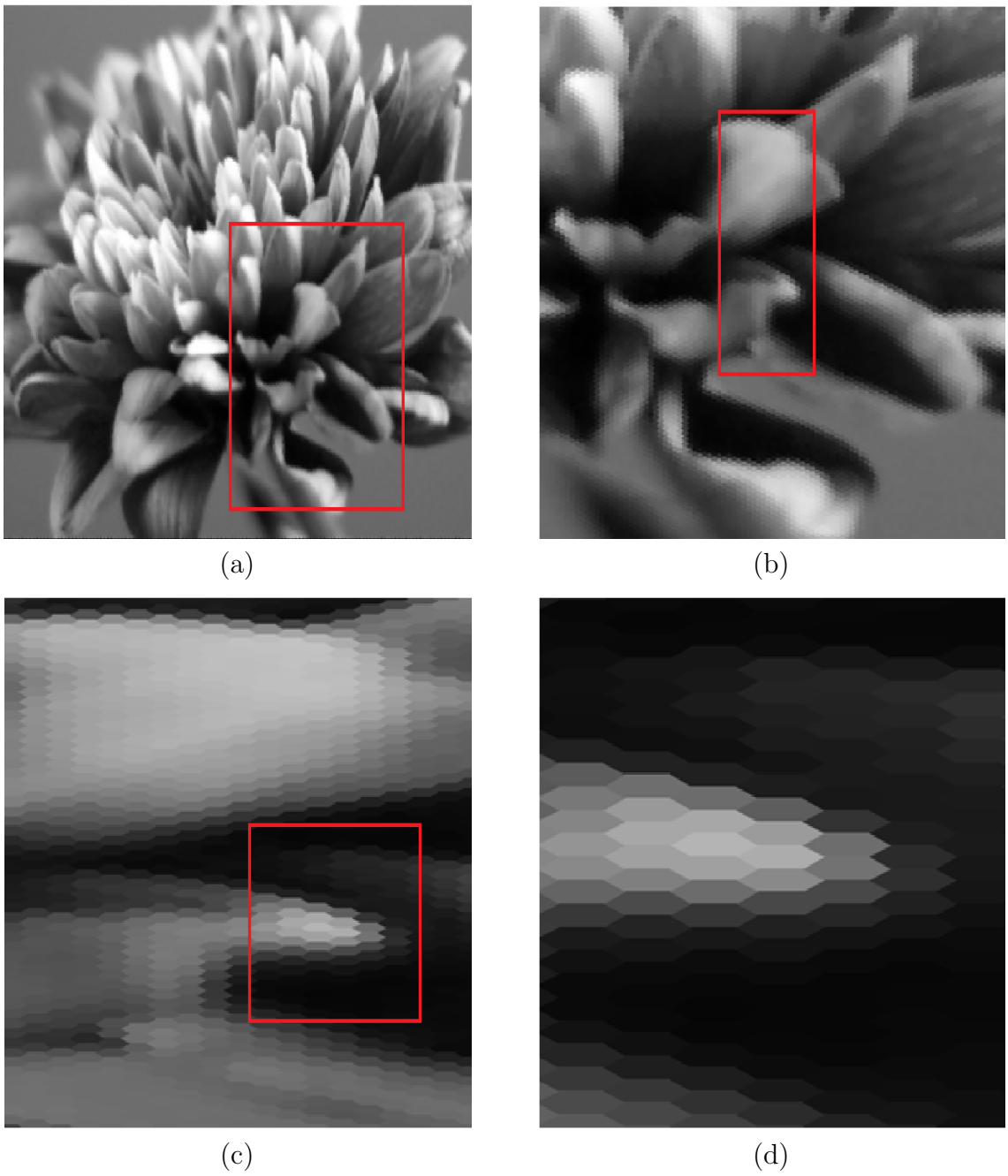

Figure. A.5 (a) Hexagonally sampled test image. (b) Magnified region of the test image. (c) Second magnification of test image. (d) Third magnification of test image.

The MATLAB toolbox is capable of resampling a 2D data or even a 3D data to hexagonal sampled version. In dealing with 3D data, the layers are resampled to hexagonal version. Considering a volumetric data in the x, y and z axis. Only the data lying in $x-y$ plane will be converted to the hexagonal domain. Once layer by layer resampling has been achieved, the resampled layers are only stacked on one another. The $x-z$ or $y-z$ resampling is not carried out.

The SA spatial domain algorithms involve arithmetic and neighborhood operations. In order to prove the working of SA toolbox consider the example of convolution on the test image. The test image has been convolved with an aggregate level 1 averaging mask. The result of convolution given by Eq. 2.25 is shown on next page. As can be seen this figure is blurred in comparison to the original image. For further clarity, the zoomed in version of the original and convolved images can be seen.

The Fourier transform of the test image is also shown. Just like regular spectral domain processing, filters can be designed to process the data in the spectral domain. Ideal low pass filters have been shown in which the passband region increases from just 49 elements i.e., 7^2 elements to 2401 elements i.e., 7^4 elements. It is evident with increase in passband region; the blurriness of the output image gets reduced. Similarly, a high pass filter has also been shown. The effect of high pass filter is an increase in the sharpness of the image. This is because all the low level frequencies are stopped and only high level frequencies are allowed to pass through.

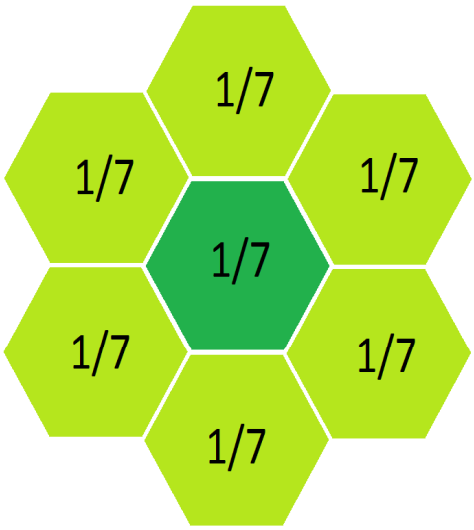

(a)

(b)

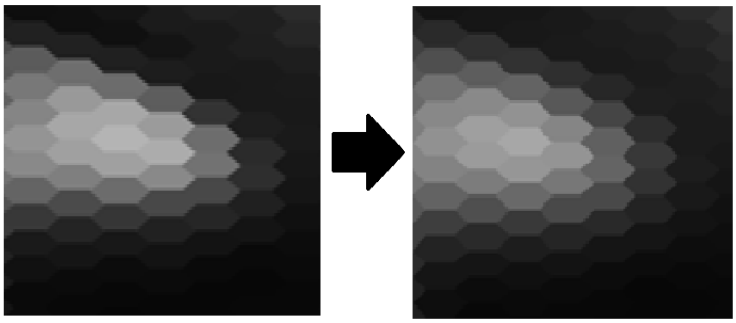

(c)

Figure. A.6 (a) Averaging/smoothing mask. (b) Test image convolved with averaging mask. (c) Magnified section of convolved test image.

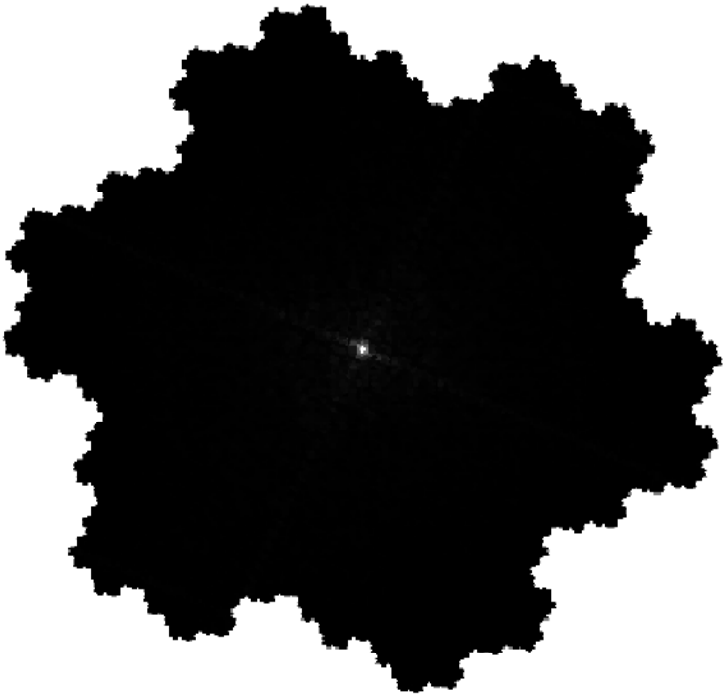

(a)

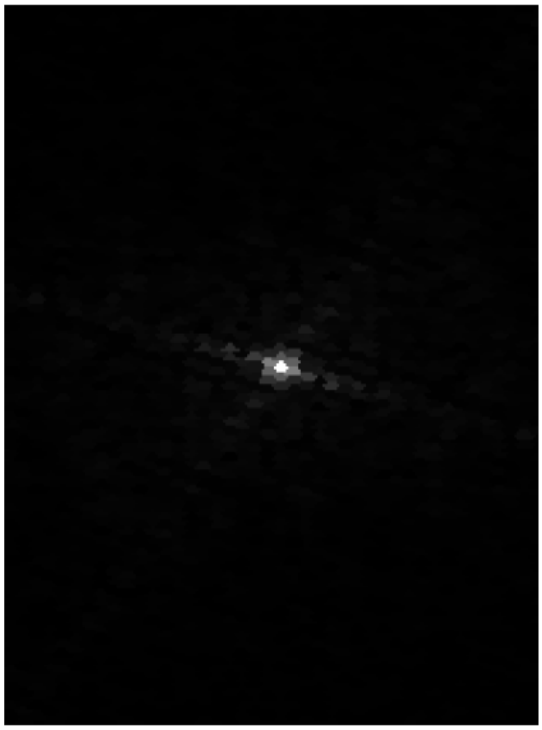

(b)

Figure. A.7 (a) Fourier transform of test image. (b)Magnified central region of Fourier transform of test image.

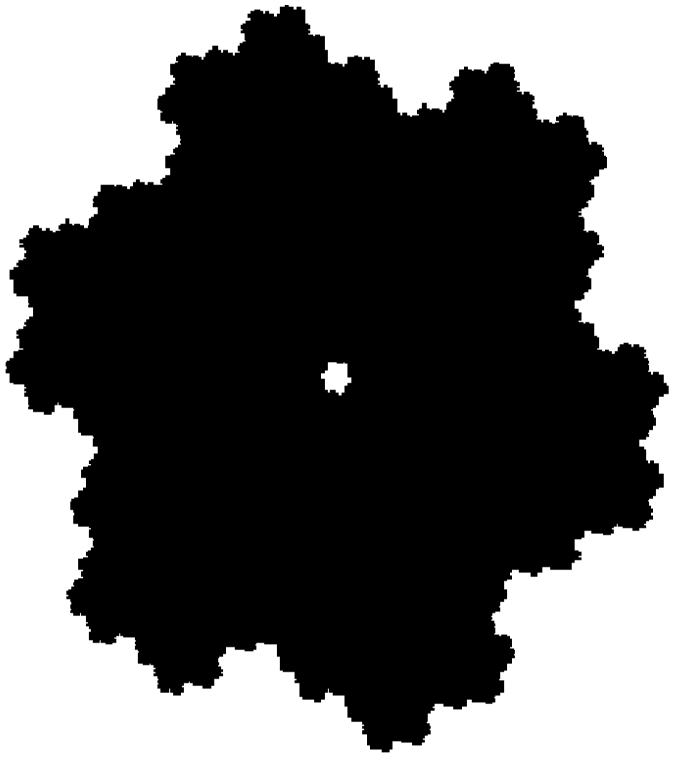

(a)

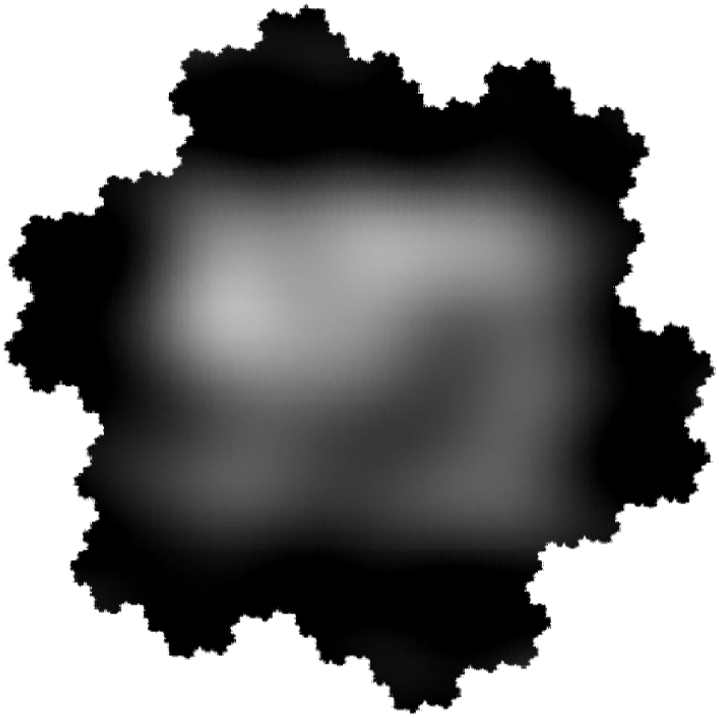

(b)

Figure. A.8 (a)An ideal low pass filter with passband consisting of aggregate level 2.
(b) Effects of an ideal low pass filter with passband consisting of aggregate level 2 on test image.

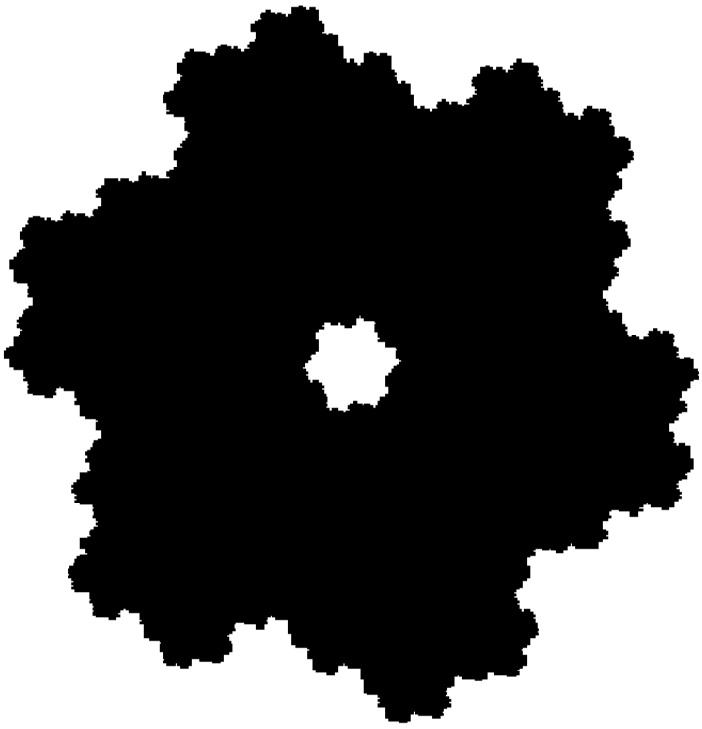

(a)

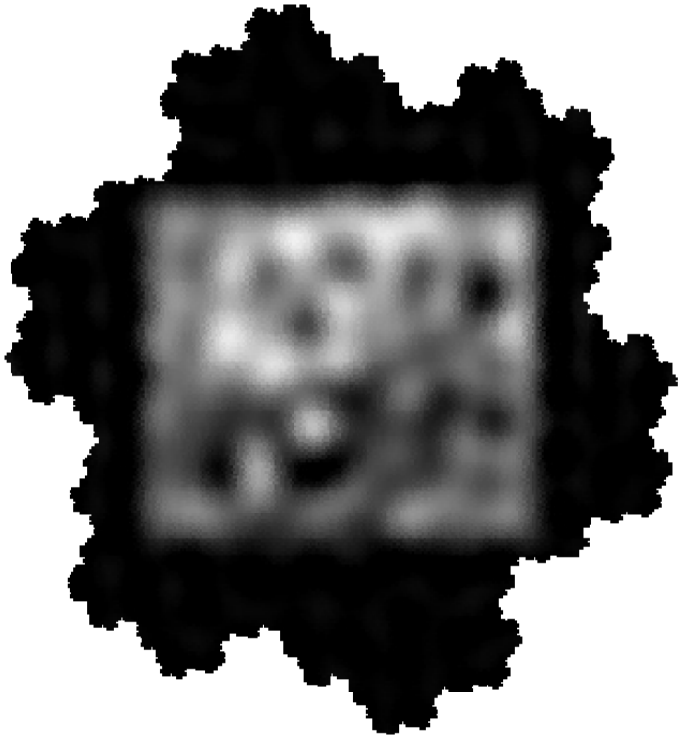

(b)

Figure. A.9 (a)An ideal low pass filter with passband consisting of aggregate level 3.
(b) Effects of an ideal low pass filter with passband consisting of aggregate level 3 on test image.

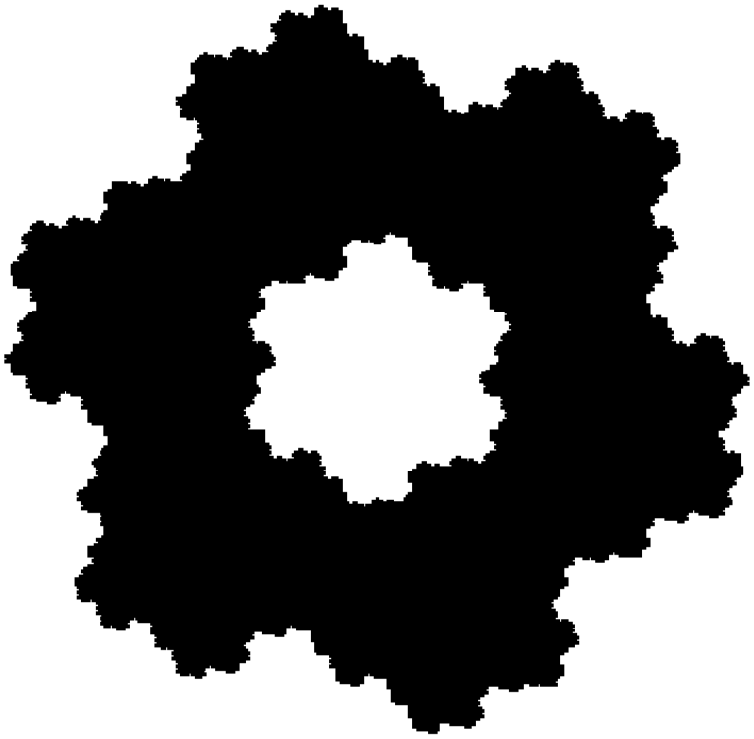

(a)

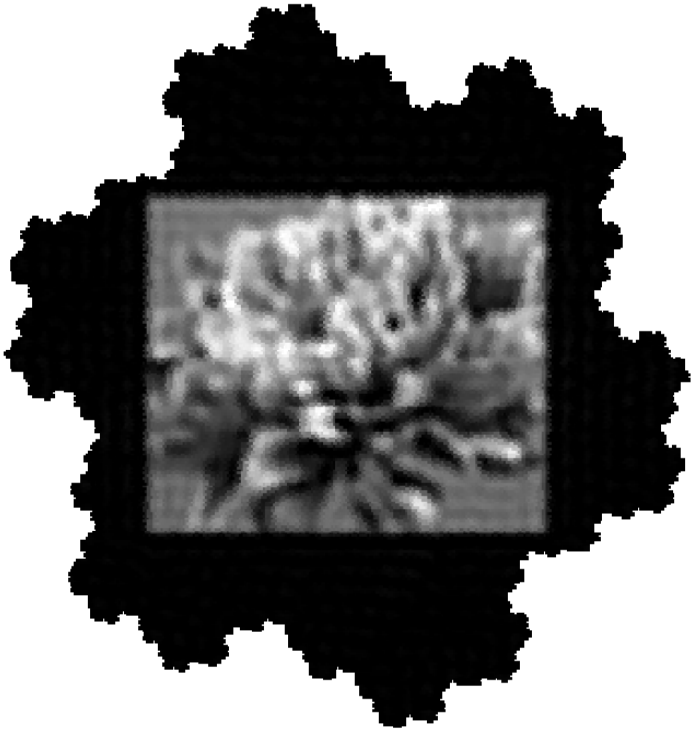

(b)

Figure. A.10 (a)An ideal low pass filter with passband consisting of aggregate level 4.
(b) Effects of an ideal low pass filter with passband consisting of aggregate level 4 on test image.

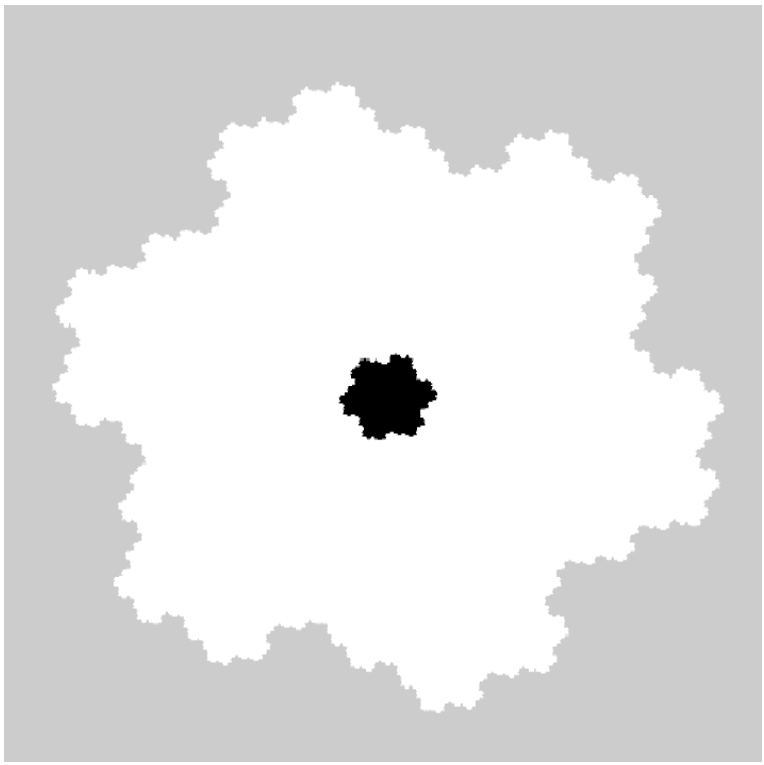

(a)

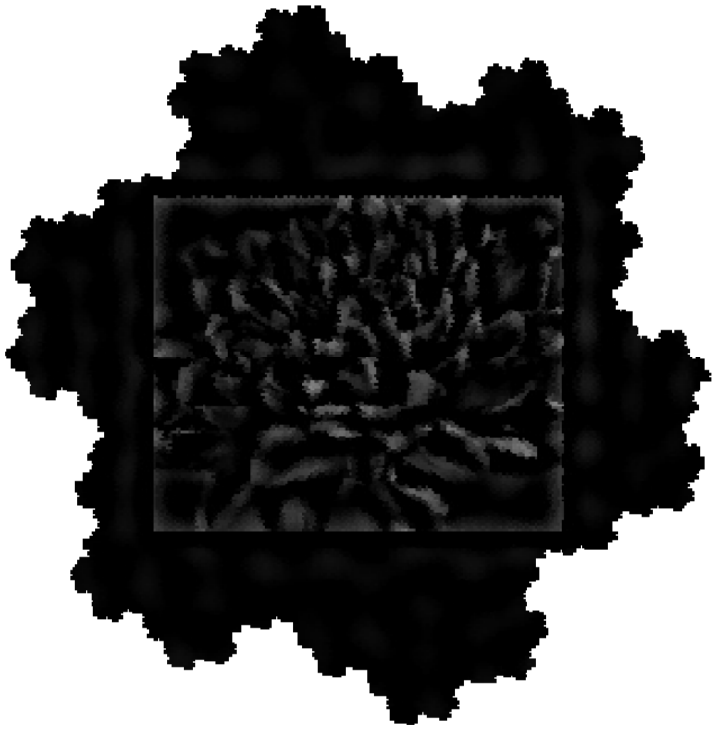

(b)

Figure. A.11 (a) An ideal high pass filter with passband consisting of aggregate level 3. (b) Effects of an ideal high pass filter with stopband consisting of aggregate level 3 on test image

REFERENCES

[1] M. D. Sacchi, "GEOPHYSICS 326 Introduction to Seismic Imaging (Refraction and Reflection Seismology)," *Response*.

[2] U. Road, "Historical development of seismic imaging technique An Overview," vol. 16, no. 3, pp. 71–86, 2012.

[3] L. Seismic, "Shifting paradigms in land data acquisition," *First Break*, vol. 31, no. January, pp. 73–77, 2013.

[4] R. J. Ferguson and G. F. Margrave, "Planned seismic imaging using explicit one-way operators," *Geophysics*, vol. 70, no. 5, p. S101, 2005.

[5] B. R. Clark, "Cover story '\," *ONPOINT*, pp. 4–7, 2007.

[6] D. Mougenot, "3D seismic onshore : should the transition be disruptive ?" 2011.

[7] J. P. Hedley, "3-D migration via McClellan transformations on hexagonal grids," p. 1048, 1992.

[8] V. Bardan, "A hexagonal sampling grid for 3D recording and processing of 3D seismic data," *Geophysical Prospecting*, vol. 45, no. 5, pp. 819–830, 1997. [Online]. Available: http://doi.wiley.com/10.1046/j.1365-2478.1997.600300.x

[9] A. Ozbek, L. Hoteit, and G. Dumitru, "3D filter design on a hexagonal grid with applications to point-receiver land acquisition," *74th Ann. Internat. Mtg.*, no. October, pp. 1965–1968, 2004.

[10] S. Gesbert, C. Haneveld, and S. Saleh, "3D hexagonal prestack depth migration of seismic data," *The Leading Edge*, vol. 26, no. 10, p. 1262, 2007.

[11] R. M. Mersereau, "The processing of hexagonally sampled two-dimensional signals," *Proceedings of the IEEE*, vol. 67, no. 6, pp. 930–949, 1979.

[12] D. P. Petersen and D. Middleton, "Sampling and reconstruction of wave-number-limited functions in N-dimensional euclidean spaces," pp. 279–323, 1962.

[13] V. Bardan, "Hexagonal sampling and hexagonal binning in 3D seismic data acquisition," *72nd Ann. Internat. Mtg*, vol. 21, no. March, pp. 1392–1395, 2002.

[14] R. Mersereau, "Two-dimensional signal processing from hexagonal rasters," *ICASSP '78. IEEE International Conference on Acoustics, Speech, and Signal Processing*, vol. 3, 1978.

[15] L. Middleton and J. Sivaswamy, *Hexagonal Image Processing : A Practical Approach*. Springer, 2005, vol. 224, no. 4. [Online]. Available: http://eprints.soton.ac.uk/262819/

[16] G. Tirunelveli, R. Gordon, and S. Pistorius, "Comparison of square-pixel and hexagonal-pixel resolution in image processing," *IEEE CCECE2002. Canadian Conference on Electrical and Computer Engineering. Conference Proceedings (Cat. No.02CH37373)*, vol. 2, pp. 867–872, 2002. [Online]. Available: http://ieeexplore.ieee.org/lpdocs/epic03/wrapper.htm?arnumber=1013056

[17] S. M. M. Sharif, A. Khalid, M. Raza, "Face Detection and Recognition Through Hexagonal Image Processing," *Sindh University Research Journal*, vol. 44, no. 4, pp. 541–548, 2012.

[18] M. Püschel and M. Rötteler, "Algebraic signal processing theory: 2-D spatial hexagonal lattice," *IEEE Transactions on Image Processing*, vol. 16, no. 6, pp. 1506–1521, 2007.

[19] R. L. Hospelhorn, "Implementation of Steerable Pyramids with Hexagonal Sampling by," *Thesis, Univeristy of New Mexico, USA*, 2006.

[20] P. Sheridan, "Spiral Architecture for Machine Vision," *Thesis, University of Technology, Sydney*, 1996.

[21] E. L. Schwartz, "Computational anatomy and functional architecture of striate cortex: a spatial mapping approach to perceptual coding." *Vision research*, vol. 20, no. 8, pp. 645–669, 1980.

[22] S. Bobe and G. Schaefer, "IMAGE PROCESSING AND IMAGE REGISTRATION ON SPIRAL ARCHITECTURE WITH saLib," *Simulation*, vol. 7, no. 3, pp. 37–43, 1996.

[23] M. Nagao and T. Matsuyama, "Edge preserving smoothing," *Computer Graphics and Image Processing*, vol. 9, no. 4, pp. 394–407, 1979.

[24] B. Grünbaum, B. Grünbaum, G. Shephard, and G. Shephard, *Tilings and Patterns*, ser. Dover Books on Mathematics Series. Dover Publications, Incorporated, 1987. [Online]. Available: http://books.google.com.sa/books?id=zY6nPwAACAAJ

[25] E. Iversen, "SEG Int ' l Exposition and 72nd Annual Meeting * Salt Lake City , Utah * October 6-11 , 2002," *SEG Int'l Exposition and 72nd Annual Meeting*, 2002.

[26] J. P. Hedley, "3-D migration via McClellan transformations on hexagonal grids," *Geophysics*, vol. 57, no. 8, p. 1048, Aug. 1992. [Online]. Available: http://library.seg.org/doi/abs/10.1190/1.1443316

[27] P. Murphy and N. Gallagher, "Hexagonal sampling techniques," *Josa*, 1982.

[28] X. He, T. Hintz, Q. Wu, H. Wang, and W. Jia, "A New Simulation of Spiral Architecture," *Conf. on Image Proc., Computer Vision & Pattern Recogn. IPCV'06*, 2006.

[29] Sahli, "An interactive Web platform development for teaching signal processing," *First Break*, vol. 24, no. February, 2006.

[30] L. Gubin, B. Polyak, and E. Raik, "The method of projections for finding the common point of convex sets," pp. 1–24, 1967.

[31] a. E. Çetin, O. N. Gerek, and Y. Yardimci, "Equiripple FIR filter design by the FFT algorithm," *IEEE Signal Processing Magazine*, vol. 14, no. 2, pp. 60–64, 1997.

[32] a. L. Tertois and T. Frank, "Data Filtering by 3D Convolution," *Image Processing*, no. c, pp. 1–10, 2004.

[33] M. Bahorich and S. Farmer, "The coherence cube," *The leading edge*, no. October, pp. 1053–1058, 1995. [Online]. Available: http://faculty.kfupm.edu.sa/ES/ashuhail/Graduate/GEOP501/Ch4/2006/Bahorich-1995.pdf

[34] A. A. Aqrawi and T. H. Boe, "Improved fault segmentation using a dip guided and modified 3D Sobel filter," *SEG Technical Program Expanded Abstracts 2011*, pp. 999–1003, Jan. 2011. [Online]. Available: http://library.seg.org/doi/abs/10.1190/1.3628241

[35] I. D. Karachentsev, R. B. Tully, a. Dolphin, M. Sharina, L. Makarova, D. Makarov, O. G. Kashibadze, V. Karachentseva, S. Sakai, E. J. Shaya, and L. Rizzi, "The Hubble flow around the CenA / M83 galaxy complex," *The Astronomical Journal*, vol. 133, no. 2, p. 31, Feb. 2006. [Online]. Available: http://arxiv.org/abs/astro-ph/0603091

[36] S. Al-Dossary, "Fault Detection and Characterization Using A 3D Multidirectional Sobel Filter," *Spe-Sas Ats&E*, 2013.

[37] Z. Jing, Z. Yanqing, C. Zhigang, and L. Jianhua, "Detecting boundary of salt dome in seismic data with edge detection technique," *SEG Technical Program Expanded Abstracts 2007*, pp. 1392–1396, 2007.

[38] X. He, W. Jia, N. Hur, Q. Wu, J. Kim, and T. Hintz, "Bilateral Edge Detection on a Virtual Hexagonal Structure," *Digital Image Computing Techniques and Applications*, vol. 4292, pp. 176–185, 2006. [Online]. Available: http://www.springerlink.com/content/l481p4401617g2u0/

[39] S. Coleman, B. Gardiner, and B. Scotney, "Adaptive tri-direction edge detection operators based on the spiral architecture," *Proceedings - International Conference on Image Processing, ICIP*, pp. 1961–1964, Sep. 2010. [Online]. Available: http://ieeexplore.ieee.org/lpdocs/epic03/wrapper.htm?arnumber=5650008

[40] S. Coleman, B. Scotney, and B. Gardiner, "Design of Feature Extraction Operators for use on Biologically Motivated Hexagonal Image Structures," *Comparative and General Pharmacology*, pp. 178–181, 2009.

[41] Q. H. Q. Hu, X. H. X. He, and Q. W. Q. Wu, "Concurrent edge detection with Spiral Architecture on Linux," *Proceedings ITCC 2003. International Conference on Information Technology: Coding and Computing*, pp. 3–7, 2003.

[42] X. He, Q. Wu, W. Jia, and T. Hintz, "Edge detection on hexagonal structure," *Journal of Algorithms & Computational Technology*, vol. 2, no. 1, pp. 61–78, Mar. 2009. [Online]. Available: http://multi-science.metapress.com/openurl.asp?genre=article&id=doi:10.1260/174830108784300321

[43] J. Y. Zhang, C. Yan, and X. X. Huang, "Edge detection of images based on improved sobel operator and genetic algorithms," *Proceedings of 2009 International Conference on Image Analysis and Signal Processing, IASP 2009*, no. 3, pp. 32–35, 2009. [Online]. Available: http://ieeexplore.ieee.org/lpdocs/epic03/wrapper.htm?arnumber=5054605

[44] N. M. AlBinHassan, Y. Luo, and M. N. Al-Faraj, "3D edge-preserving smoothing and applications," *Geophysics*, vol. 71, no. 4, p. P5, 2006.

[45] D. Harwood, M. Subbarao, H. Hakalahti, and L. S. Davis, "A new class of edge-preserving smoothing filters," *Pattern Recognition Letters*, vol. 6, no. 3, pp. 155–162, 1987.

[46] S. Reich, A. Abramov, J. Papon, and B. Dellen, "A novel real-time edge-preserving smoothing filter segmentation."

[47] C. Garnica, F. Boochs, and M. Twardochlib, "A New Approach to Edge-Preserving Smoothing For Edge Extraction and Image Segmentation," *International Archives of Photogrammetry and Remote Sensing*, vol. XXXIII, pp. 320–325, 2000.

Vitae

- Name: Haroon Ashraf
- Nationality: Pakistani
- Date of Birth: June 27th, 1988
- Email: *aharoonashraf@gmail.com*
- Permenant Address: H No. 271, Lane 4, Askari 10, Rawalpindi, Pakistan
- Undergraduate Degree: B.E. Mechatronics Engineering, NUST, Islamabad, Pakistan
- Patent: Efficient Management,Acquisition,Processing & Interpretation of 3D Hexagonally Sampled Seismic Data.